

UNIVERSITY OF OKLAHOMA

GRADUATE COLLEGE

FRACTURE CHARACTERIZATION AND ANALYSIS ALONG THE BLAINE  
ESCARPMENT OF NORTHWESTERN OKLAHOMA

A THESIS  
SUBMITTED TO THE GRADUATE FACULTY  
in partial fulfillment of the requirements for the  
Degree of  
MASTER OF SCIENCE

By  
Paul Gilbert  
Norman, Oklahoma  
2021

FRACTURE CHARACTERIZATION AND ANALYSIS ALONG THE BLAINE  
ESCARPMENT OF NORTHWESTERN OKLAHOMA

A THESIS APPROVED FOR THE  
SCHOOL OF GEOSCIENCES

BY THE COMMITTEE CONSISTING OF

Dr. Brett M. Carpenter, Chair

Dr. Ze'ev Reches

Dr. Richard Elmore

© Copyright by PAUL GILBERT 2021

All Rights Reserved

## ABSTRACT

Detailed fracture mapping and analysis along the Blaine Escarpment of northern Oklahoma demonstrates that zones of deformation previously assigned to solution collapse and desiccation failure appears to play a role but may not be the only or even the primary driving stressor of the region. This implication is strengthened by a thematic strike orientation in fracture sets, mineral veins and regional linear features including surface geomorphology and subsurface fault systems. The maximum compressive stress orientations of the area trend almost exactly E/W, at about  $85\pm 5^\circ$ . This regional stress drives the compressional strike-slip regime of the basement and sedimentary faults systems in this portion of the state. These strike-slip faults of northwestern Oklahoma display a dominant NE/SW trend which is heavily reflected in the linear features of the surface. Large scale, relatively shallow, westward retreating salt bodies are present in the area as well, with certain zones exhibiting active subsurface dissolution and surface precipitation. This active dissolution suggests subsidence at an unknown scale. The surface influence is dependent upon the scale of vertical and horizontal salt front retreat and likely manifests itself in upward propagating sets of extensional fractures. Of the 1,406 mapped fractures and fracture traces, there is a primary trend with a NE/SW orientation. Dominant fracture trends throughout the research stations that are oriented in nearly the same direction as sub-surface features suggests a relationship between the two. However, fracture characteristics, including bed-boundedness, bedding-parallel veining, and others that occur in regions of heavy sub-surface salt dissolution suggests subsidence-related deformation. This study demonstrates, in lieu of the aforementioned characteristics, that: (1) Dissolution subsidence played an active role in shale fracture, as inferred through magnitude of deformation that varies with proximity to dissolving salt fronts; and (2) Fault activity or contemporary stress trends influenced shale fracture

propagation and orientation, as inferred through strong trends of fracture strike in association with regional sub-surface fault systems and previous stress field measurements.

## ACKNOWLEDGEMENTS

First and foremost, I would like to thank my wife, Leah. Without her support and sacrifice I would never have had the opportunity nor the fortitude to continue on with completing a graduate degree. This thesis is dedicated to her. I hope to be as much of a strong pillar of support to her in her life and endeavors as she has been in mine. To my mother, Vanessa, who has always encouraged me to pursue my dreams and who gave me a wonderful childhood despite setbacks and hardships, for which I will be forever grateful. Also, my father Mark, my two sisters Rachel and Rebecca and their husbands and children, my step mother Bobby, and my step sister Lindsey. Additionally, my father and mother-in-law and many brothers-in-law as well as their significant others and family members. Their support was immense and their faith in me was invaluable.

My most sincere thanks goes out to my advisor Dr. Brett M. Carpenter, who gave me the opportunity to pursue this degree under his guidance and who offered assistance and advice throughout the experience. I would also thank Dr. Ze'ev Reches and Dr. Richard Elmore for their instruction and helpful assistance throughout my education and thesis compilation. Thanks to the Oklahoma Energy Resource Board for their financial support and to Tim Munson for his career advice, guidance, and instruction.

A special thanks to Viersen Oil and Gas for allowing me to access their land throughout the years to complete my research. Also, to the Boeckman family of Blaine County for access to their property and Salt Creek Canyon. Finally, a special thanks to my good friends Ben, Brian, Kane, Garrett, Seth, and Tad. They may be a group of disgruntled punks who will never read this, but they are good and true friends.

# CONTENTS

	<u>Page</u>
ABSTRACT .....	iv
ACKNOWLEDGEMENTS .....	vi
LIST OF FIGURES .....	ix
LIST OF TABLES .....	xii
INTRODUCTION .....	1
Objective and significant questions of research.....	1
Location of study and description.....	4
GEOLOGIC SETTING AND RELATED WORKS .....	7
Middle Permian stratigraphy.....	7
Blaine Formation.....	8
Flowerpot Shale.....	10
Chickasaw Formation.....	11
Evaporite salts.....	12
Regional structure and setting.....	14
Local stress and structures.....	14
Regional linear features.....	16
Salt distribution and dissolution.....	18
APPROACH/METHODS OF DATA COLLECTION .....	22
Fracture inventory.....	26

RESULTS .....	28
Station 1 (Hitchcock, OK).....	28
Station 2 (Salt Creek Canyon). ....	35
Stations 3 & 4 (Gloss Mountain State Park and parts of Woods County).....	38
Station 5 (Freedom, OK). ....	40
Station 6 (Big Salt Plains) .....	42
Results Summary. ....	44
DISCUSSION .....	47
Mineral fill.....	47
Selenite.....	47
Satin spar.....	49
Vertical/Sub-Vertical Fracture Orientation.....	51
Aperture/Persistence.....	53
Fracture Interactions.....	58
Bed-Bounded Fractures.....	63
Shale Character.....	66
Subsurface Salt Layer Proximity.....	70
Research Comparison .....	71
Comparable Fracture Studies .....	71
Stress Regime Deformation .....	73
CONCLUSIONS .....	74
REFERENCES .....	79
APPENDIX A .....	86
APPENDIX B .....	94



## LIST OF FIGURES

**Figure 1.** Area of study within Oklahoma, blue polygons represent counties of research, red lineation represents Blaine Escarpment, numbers represent station locations, and black dots represent towns (after Fay, 1964). .....4

**Figure 2.** Stratigraphy of study area (after Johnson, 2019). .....7

**Figure 3.** a) Landsat image of concentric fracture patterns running parallel to cliff edge of escarpment mesas and plateaus. b) Stratigraphic column showing the Blaine Formation gypsum units and associated shales and dolomites at Station 1 (after Fay, 1964). c) Station 1 roadcut showing middle gypsum units of Blaine Formation. d) Graphic showing development of edge parallel fracture due to weathering of gypsum, shale, and potentially salts below or within the shale units. ....9

**Figure 4.** County map showing surrounding regions of Blaine Escarpment (after Fay, 1964) and measured stress orientations from borehole breakout, drilling induced tensile fracture and shear wave splitting measurements as well as subsurface faults of the study area (after Heidbach et al., 2018). .....15

**Figure 5.** a) Northwest Oklahoma linear feature orientations with dominant trends towards the NE/SW, NW/SE (after Guo and George, 1999). b) Cavern passageway orientations of Barber County, KS (after Gauvey, 2019). .....17

**Figure 6.** a) Midcontinent region underlain by evaporite sequences and salt layers (after Johnson, 2019). b) Figure showing salt removal through dissolution and subsequent rock failure through fracture and layer parallel extension (after Warren, 2016). .....19

**Figure 7.** Map of study zones in northwest Oklahoma showing stations 1-6 in relation to salt dissolution fronts as interpreted by Vosburg (1963) along the Blaine Escarpment (after Fay, 1964). Stations 1, 2, 5, and 6 are located near to shallow salt fronts where active precipitation has been observed on the ground surface. ....23

**Figure 8.** a) Fracture density measurement using ½ m<sup>2</sup> square. b) Drawing of fracture density measurement. c) Fracture spacing measurement using scanline. d) Drawing of fracture spacing measurement. ....24

**Figure 9.** (a) Fractures may be divided into various modes dependent upon the direction of wall rock movement. (b) Terms of different modes based upon no mineral infill. (c) Terms of different features based upon mode of fracture and banded or zones regions (after Peacock et al., 2017). .....27

**Figure 10.** a) Column of measured section of upper Flowerpot Shale immediately underlying basal Blaine Formation gypsum at Station 1. b) Crosscutting veins of both sub-horizontal and sub-vertical orientations. c) Transition zone between thick red/brown shales and thin green/grey shales showing the change from massive shale character with dense horizontal satin spar networks to granular/blocky, pedogenic shales where selenite veins dominate. d) Thick, glassy selenite vein outcropping through weathered red bed shales. ....29

<b>Figure 11.</b> a) Rose diagram showing vein orientations in upper selenite layer of Flowerpot Shale. b) Histogram of aperture sizes of selenite veins in upper selenite layer. ....	31
<b>Figure 12.</b> a) Sub-horizontal satin spar veins within massive, clay-rich layer of Station 1 Flowerpot Shale. b) Histogram showing sub-horizontal vein apertures in middle satin spar layer of Flowerpot Shale. ....	32
<b>Figure 13.</b> a) Thick (~150 mm) vertical selenite vein within lower shale layer. b) Histogram showing aperture sizes of selenite veins. c) Rose diagram showing vein strike of basal layer of measured section within the upper Flowerpot Shale. ....	34
<b>Figure 14.</b> a) Satellite imagery of Salt Creek Canyon. b) Fracture with reduced zone due to organic reduction along fracture border. c) Regularly spaced fracture sets in mudstones. d) Rose diagram showing fracture orientations in Chickasaw Formation of Salt Creek Canyon. e) Histogram showing Station 2 fracture persistence frequency distributions. ....	37
<b>Figure 15.</b> a) Sub-horizontal satin spar veins of Station 3. b) Sub-horizontal satin spar veins of Station 4. c) Histogram showing Station 3 aperture size distribution. d) Histogram showing Station 4 aperture size distribution. ....	39
<b>Figure 16.</b> a/b) Common bedding-parallel antitaxial satin spar vein found at Station 5. Bent growth fibers indicate lateral shear movement in conjunction with fracture dilation and mineral precipitation. c) Histogram showing Station 5 vertical vein aperture distribution. d) Rose diagram showing vertical vein orientation distribution. e) Histogram showing horizontal vein aperture distribution. ....	41
<b>Figure 17.</b> a) Rose diagram showing vein orientation distributions at Station 6. b) Histogram showing aperture size distribution. ....	43
<b>Figure 18.</b> Two coarse grained selenite veins with linear, layered plating. ....	48
<b>Figure 19.</b> Fibrous satin spar vein showing multiple growth generations as identified through vein color variation zones radiating from medial suture. ....	49
<b>Figure 20.</b> Density graph showing aperture of satin spar unit found continuously in uppermost Flowerpot Shale. ....	55
<b>Figure 21.</b> Graphs showing density distributions of vein aperture and fracture persistence by station and set. a) Aperture density distribution of sub-vertical selenite veins at Station 1. b) Aperture density distribution of sub-vertical satin spar veins at Station 5. c) Fracture length density distributions of jointed rocks at Station 2. ....	58
<b>Figure 22.</b> a/b) Vertical selenite veins of Station 1 intersecting at T-node with NE vein cutting NW vein. c/d) Thick (~120 mm) NE trending vertical selenite vein of Station 1 with NW vein abutting against it in T-node orientation. ....	60

**Figure 23.** Density plots showing distributions of terminating and terminated against (original) veins and fractures for both Station 1 (a) and Station 2 (b). Both show the vein terminations distributed by strike orientation. For both locations, the most common event is NE/SE and NW/SE trending fractures cutting and arresting NW/SE and NNW/SSE fractures. ....61

**Figure 24.** a/b) Gypsum vein bifurcating upon contact with gypsum nodule at Station 1. c/d) Gypsum vein thinning upon encountering gypsic unit and thickening past it. ....62

**Figure 25.** a/b) Non-bed bound, vertical selenite vein crosscutting through nodular gypsum layer at Station 1. c/d) Non-bed bound satin spar vein crosscutting multiple shale and vein layers at Station 5. ....64

**Figure 26.** a/b) Near perfect bed bounded or top bounded satin spar veins of Station 5 near river escarpment with small deformational folds present. c/d) Near perfect bed bounded or top bounded satin spar veins of Station 5 at roadcut. ....65

**Figure 27.** Station 1 transitional layer from red/brown shale to green/grey back to red/brown. There is a change in shale structure from the top red shales to the bottom. The top is mostly massive and structureless with dense sub-horizontal satin spar veining. The bottom has changed to a more granular and blocky shale with root traces (left) and vertical selenite veins (right). ....67

**Figure 28.** Photographs showing various paleosol and reduction-related features found throughout the study area. a) Photo showing multiple layers of reduced horizons that are slightly richer in silt content at Lone Peak near Station 3. b) Closed and closely spaced fractures within blocky pedogenic shale that strike NW/SE at Station 1. c) Nodular gypsum horizon with layer of water retentive clay located immediately below it at Station 1. ....69

LIST OF TABLES

**Table 1.** Station latitude and longitude. ....6

**Table 2.** Vertical fracture orientation trends by station. ....52

**Table 3.** Upper layer satin spar veining aperture and spacing for Stations 1, 3, and 4. ....57

**Table 4.** Sub-vertical veining aperture and spacing for Stations 1, 5, and 6. ....57

**Table 5.** Station 2 joint persistence and spacing. ....57

## INTRODUCTION

The Glass Mountains of northwestern Oklahoma have been so named from the hills created by the erosion of red Permian shales. Topped by resistant gypsum units, this region of Oklahoma is well known and picturesque. In addition to this caprock of gypsum sitting atop these red shales, gypsic veins cut through the underlying rock layers in many places. These veins represent opening and shearing mode fractures that have been filled with precipitated gypsum ( $\text{CaSO}_4 \cdot 2\text{H}_2\text{O}$ ). Due to intense weathering of the shales, these veins are the only indications that the rocks experienced structural deformity of any sort.

Fractures and associated mineral veins have had a long history of extensive and thorough research in many academic and industrial related geological studies. The discontinuities within a rock structure can tell us many things, such as; principle stress directions during fracture initiation, fluid transport information, directional movement along a fault plane, etc. The Blaine Escarpment (a prominent geographic feature in northwest Oklahoma of which the Glass Mountains are attributed to (Fig. 1)) exhibits a varied array of deformational features. The features most often appear in the form of rock fracture. These fractures are either open or closed, with the open fractures being identified through their mineral fill, which is typically in the form of selenite (clear, glassy gypsum polymorph), satin spar (fibrous polymorph of gypsum, often referred to as a “beef” structure) or, in very few cases, rock gypsum (general massive form of gypsum)(McGregor, 1954).

### **Objective and significant questions of research**

The purpose of this study is to characterize, analyze and interpret fracture systems and patterns within the Permian strata of Blaine County, Oklahoma, and the surrounding regions,

with special interest being paid to formations exposed near the Blaine Escarpment. To achieve the purpose of this study some fundamental questions regarding the expressions of subsurface stress on surface geological features need to be answered. These questions include: 1.) What are the nature and characteristics of surface fractures in the area and along the escarpment? 2.) What role does regional stress and current or paleo tectonic activity play upon the local study area and is there a relationship between it and surface structures? 3.) In an area of stratified salt layers, does an active/ancient dissolution front play a role in surface deformation?

Fractures and veins along the Blaine Escarpment and within the study area have been noted throughout different research projects (e.g., Wu, 1969; Sweet at al., 2013; Johnson, 2019). They have undergone no further study aside from location and general orientation. Wu (1969) conducted research on the geochemistry of the upper Flowerpot Shale and made complete stratigraphic compilations with in-depth descriptions of the shale and the veining that occurred within it. Sweet at al. (2013) conducted research interpreting the depositional environment of the Flowerpot Shale and made note of what she interpreted to be chaotic mineral veins resulting from desiccation cracks. Johnson (2019) completed research over the salt plains of northwestern Oklahoma, in which he noted that saline fluids were expelled from E/W trending joints within the rocks of Salt Creek Canyon. These mentions and general observations form the majority of fracture and vein study along this escarpment. Additional data including detailed strike orientation, vein width, length, etc., juxtaposed with regional characteristics of stress and subsurface structure will provide further information for the nature and genesis of these fracture sets.

Fracture and rock deformation in response to regional stress and fault reactivation is a broad topic. In a study over regional stress influenced rock fracture completed by Terry Engelder (1982) concerning opening mode joints striking parallel to maximum horizontal stress orientations, it was concluded that the formation of these features was the result of tectonic events that were overlooked in favor of events that produced more spectacular structures. These structures might include upward fault propagation and unloading. Jointing as a result of a contemporary stress field, as is hypothesized in Engelders work, may happen in conjunction with or as a result of these events, however, the joint orientation is controlled by the stress regime rather than the events or structures themselves. It is somewhat difficult to ascertain whether these orientations are controlled by the contemporary stress field, considering that loading conditions and propagation timing are not evident. In order to relate the fractures with the field, one must rule out potential mechanisms. This includes propagation of subsurface faults (likely resulting in surface deformation aligned with the deeper or regional structure) and propagation of residual stress from unloading (Engelder, 1982). If the joints do not align with stress fields related to these mechanisms, they may be related to contemporary stress of the region, otherwise they may result from surface deformation caused by propagation of subsurface structures.

Rock deformation as the result of stratified salt dissolution and subsidence is a well-studied topic in the area surrounding this project, such as the Texas panhandle and Kansas. Previous authors have completed research concerning Permian salt layer distribution (e.g., Vosburg, 1963), gypsum veining in the Texas panhandle as the result of dissolution subsidence of Permian Salts (e.g., Goldstein and Collins, 1984; Gustavson and Simpkins, 1989), and salt plain formation through the dissolution, migration, and precipitation of bedded salt in northwestern Oklahoma (e.g., Johnson, 2019). The similarities and close proximity of these prior

works supply valuable information and insight into the relatable events and observations of this thesis.

Summarily, various authors and researchers have conducted studies on the geology of Blaine county and the surrounding regions, as well as relatable works. However, due to the lack of substantial geologic structures in this region, stress orientations and the resultant surface features have undergone less investigation. Further research into this subject will grant discernment into the influence and relationship of salt dissolution and tectonic stresses in addition to their impact on surficial features.

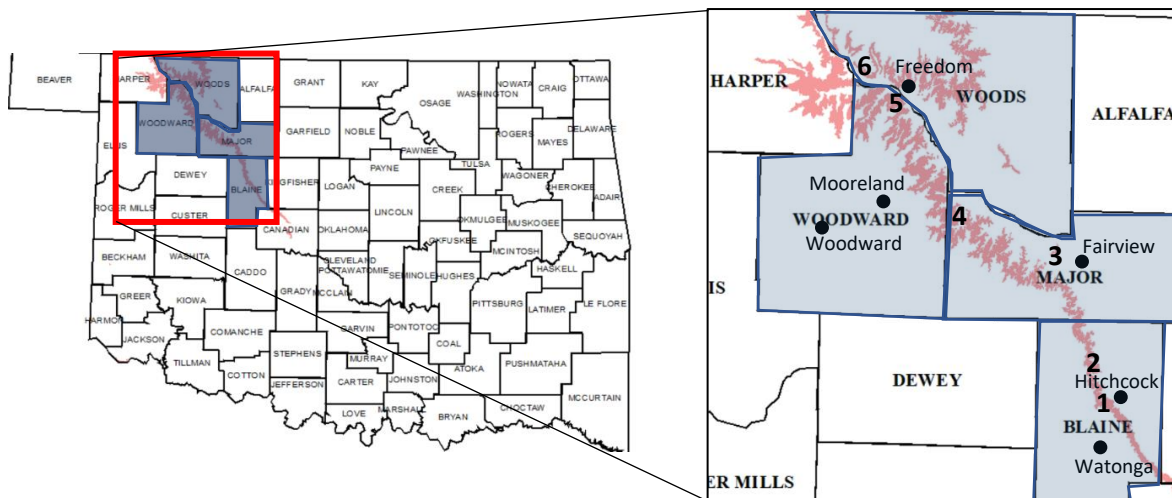


**Figure 1.** Area of study within Oklahoma, blue polygons represent counties of research, red lineation represents Blaine Escarpment, numbers represent station locations, and black dots represent towns (after Fay, 1964).

### Location of study and description

The region of investigation primarily includes the slopes and adjacent areas of the Blaine Escarpment. This escarpment runs in a linear fashion from south-central Oklahoma to southern Kansas. It makes up portions of the topography in many Oklahoma counties. However, the



counties of interest to this study include Blaine, Major, Woods and Woodward Counties (Fig. 1). These counties are located approximately 50, 80, 130, and 170 miles northwest of Oklahoma City, respectively.

Specifically, within these counties and along this escarpment, stations were chosen for their proximity to subsurface salt layers, river contiguity, surface salt precipitation, and accessibility. The latitude and longitude coordinates of these stations can be found in Table 1. Research was highly dependent upon land accessibility and observable fracture propagation. The primary station (Station 1) is located within Blaine County, approximately five miles west of Hitchcock, OK. This location has served as a station for past studies of Flowerpot Shale depositional environments and paleosol interpretations done by Sweet et al. (2013). Within her work she interprets the deposition of the local shales to be of loess origins and makes mention of chaotic mineral veins within the shales and siltstones, however, she does not go into detail regarding these features. In the current study, hundreds of veins measurements were taken at this location to further describe these features. Station 1 is the primary and most thoroughly studied station of this research and was chosen for its accessibility and abundant mineral vein occurrence. The shale slopes, roadcuts, and washouts of the area provide excellent vein observation and study.

The subsequent stations were studied to ascertain a macroscopic relationship between various regional points along the exposed shales of the Blaine Escarpment. Station 2 is in Blaine County approximately 5 miles northwest of Station 1 at the headwaters of Salt Creek. This location is appropriately named Salt Creek Canyon and consists of a creek bed of mudstone with about 120 m of canyon wall relief consisting of shale and gypsum. Station 2 was chosen for its accessibility and proximity to the Upper Cimarron Salt front (according to Jordan and Vosburg,

1963 and Johnson, 2019), which lies, or at one point did lie, between 90-180 m below the surface. This is also a region in which there is active surface salt precipitation indicating active subsurface dissolution at or near the study area.

Station 3 is located at Gloss Mountain State Park, approximately six miles northwest of Fairview, OK. It is a popular road stop that offers a spectacular view of the mesas and plateaus of the Blaine Escarpment. Station 3 was chosen for accessibility and its lack of proximal salt layers. Station 4 is located along Highway 412 at various roadcuts in Woodward and Major Counties, approximately ten miles east of Woodward, OK. Station 4 was chosen for its nearness to public lands and highways as well as its proximal vertical distance from subsurface salt, however, there are no nearby bodies of water and no present or historical evidence of surface salt precipitation (as observed through land satellite data analysis).

Station 5 is located along the Cimarron River approximately two miles south of Freedom, OK in Woods County and consists of two roadcuts and the escarpment ledges along the river. Station 6 is located just north of Big Salt Plain, approximately eight miles northwest of Station 5 and consists of a singular mesa of highly weathered shales. Stations 5 and 6 were chosen for their proximity to the Great Salt Plains, where the Flowerpot Salt is dissolving large volumes of material and reprecipitating it on the surface near the Cimarron River. See Appendix B for further information on site locations.

**Table 1.** Station latitude and longitude.

<b>Station</b>	<b>1</b>	<b>2</b>	<b>3</b>	<b>4</b>	<b>5</b>	<b>6</b>
<b>Latitude</b>	35°57'15"N	36°01'03"N	36°21'50"N	36°25'14"N	36°45'19"N	36°48'42"N
<b>Longitude</b>	98°24'19"W	98°27'00"W	98°36'05"W	98°52'32"W	99°07'06"W	99°15'32"W

## GEOLOGIC SETTING AND RELATED WORKS

### Middle Permian Stratigraphy

Located on the northeastern shelf of the Anadarko Basin in Blaine County, the study area includes the gently westward dipping ( $< 1^\circ$ ; Fay, 1964) middle Permian strata. The Permian rocks of interest to this study are within the El Reno Group of the Guadalupian Series which, according to Carter et al. (1998) and Hemmerich and Kelley (2000), have undergone minimal burial, attaining a maximum depth of approximately 2 km according to vitrinite reflectance studies and reemerging sometime in the early Cenozoic.

The major components of this group and study are the Blaine Formation, the Flowerpot Shale, and the Chickasha Formation (Fig. 2). The Flowerpot Shale contributes to most mineral

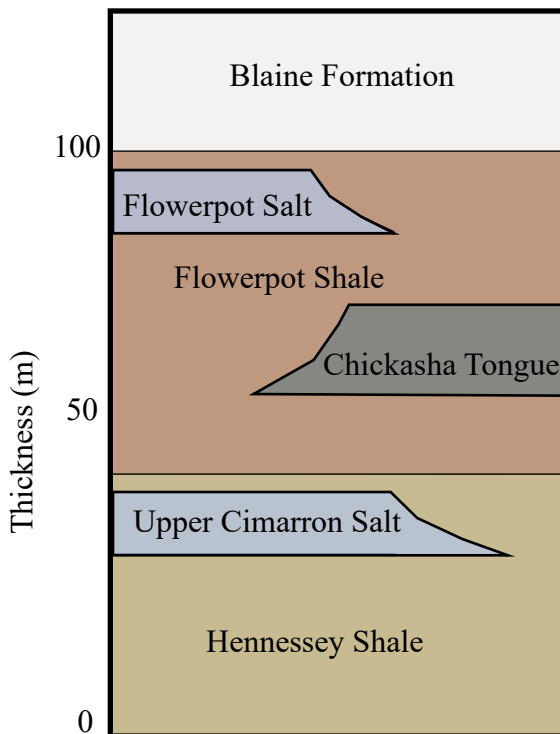


**Figure 2.** Stratigraphy of study area (after Johnson, 2019).

veins that have been measured and analyzed for this project. To the west of the Blaine Escarpment the Dog Creek Shale overlies the Blaine Formation and to the east the Cedar Spring Sandstone and the Hennessey Shale underlie the Flowerpot Shale. The Chickasha Formation is interpreted to be a deltaic deposition (Fay, 1964) which interfingers the Flowerpot Shale and outcrops at Salt Creek Canyon (Station 2). Further detail regarding these three main units in descending order is as follows:

### *Blaine Formation*

The Blaine Formation of Blaine County is approximately 22-130 m thick with sequences of gypsum beds and thick interbedded red/brown and green/grey shales and thin dolomites (Fay, 1964). The layers of gypsum act as a resistant caprock overlying the sub-caprock shales within the Blaine and Flowerpot Formations, creating the escarpment (Fig. 3a). Precisely four gypsum beds make up the formation. These include, in ascending order, the Medicine Lodge Gypsum, the Alabaster (or Kingfisher Creek) Gypsum, the Nescatunga Gypsum and the Shimer Gypsum, with a thin layer of dolomite (the Cedar Springs Dolomite) separating the basal Medicine Lodge Gypsum from the Flowerpot Shale (Fay, 1964). These gypsum beds vary in thickness throughout the escarpment but in the areas of Stations 1 and 2 the Shimer Gypsum runs ~ 9 m thick, the Nescatunga Gypsum runs ~2-4 m thick, the Alabaster (or Kingfisher Creek) Gypsum runs ~ 0.5 m thick, and the Medicine Lodge Gypsum runs ~ 1-2 m thick (Fig. 3b, 3c). The central portion of the Nescatunga Gypsum is marked by a continuous zone of anhydrite (Everett, 1962). The tops of these gypsum units are marked with dense, systematic, and concentric slump and lateral unloading induced fracture sets in the northwest portion of the Blaine Escarpment, but less dense sets in the southeast portion of the escarpment (Fig. 3a, 3d). It is also marked with various collapse features and caverns throughout from the dissolution of the gypsum.

Fracture networks similar to those of the Flowerpot Shales also exist within the Blaine Formation interbedded shales. These networks resemble the dense, thin, sub-horizontal satin spar veins located within the uppermost portions of the Flowerpot Shale. At Station 1, these veins outcrop immediately below the thin Alabaster (or Kingfisher Creek) Gypsum unit within the red/brown and thin green/grey shales and are present halfway to the Medicine Lodge Gypsum (about 3.6 m).

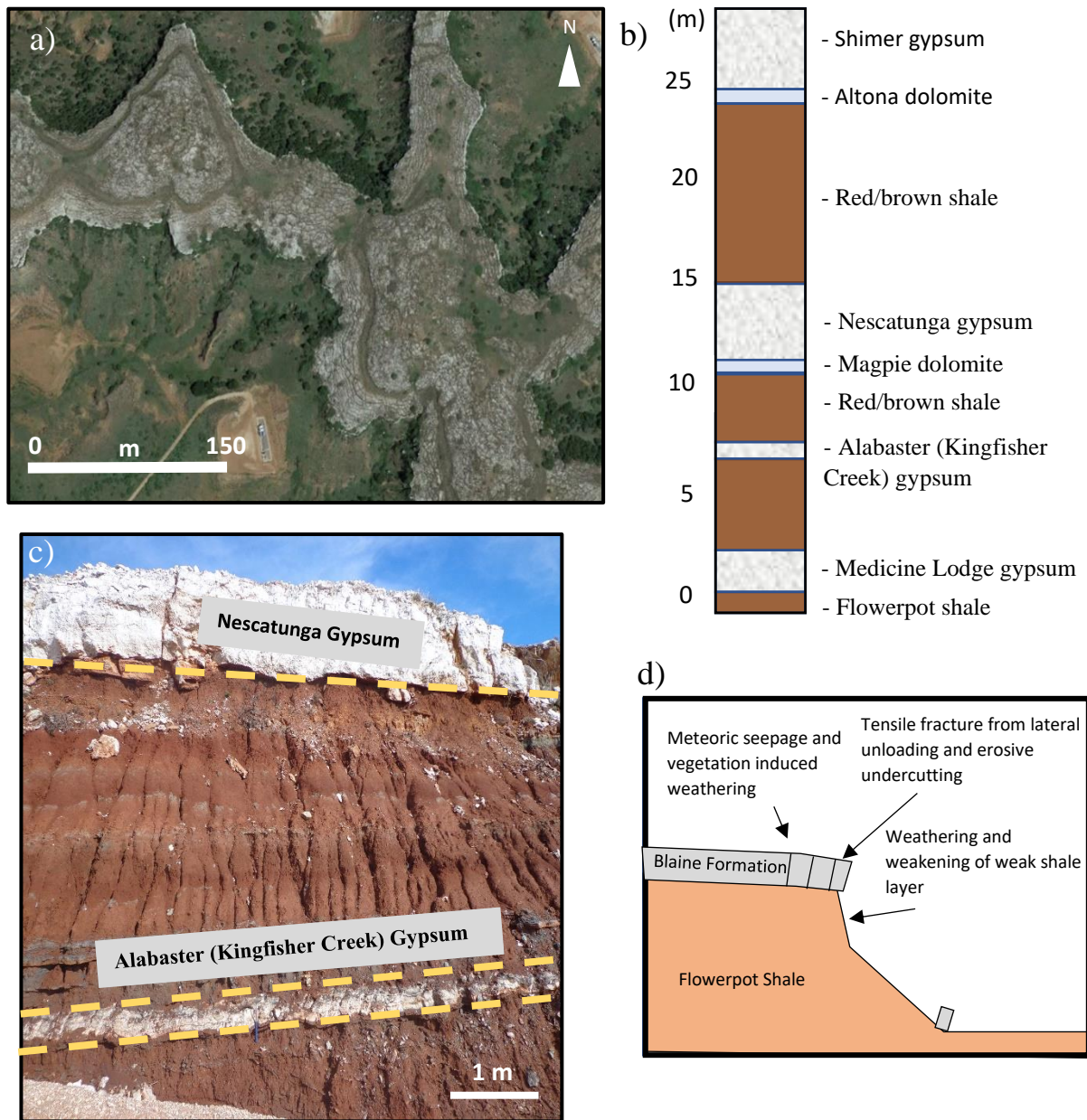


**Figure 3.** a) Landsat image of concentric fracture patterns running parallel to cliff edge of escarpment mesas and plateaus. b) Stratigraphic column showing the Blaine Formation gypsum units and associated shales and dolomites at Station 1 (after Fay, 1964). c) Station 1 roadcut showing middle gypsum units of Blaine Formation. d) Graphic showing development of edge parallel fracture due to weathering of gypsum, shale, and potentially salts below or within the shale units.

These veins are not included in the study of the Flowerpot Shale veins and fractures because they outcrop only at Station 1, where the various gypsum layers of the Blaine Formation were observed. At the other stations, typically, the Medicine Lodge Gypsum is the only layer of the Blaine Formation present, or the other layers are inaccessible. Therefore, this satin spar vein-rich layer lying above the Medicine Lodge Gypsum was not recorded or sought after at subsequent locations. These mineral veins were attributed to weathered Kingfisher Creek Gypsum that dissolved and re-precipitated in the shale units underneath by Everett (1962).

### *Flowerpot Shale*

The Flowerpot Shale is the primary rock unit of this study. It is a unit of reddish/brown and greenish/grey gypsiferous shales and siltstones with beds of dolomite and gypsum (Everett, 1962; Fay, 1964; Wu, 1969). According to Fay (1964), the Flowerpot Shale within Blaine County is 133-141 m thick and contains beds of gypsum, dolomite and siltstone within the upper 15 m, silty clay-rich shale with little or no gypsum, dolomite, or siltstone in the next lower 12 m, and the next 48 m contains red/brown gypsiferous shales and siltstones. This layer grades into the Chickasha Formation near Blaine County. Below the Chickasha Formation lies another 50 m of Flowerpot Shale with red/brown silty clay-rich shale and some siltstone beds (Fay, 1964).

This thesis focuses upon the upper 30 m of the Flowerpot Shale. Specifically, the uppermost 15-18 m of the shales are the primary focus of Station 1, which constitutes the most in-depth study of the stations. A 15 m section of Flowerpot Shale was measured at Station 1 along a roadcut and washout to determine the various facies within the unit of this station and is discussed in the results section of this work.

Suspected paleosol formation within the Flowerpot Shale is another important feature of this unit. Protosols (Mack et al., 1993), or Inceptisols (Retallack, 2001), and Gypsols are interpreted throughout Station 1 and may be seen in a less distinct manner throughout the exposed Flowerpot Shale (Sweet et al., 2013). Protosols and Inceptisols represent minimal duration of soil development and retain original features of the parent material as well as weak horizonation and development (Kraus and Aslan, 1993; Sweet et al., 2013). According to Sweet et al. (2013), these Protosols and Inceptisols are slightly enriched in clay content relative to surrounding strata and show local development of slickensides and wedge-shaped pedes from shrinking and swelling. Throughout these layers are further indications of paleosol development including downward bifurcating root traces and green/grey shale layers that may be attributed to organic reduction (Wu, 1969) along an ancient soil horizon.

The other paleosols present are Gypsols. These are interpreted from the presence of nodular gypsum horizons that can be found throughout these upper Flowerpot Shales and typically form within the vadose zone (Mack et al., 1993). These nodular gypsum horizons often have a clay-rich unit immediately underlying the gypsum which may have sparse, thin satin spar veining.

### *Chickasha Formation*

The Chickasha Formation is a northward thinning deltaic mudstone in Blaine County and, according to Fay (1964), reaches a thickness of approximately 12-15 m. It is interfingered with the Flowerpot Shale and appears near the middle of the unit. The bedding planes of these mudstones and thin shale interbeds have erratic dips throughout, as seen in the only exposure

within Blaine County at Salt Creek Canyon (Station 2). These erratic dips may result from dissolution and collapse or may be a feature of deltaic deposition.

### *Evaporite Salts*

Evaporite layers are regular throughout the Permian Strata in the Anadarko Basin. These evaporites consist of alternating layers of halite salt and gypsum/anhydrite. Salt layers within this region interfinger shale or other units and thin/pinch out as they near the surface on the upward dip of the strata. In the down dip (westward) direction they thicken towards the center of the Anadarko Basin. The combined thicknesses of these salt units are ~760 m thick and, in ascending order, consists of the Wellington salt-anhydrite member, the Lower and Upper Cimarron Salts (between both of these salt layers lies an anhydrite member), the Flowerpot Salt and the Yelton Salt (Jordan and Vosburg, 1963). The Wellington member occurs at depths of 917 m in Blaine County and should be far enough below meteoric influence to have a deformational effect on the surface within the study zones. The Yelton Salt (the uppermost salt within this Permian sequence) is not present within the study location strata and lies above the rocks of interest, thus eliminating its deformational influence. The two evaporite layers of interest that could contribute to salt-related deformation are the Flowerpot Salt and the Cimarron Salts (specifically the Upper Cimarron Salt).

The Cimarron Evaporites have different areal distributions, with the lower salt, middle anhydrite, and upper salt pinching out at separate locations. The upper Cimarron Salt is a focus of this study because of its proximity to some study stations and its migration to the surface at Salt Creek Canyon as concluded by Johnson (2019). It consists of salt and salty shales and,



according to Jordan and Vosburg (1963), the top of this salt unit is difficult to establish due to progressive shaling upwards of the strata.

The Flowerpot Salt is part of the Beckham Evaporite unit (conjoined term for Blaine Formation and Flowerpot Salt) and is the other salty unit that plays a role in this study. It consists of beds with varying thicknesses of salt and salty shale between the Flowerpot Shale and the Blaine Formation. The front of this unit occurs further west than the Cimarron salt fronts. In Blaine County this salt is non-existent. Further to the northwest, in Woods and Woodward Counties, at Big Salt Plains, the Flowerpot Salt has been observed very near to the surface (Ward, 1961). Drilling done by the U.S. Army Corps of Engineers found salt from 9-53 m below the surface at Big Salt Plains, as stated by Ward (1961), who wrote that the upper 27 m of the surface was mostly shale, however, after this interval, the next 18 m were salt. This salt filled vertical cracks in the shale. Gypsum veining also occurred within the shale in what Ward (1961) characterized as selenite. The shales of this drill hole were blocky and granular.

This important observation makes note of selenite veining below the surface of Big Salt Plains and within blocky Flowerpot Shales. During this study, no selenite veining was observed in this region, only satin spar, and no blocky shales were observed, only massive and granular. This occurrence of selenite, as well as the character of the shale, may play an important role in the interpretation of fracture formation.

## Regional Structure and Setting

### *Local Stress and Structure*

According to multiple studies, the stress state in northwestern Oklahoma has an ENE trending maximum horizontal stress ( $\sigma_{Hmax}$ ) (e.g., Dart, 1990; Alt and Zoback, 2017; Heidbach et al., 2018; Levandowski, 2018; Qin et al., 2019). Generally, for northern Oklahoma and the study area region, this trend is approximately N85°(±5°)E (Fig. 4)(Alt and Zoback, 2017). This assertion is calculated from in-situ stress analysis of wellbore breakouts and tensile drilling induced fractures (Dart, 1990), the World Stress Map (WSM) (Heidbach et al., 2018), an updated world seismic map (Levandowski et al., 2018) and stress inversion from focal mechanisms and wellbore measurements (Alt and Zoback, 2017). Central and northern Oklahoma is characterized by strike-slip faulting regimes while further into western Oklahoma and the panhandle oblique normal faulting becomes prevalent (Qin et al., 2019). This trend in stress and faulting orientations is crucial to understanding whether fracturing in the surface pre-exists dissolution influence or if it is unrelated to the direction of regional compressive stress.

In the work of Qin et al. (2019), seismogenic faults within NW, north-central Oklahoma and southern Kansas were mapped using high-precision earthquake relocations. Most of these faults were found to trend in the NE and NW directions, an optimal direction to the local stress field for a strike/slip regime. This optimal orientation in comparison to sedimentary faults and basement fracture (Kolawole et al., 2019) suggests tectonic origins of the seismogenic fault systems.

According to the comprehensive fault map of Oklahoma by Marsh and Holland (2018) that was compiled from numerous studies and petroleum company releases, subsurface faults

along the Blaine Escarpment and near the study region have a typical northeast trend (Fig. 4). To the east fault orientations are mostly N/S and NE/SW as the Nemaha Ridge is approached. To the southwest of the study region around Beckham county, faults strike in a more east/west orientation, attributed to features related to the Wichita megashear system (Zabawa, 1976). The basement faults in the northern portion of the study area show an offset to the regional maximum horizontal stress direction consistent with angular deviations of strike-slip systems to current  $\sigma_1$  orientations.

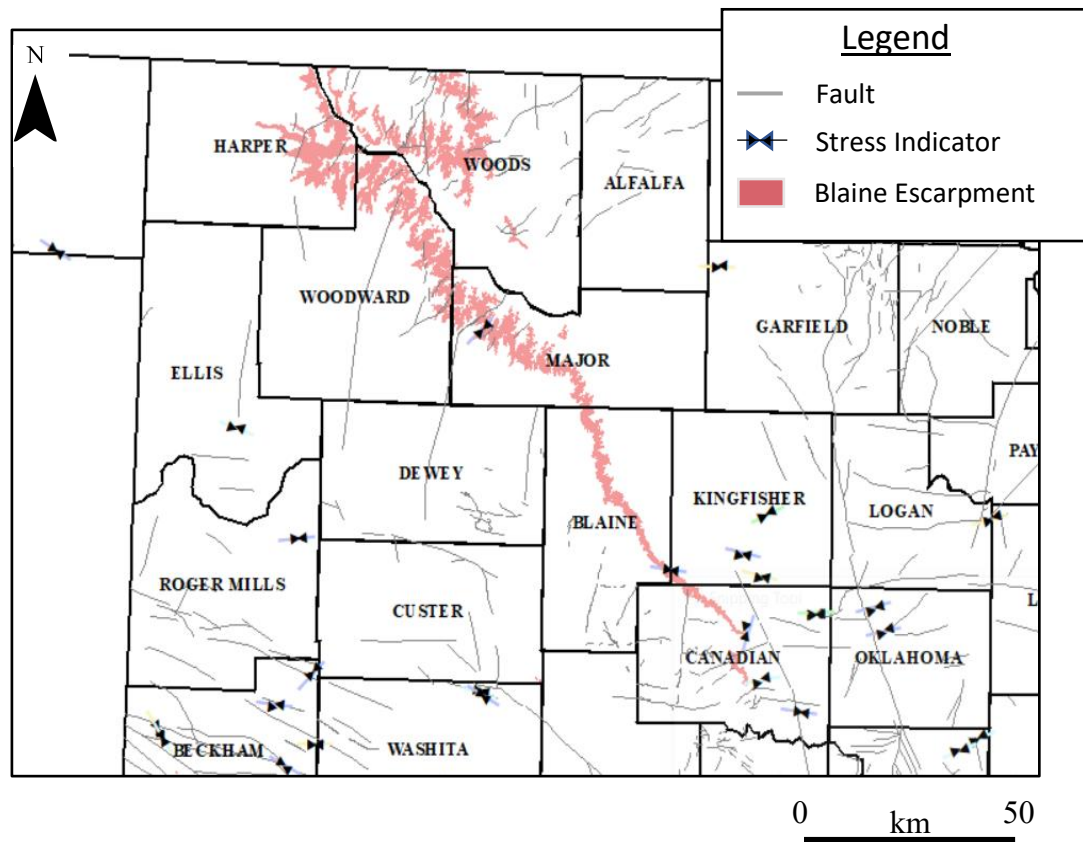


**Figure 4.** County map showing surrounding regions of Blaine Escarpment (after Fay, 1964) and measured stress orientations from borehole breakout, drilling induced tensile fracture and shear wave splitting measurements as well as subsurface faults of the study area (after Heidbach et al., 2018).

### *Regional Linear Features*

Often, surface lineations such as straight river segments, topography, lithologic contacts, etc., will be impacted by structural influences. This might include fractures, faults, and folds. Understanding the regional trends, if any exist, of surface lineations, as well as regional fracture trends is important to discovering a relationship between these features and underlying formation causes.

Collins et al. (1974) conducted a study throughout the Anadarko Basin of surface linear features in an attempt to apply the knowledge gained to current and future petroleum reservoir identification. Using Earth Resources Technology Satellite-1 (ERTS-1) imagery, the team analyzed black, white, and color photos of differing color bands at various times throughout the year to distinguish linear anomalies in the surface of the region. The linear anomalies that they characterized were the lineations mentioned above, as well as tonal anomalies in topography, drainage patterns and vegetation. Further research combining both surface linear features with subsurface features such as gravitational, magnetic, and subsurface fault lineations conducted by Guo and George (1999) indicate even further dominant NE/SW and NW/SE directional trends in western, northwestern Oklahoma and western Kansas (Fig. 5a). Using data for the entire mid-continent region, they concluded that there was a very high consistency between surface linear features and linear gravitational and magnetic anomalies, as well as subsurface fault orientations. The reasons for this consistency were attributed to vertical propagation of subsurface fault activity to the surface. Activation and reactivation of these faults created topographic and surface fracture patterns that mirrored the orientation of faults in the subsurface.

Further studies within the cavern systems in the Blaine Formation of Barber County, Kansas (immediately north of Stations 5 and 6), have recorded linear passageways following

NE/SW and NW/SE striking joints within the Flowerpot Shale and the Blaine Formation gypsum (Fig. 5b)(Gauvey, 2019). The corridors form as fluids migrating through permeable fractures dissolve the surrounding gypsum.

Linear features of northwestern Oklahoma that mirror subsurface anomalies and discontinuities suggest a relationship between the two as opposed to a relationship between contemporary stress orientation and surface features. The offset of the feature alignment with regional stress fields likely indicates little or no direct relation between the two. Fracture zones that may form some of these relatively uniform lineations seem, based on current research and conclusions, to propagate in response to movement in the subsurface as opposed to contemporary stress fields.

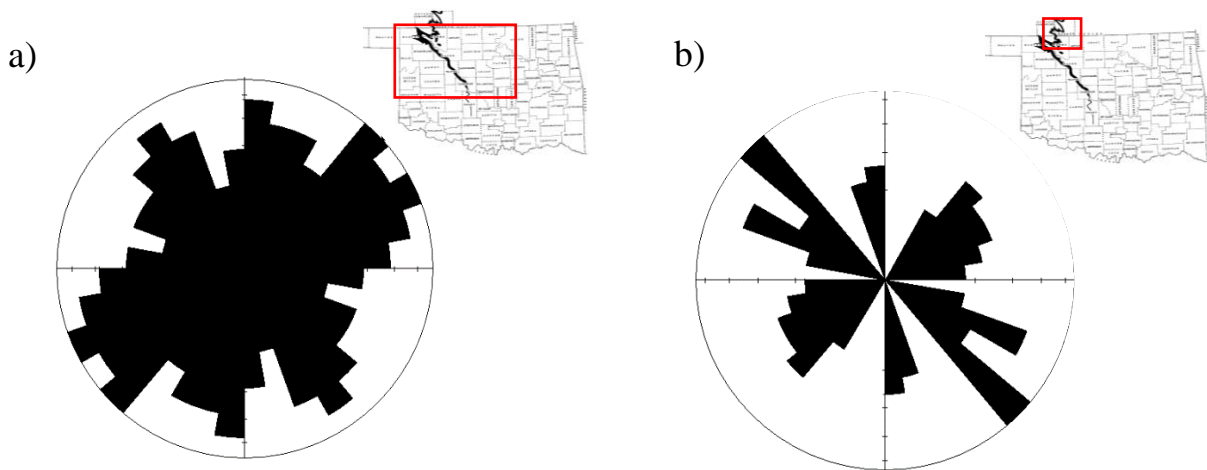


**Figure 5.** a) Northwest Oklahoma linear feature orientations with dominant trends towards the NE/SW, NW/SE (after Guo and George, 1999). b) Cavern passageway orientations of Barber County, KS (after Gauvey, 2019).

### *Salt Distribution and Dissolution*

Stratified salt layers exist throughout many areas of the midcontinent region (Fig. 6a). Sub-surface salt dissolution is one other prime suspect for fracture initiation and surface deformation in northwest Oklahoma. Several studies have been conducted in relation to surface effects of the dissolution of Permian salts in southern Kansas, the panhandle of Texas, and northwestern Oklahoma (e.g., Goldstein and Collins, 1984; Gustavson, 1986; Morton et al., 2018; Johnson, 2019).

Gustavson, Goldstein, and Collins have done extensive work regarding dissolution, rates of retreat of geomorphic features, sub-surface salt fronts, and gypsum veins of evaporite basins in the Texas panhandle (Goldstein and Collins, 1984; Gustavson, 1986; Gustavson and Simpkins, 1989; Gustavson and Hovorka, 1994). Goldstein and Collins (1984) conducted a study within the Palo Duro Basin of Texas, focusing on collapse structures and systematic regional joints. They interpreted the joint systems as pre-dating the collapse structures and expressed that these jointed zones controlled dissolution rates along the salt front, creating a mosaic of local areas with variable rates of dissolution. Their proposed theory of dissolution related stress in the area was initial jointing due to burial, early dissolution layer-parallel extension with faulting, and, finally, mid to late dissolution related subsidence and collapse (Goldstein and Collins, 1984). Tension in layers above vertically dissolving salt, as opposed to a laterally dissolving front, is created through gravitational stretching of overlying strata, resulting in normal faulting and horizontal vein networks (Fig 6b).

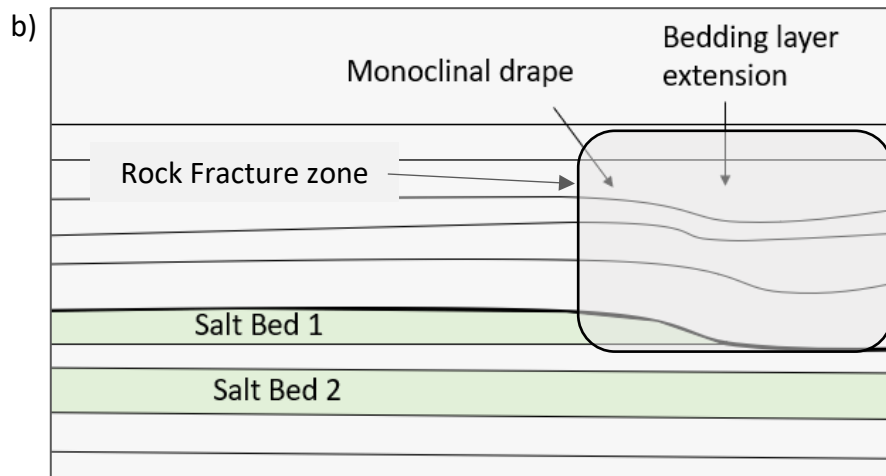
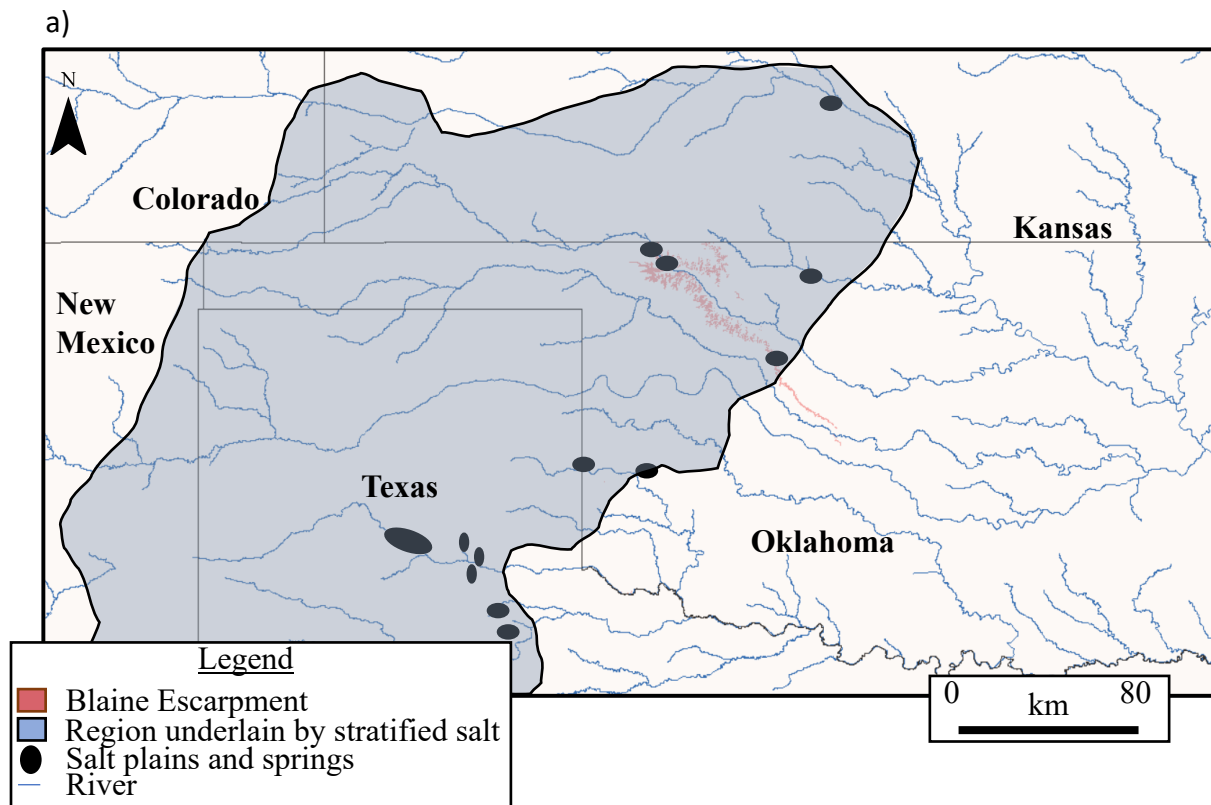


**Figure 6.** a) Midcontinent region underlain by evaporite sequences and salt layers (after Johnson, 2019). b) Figure showing salt removal through dissolution and subsequent rock failure through fracture and layer parallel extension (after Warren, 2016).

Gustavson and Simpkins (1989) attributed the Canadian River Valley in the Texas Panhandle to regional subsidence following Permian salt dissolution. They concluded that thick regions of layered salt formerly occupied space underneath of the current river valley using five lines of evidence: 1) interpretation of log data showing structural collapse of overlying beds and the presence of salt layers abruptly disappearing between wells, 2) brecciated zones and extensional features overlying uppermost salts in core, 3) outcropping rocks contain folds and gypsum filled veins, 4) hydrologic tests above upper salts produced sodium chloride brines and 5) high chloride contents in the nearby Canadian River indicating active dissolution (Gustavson and Simpkins, 1989). Similar methods were used by Vosburg (1963) to identify Permian salt distributions in northwestern Oklahoma.

The work of Kenneth Johnson (2019) has contributed significantly to the understanding of Permian stratigraphy and evaporite processes in much of northwestern Oklahoma. Having conducted studies to measure brine emission along the Cimarron River, Johnson (2019) found large loads of chloride increasing as the river ran south through the northwest portion of the state, indicating active salt dissolution. At Salt Creek Canyon (Station 2) it was discovered that brines were being introduced to the system through E/W and NE/SW trending fracture sets where the Upper Cimarron Salt is approximately 90 m below the surface of the Chickasaw Formation. It was also discovered that the vast majority of chloride load being introduced to the Cimarron River was occurring at Big Salt Plain (Stations 5 and 6). This region of the state is where the shallow Flowerpot Salt front is actively dissolving approximately 40 m below the surface (Vosburg, 1963). It is in close proximity to the river, introducing enormous amounts of freshwater that contributes to salt dissolution in the near surface and precipitation at ground level. As with Gustavson and Simpkins (1989), it was found through well log and core data that



in regions east of the Cimarron and Flowerpot salt fronts, brecciated and collapse zones were left where salt should have formerly existed.

In zones of active or historic dissolution of subsurface bodies, the geomorphic properties of the region will be affected to some degree. The Canadian River in the Texas Panhandle is an example of a river with high levels of chloride following a zone of dissolution which applies a control on the rivers orientation throughout a portion of the High Plains (Gustavson, 1986). In salt zones where the layers are introduced to a large amount of unsaturated water, dissolution may be quite rapid and result in collapse features and subsidence, and in turn may have a significant impact on regional drainage patterns (Frumkin, 2013).

#### Subsurface salt-related deformation summary

- Surface deformation including jointing and mineral veins over dissolving Permian salts in the Texas panhandle (Goldstein and Collins, 1984).
- Satin spar veining within evaporite basins (Gustavson, 1994).
- Caprock retreat attributed to regional subsidence following salt dissolution and subsidence (Gustavson and Simpkins, 1989).
- Brine emission through pre-existing joints within Salt Creek Canyon, OK (Johnson, 2019).
- Drainage patterns impacted by salt deformation zones resulting in collapse and subsidence (Frumkin, 2013).

## APPROACH/METHODS OF DATA COLLECTION

The discontinuities along the Blaine Escarpment form as a result of some stress induction, either paleo or current, which, being local or regional, may be attributed to horizontal stress patterns related to regional tectonic fields, vertical fault propagation, and/or dissolution subsidence. These potential deformation causes will be discussed, analysed, and juxtaposed with field measurements.

Data collection of multiple fracture zones were mapped along the Blaine Escarpment, with particular interest being paid to fracture zones near or intersecting receding salt fronts, as inferred through log data (Jordan and Vosburg, 1963; Johnson, 2019) . This involved six separate stations needed to compare and contrast fracture features (Fig. 7). These stations were important in their proximity to receding salt as well as the depth of salt layers in the area.

At these various regions, the discontinuities were analyzed for their azimuthal orientation (strike), dip (where possible), aperture, persistence, spacing, density, connectivity, fill, elevation, and any sign of displacement as described by Singhal and Gupta (1999). Orientation and dip magnitudes were taken with a Brunton to accurately gauge direction of vein and joint strike and dip. The dip of these fractures was measured in various locations but was not used for analysis because most of the features were vertical or nearly so.

Fracture aperture is a term that refers to the width of the fracture opening from wall to wall. This was measured on sealed fractures within the study zones. To obtain these measurements a caliper was used to measure in millimeters. This caliper was also used to determine mineral vein fiber widths. Persistence is a term that refers to the length a fracture runs on a surface. To obtain measurements of persistence a measuring tape was used in most cases.

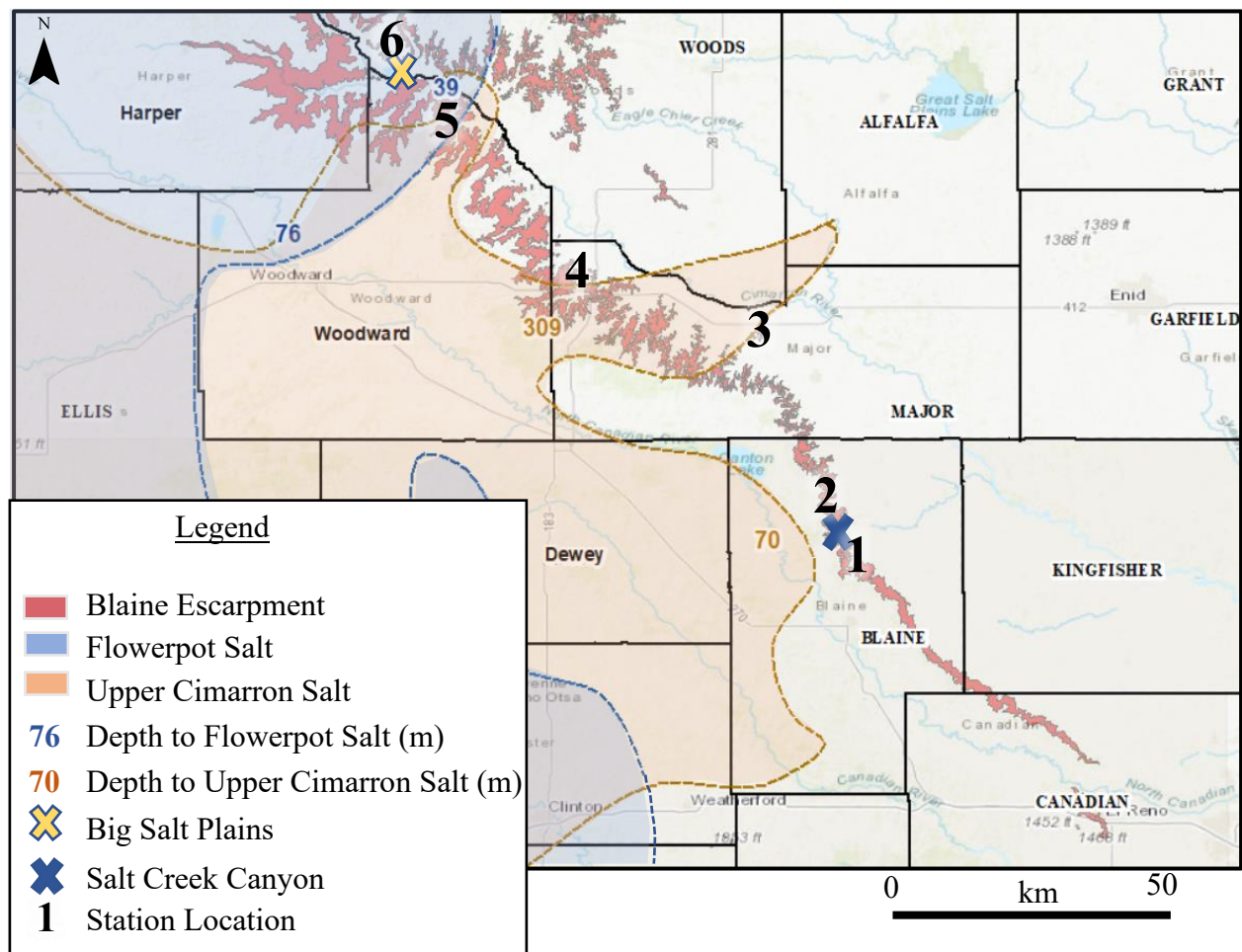


**Figure 7.** Map of study zones in northwest Oklahoma showing stations 1-6 in relation to salt dissolution fronts as interpreted by Vosburg (1963) along the Blaine Escarpment (after Fay, 1964). Stations 1, 2, 5, and 6 are located near to shallow salt fronts where active precipitation has been observed on the ground surface.

Aperture and persistence were highly variant throughout singular study areas, thus these numbers were averaged and given with their minimum and maximum values.

Linear and areal fracture densities and spacings were recorded using the  $\frac{1}{2}$  m<sup>2</sup> square (Fig. 8a, 8b) and measuring tapes (Fig. 8c, 8d) using the methods of Singhal and Gupta (1999). Connectivity was traced to determine relative fracture ages and to identify relative timing of

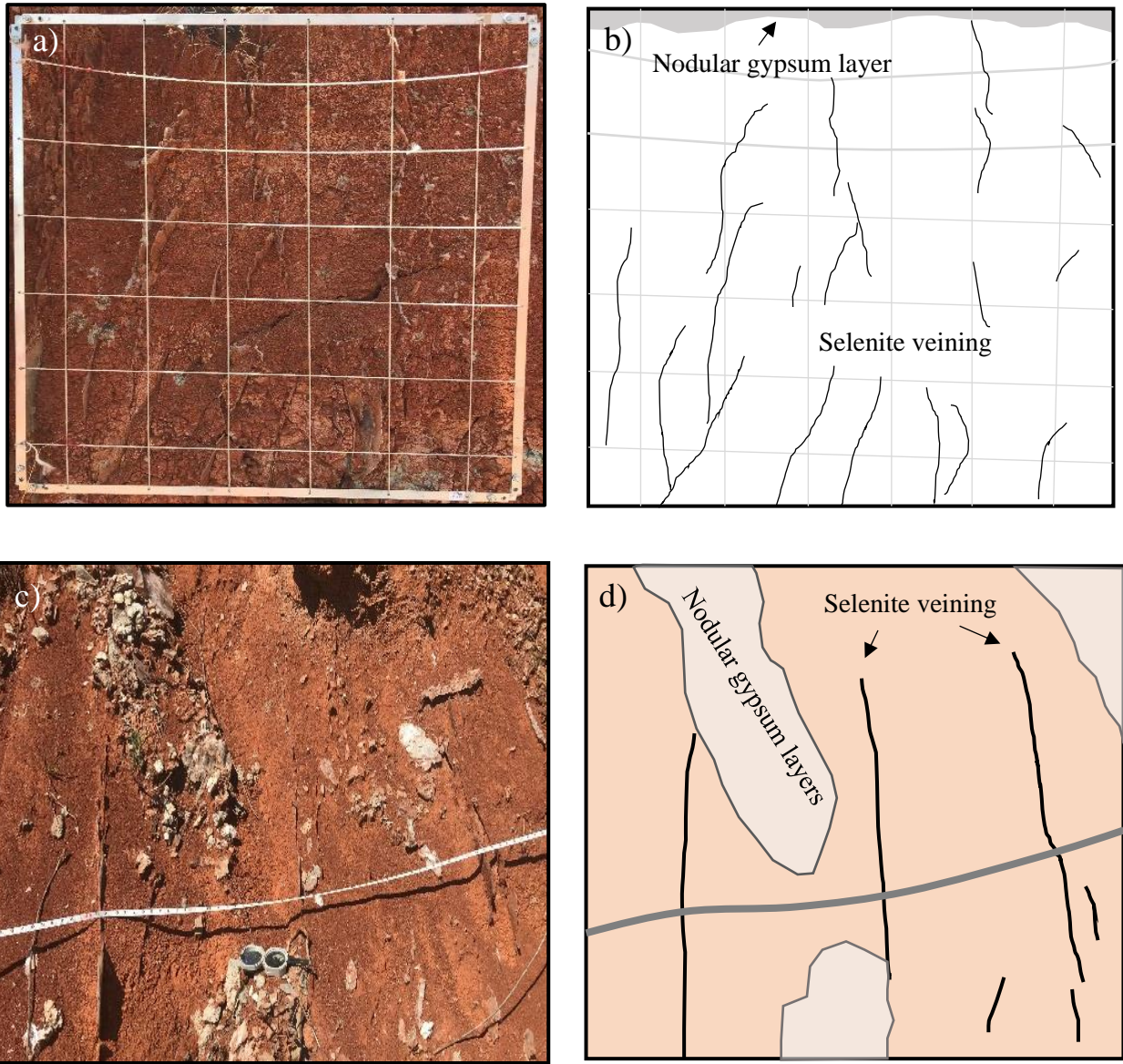


**Figure 8.** a) Fracture density measurement using  $\frac{1}{2}$  m<sup>2</sup> square. b) Drawing of fracture density measurement. c) Fracture spacing measurement using scanline. d) Drawing of fracture spacing measurement.

dominant trends. Lateral displacement was measured and analyzed to determine if any shear offsets are present, as well as vertical displacement to determine if subsidence exists in a zone or blocks. The material that the veins or joints occurred in was an important observation that was taken (whether the material was massive, granular, etc.). Bed-boundedness was also noted for individual fractures so that it could be observed in accordance with the work of Hooker et al. (2013). The fill of the fractures was analyzed to describe the fracture growth structure and fluid movement (Ramsay, 1980). These data points were stored in a field notebook as well as a Garmin GPS unit and were immediately transferred to an excel spreadsheet. Sketches were made of representative samples of fracture patterns to clarify specific details concerning the relationship between the nature of the vein and host material.

The data was robustly analyzed using various statistical methods and software. ArcMap was utilized for placement of the two important inferred salt fronts using data and maps created by Vosburg (1963) on the Permian salts of northwestern Oklahoma. Data from ArcGIS Online was utilized to import information concerning stress fields from the World Stress Map (after Heidbach et al., 2018), as well as fault data, river data, escarpment outcrops, county, and city locations, etc.

Maps were also created from the satellite imagery of Google Earth and Google Earth Pro. These programs were indispensable in the reconnaissance phase of this project. They allowed for the identification of potential outcrops and access locations as well as accurate measurements of landforms and distances.

Data visualization techniques and statistical analysis were completed on RStudio and GeOrient. Histograms and density plots were created using the programming language R in RStudio to show various distributions of fracture properties including aperture vs. strike,

persistence vs. strike, interaction comparisons, etc. Area weighted rose diagrams for the separate stations and rock layers were created within GeOrient to show the distributions of vein and joint trends, and to allow for the identification of dominant sets. These sets were identified and separated and put into bins of specific ranges. Once the sets were binned individually, they were run through the program again to obtain an accurate average strike. Fractures were then placed into their appropriate sets if they fell within one standard deviation of the set average. Using these various programs and techniques, relationships and trends were sought out with the available data.

## **Fracture Inventory**

Before analysis, it is important to define the appropriate terms and to recognize the types of features that were observed and will be referred to. Throughout this work the term fracture is used in conjunction with veins and joints. A fracture is used within the geologic literature to define a broad range of structures. These structures include joints, veins, dykes and sills, faults, deformation bands, stylolites, etc. (Fig. 9)(e.g., Schultz and Fossen, 2008; Peacock et al., 2016). The failure of the rock itself creates a discontinuity termed “fracture” and is then specified down to a more distinct label. The fractures observed throughout this study fall within the scope of extension fractures and shearing-mode fractures. Extension (opening mode) fractures occur as the walls of a discontinuity move apart from each other perpendicularly and include veins (mineral filled fractures) and joints (unfilled fractures)(e.g., Peacock et al., 2016). Shearing-mode fractures are discontinuity planes along which the wall rock moves sub-parallel to the plane of fracture and when filled with precipitating fluids may develop veins with bent fibers, depending upon dilation and precipitation rates.

Vertical/sub-vertical/high angle to bedding fractures all refer to the fractures of this study that are between 45° and 90° to the bedding in which they occur, which is near horizontal for all stations. Horizontal/sub-horizontal/bedding-parallel refer to fractures that are between 0° and 45° to the bedding in which they occur. Bedding-parallel is typically used more in relation to fractures that occur along a bedding plane surface while horizontal/sub-horizontal is often used to describe smaller fracture sets that occur within the beds themselves. Varying types of fill reside within these fractures, mostly gypsum (satin spar, selenite, or rock gypsum).

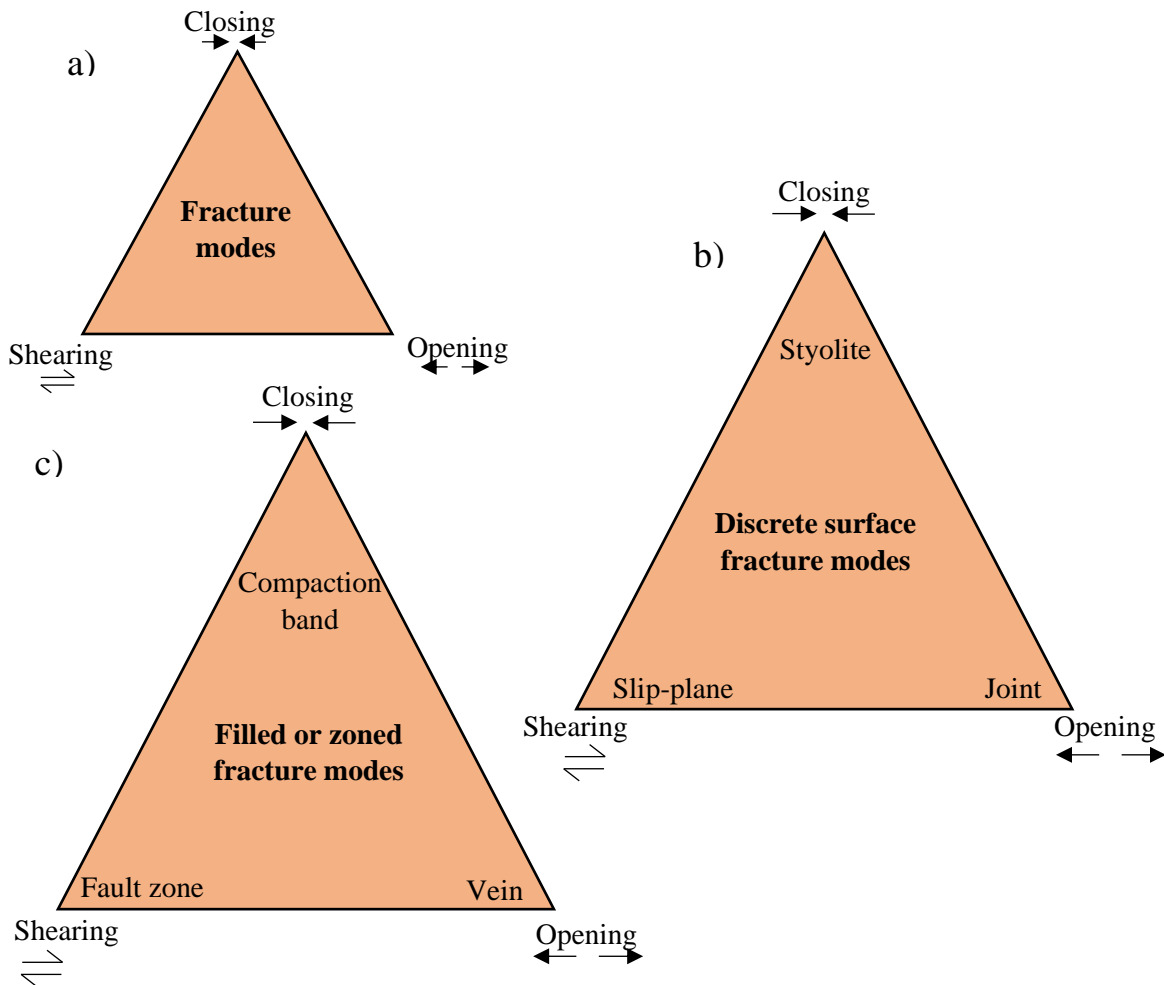


**Figure 9.** (a) Fractures may be divided into various modes dependent upon the direction of wall rock movement. (b) Terms of different modes based upon no mineral infill. (c) Terms of different features based upon mode of fracture and banded or zones regions (after Peacock et al., 2017).

## RESULTS

### **Station 1 (Hitchcock, OK)**

Station 1 (the primary station) is the location at which a comprehensive stratigraphic column was measured and interpreted (Fig. 10a). The measured column of approximately 15 m divides thick beds of red/brown shales/siltstones and thin beds of green/grey shale/siltstone with varying degrees of gypsum content, some of which is nodular. These bedded shales contain mineral vein networks throughout the section. Layers display varying degrees of fracture nature, some of which are dominantly sub-horizontal or sub-vertical, some have very high densities compared to others, and in some satin spar dominates over selenite.

Selenite is the most common vein type in the area (Fig. 10). The glassy and platy nature of the fill is highly variant. Some veins exhibit thin glassy or blocky plates of selenite that strike parallel to the fracture walls, some have plates at an angle or perpendicular to the walls, and some alternate sporadically between these orientations with varying plate thickness.

Satin spar occurs in the region as well, although it is mostly confined to a single layer within the measured section and is predominantly quite thin. The satin spar vein fibers are mostly white with some yellowish discoloring. The veins in which the aperture is wide enough to observe display fibers normal to fracture walls, with no evidence of slippage during precipitation. Antitaxial (outward growing) veins with medial scars that are roughly parallel to the fracture walls show singular or multiple generations of growth, mostly observed within the wider veins. This can be seen through regularly spaced zones radiating from the median in which fibers change characteristics, such as color or width. The vein seams are dominantly equal to



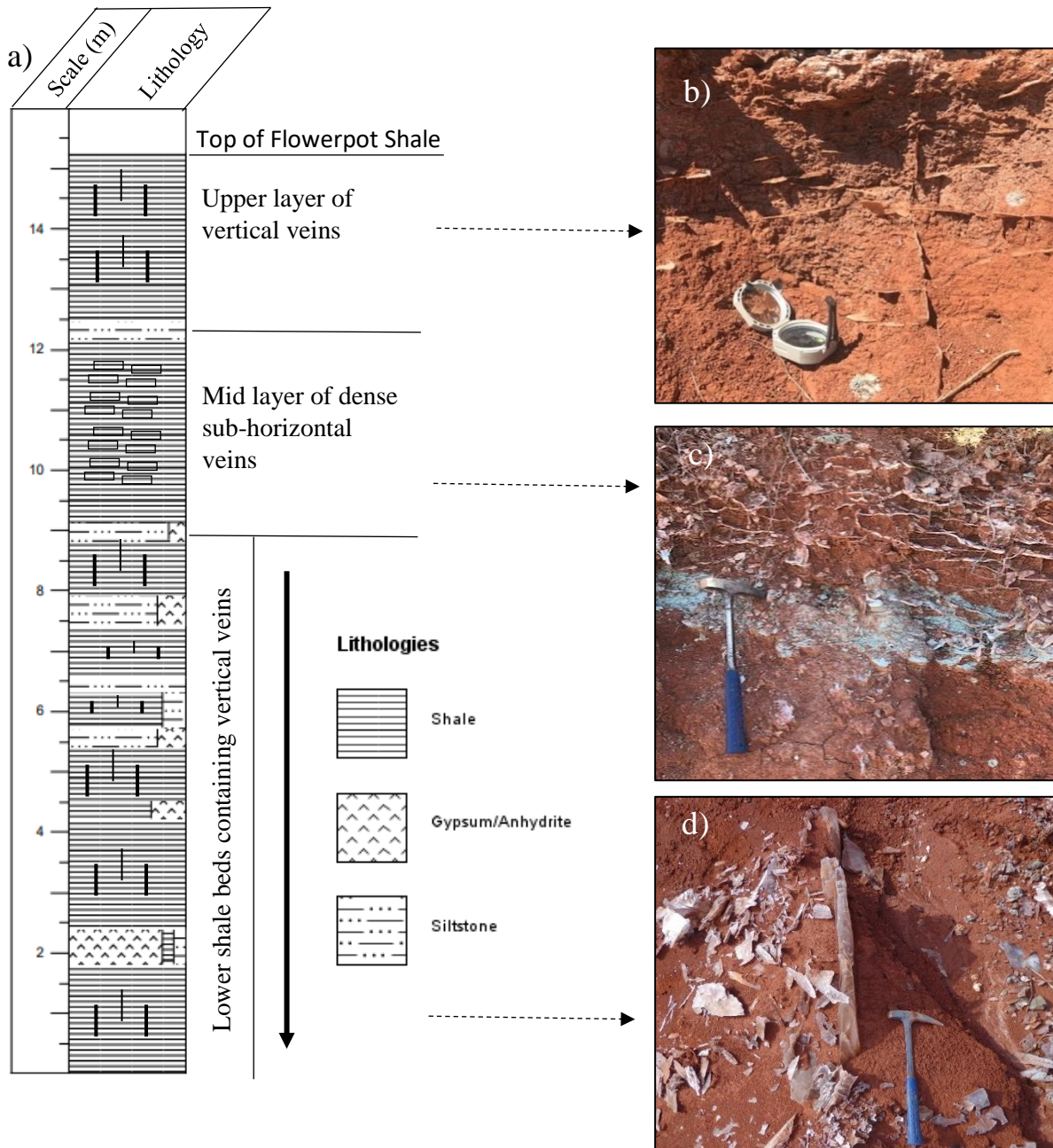


**Figure 10.** a) Column of measured section of upper Flowerpot Shale immediately underlying basal Blaine Formation gypsum at Station 1. b) Crosscutting veins of both sub-horizontal and sub-vertical orientations. c) Transition zone between thick red/brown shales and thin green/grey shales showing the change from massive shale character with dense horizontal satin spar networks to granular/blocky, pedogenic shales where selenite veins dominate. d) Thick, glassy selenite vein outcropping through weathered red bed shales.

approximate in widths, with exceptions being seen throughout of thicker or thinner upper and lower seams.

Throughout the measured section, especially in the bottom half, paleosol structures occur more distinctly than other station locations. These structures include blocky peds, columnar peds, reduced root traces and horizons, and reduction haloes. Changes in silt and clay material throughout the layered shales contribute to changes in layer structures, including pedogenic fractures (Sweet et al., 2013).

There are three dominant vertical vein strike sets recorded at Station 1 (NE/SW (Set 1), NW/SE (Set 2), N/S (Set 3)). Set 1 averages  $066/246^\circ$  with a standard deviation of  $18.4^\circ$ , Set 2 averages  $137/317^\circ$  with a standard deviation of  $21.6^\circ$ , and Set 3 averages  $179.6/359.6^\circ$  with a standard deviation of  $3.19^\circ$ . These sets are the accumulated orientations of the three layers discussed in detail in the next several paragraphs.

Station 1 was measured in terms of the shale layers with alternating fracture patterns and will be separated between the upper selenite, middle satin spar, and the lower selenite layers (Fig. 10). There were 672 fractures measured in total at this location (Appendix A). The lower section consists of multiple shale layers and will thus have the most recorded measurements. The reason for the lower shale consolidation is because of the indistinct and weathered nature of the shale slopes, making layer discrimination difficult to determine. The section column was measured along a roadcut and washout that displayed layering well but did not display a wide array of mineral veins.

In descending order, the topmost layer of red/ brown shales underlies the Medicine Lodge Gypsum (the basal layer of the Blaine Formation). This layer consists of silty, granular, and blocky shale and siltstone material (Fig. 10b). At the location of measurement this shale is

approximately two meters thick, although this varies throughout the area and seems to disappear completely away from this study zone. Selenite veins of variable size ranges occupy this space, 42 of which were recorded with eight measurements taken along a 15 m scanline. Vein sets within this layer strike in the NE/SW and NW/SE directions (Fig. 11a). Aperture measurements had an average of 13 mm and a range from 5-39 mm with lengths and heights being indeterminate (Fig. 11b). Average spacing between NW/SE sets were 0.5 fractures/m or 2.2 m between fractures and 0.7 fractures/m or 1.5 m between fractures for the NE/SW sets.

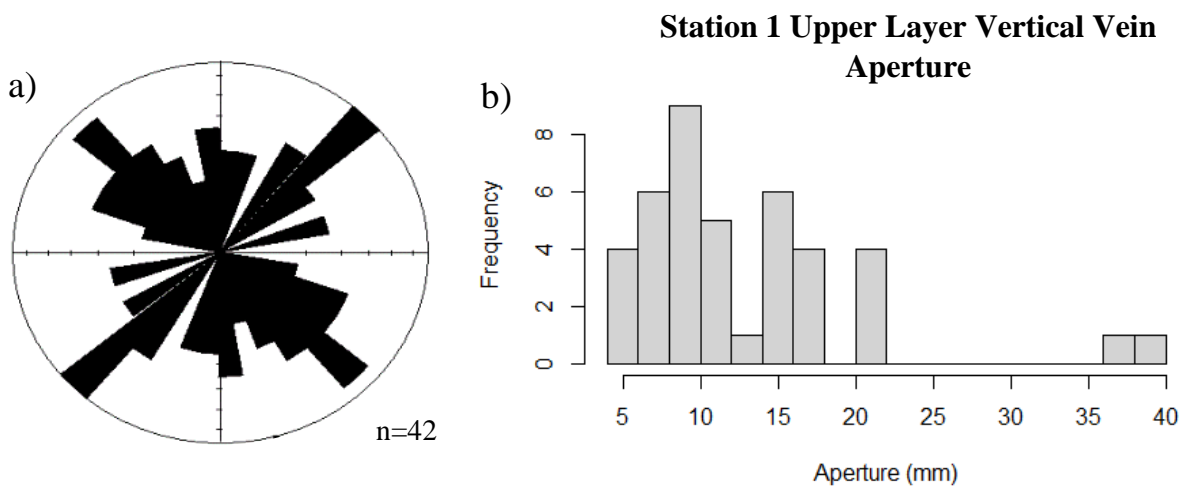


**Figure 11.** a) Rose diagram showing vertical vein strike in upper selenite layer of Flowerpot Shale. b) Histogram of aperture sizes of selenite veins in upper selenite layer.

Immediately underlying the upper selenite vein layer of the Flowerpot Shale is a thin green silty/shale layer rich in horizontal satin spar veins that separates the upper selenite veins from the middle satin spar veins. The middle satin spar-rich layer is a red-brown shale of more

massive-granular character than the surrounding layers and is approximately three meters thick (Fig. 12a). Veins in this layer are sub-horizontal with occasional subvertical orientations. This satin spar layer is continuous throughout large distances within the Flowerpot Shale, as observed through the various locations of this study and the observations of Wu (1969). There is no organized pattern of vein crosscutting and many appear to cut, abut, and splay into bifurcating networks.

At this location 160 mineral veins apertures were measured within a 15 m section. There were three vertical scanlines measured for 2.5 m each and two horizontal scanlines taken for 7.5 m each. Two areas within this section were also measured for areal density using a  $\frac{1}{2}$  m<sup>2</sup> grid. Sub-horizontal vein aperture sizes within this unit range from 0.9-14.05 mm and have an average of 5.6 mm (Fig. 12b). The sub-vertical aperture sizes range from 2.6-33.7 mm with an average of 10.8 mm.

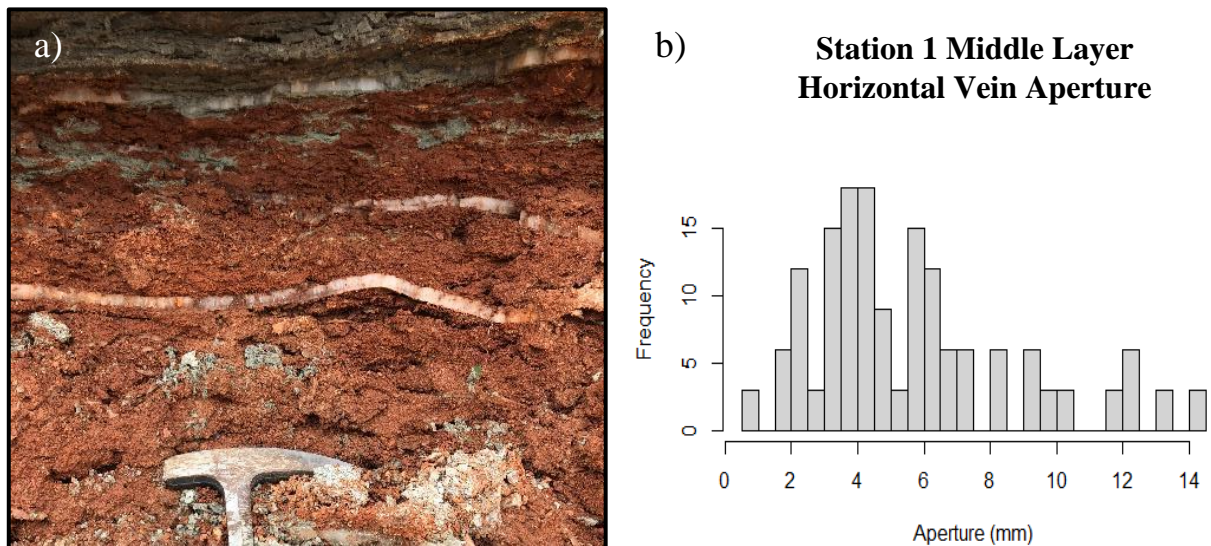


**Figure 12.** a) Sub-horizontal satin spar veins within massive, clay-rich layer of Station 1 Flowerpot Shale. b) Histogram showing sub-horizontal vein apertures in middle satin spar layer of Flowerpot Shale.

Density measurements for the veins averaged 18 fractures/ m<sup>2</sup>. The average spacing for the sub-horizontal veins using the measurements obtained from the three vertical scanlines was 23.3 fracture/m, while the average spacing for the sub-vertical veins was 2.2 fractures/m. Of the few vertical/sub-vertical veins measured, the dominant trends were oriented in the NW/SE and E/W directions.

The basal section of the measured section at Station 1 is approximately nine meters thick and is comprised of alternating layers of thick red/brown shales, thin layers of green/grey shales and gypsum nodules and concretions. The shales of this section range from a massive-blocky structure that is definitive of these basal rocks. Veining within this layer consists of glassy selenite that can be identified within the weathered shales by clear platy structures running through the dirt (Fig. 13a).

The behavior of the mineral veins is markedly diverse, with some exhibiting a curved orientation and some linear fracture sets of regular spacing. The aperture width is also highly variable, with sizes ranging from 0.8-153 mm and an average of 8.2 mm (Fig. 13b). While vein persistence was not measured outright due to the highly eroded and discontinuous structures, it was noted that of the many fractures that penetrated various shale beds, the highest frequency of non-bed bounded fractures were often the thickest and some could be traced for over 20 m. These would fall within the hierarchical patterns defined by Hooker et al. (2013), where bed boundedness is related to or dependent upon a specific characteristic of the fracture such as aperture, orientation, etc.

Most measured veins within the basal section were vertical to subvertical, with very few thin, sub-horizontal selenite veins being observed. Within this section, 470 fractures were measured for various characteristics with three scanlines being ran at 90, 30, 12 m lengths. The

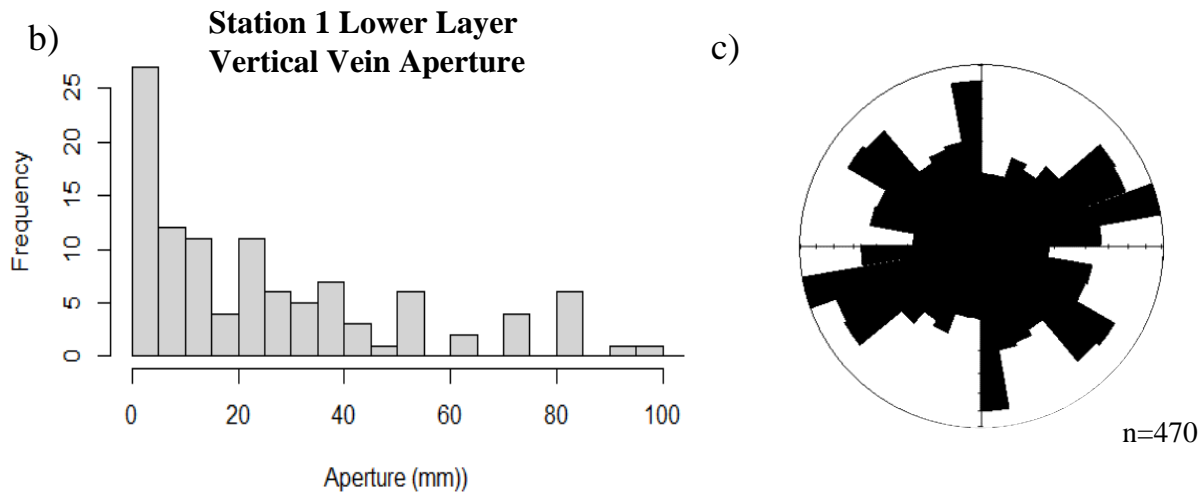


**Figure 13.** a) Thick (~150 mm) vertical selenite vein within lower shale layer. b) Histogram showing aperture sizes of selenite veins. c) Rose diagram showing vein strike of basal layer of measured section within the upper Flowerpot Shale.

dominant orientations of the fractures trended in the NE/SW, NW/SE, and N/S directions for all scanline and individually measured fractures (Fig. 13c). Within the fracture sets of the individual scanlines: Scanline 1 recorded an average vein aperture of 23.3, 18.3, and 17.4 mm and an average spacing of 5.9, 6.2, and 7.9 m/fracture for the NE/SW, NW/SE, and N/S sets, respectively. Scanline 2 recorded a set of NE/SW trending veins with an average aperture of 29.3 mm and an average spacing of 1.05 m/fracture. Scanline 3 recorded an average aperture of 28.5

and 13.6 mm with an average spacing of 3.14 and 3.23 m/fracture for NE/SW and NW/SE sets, respectively. Within the fracture sets of the individual scanlines: Scanline 1 recorded an average vein aperture of 23.3, 18.3, and 17.4 mm and an average spacing of 5.9, 6.2, and 7.9 m/fracture for the NE/SW, NW/SE, and N/S sets, respectively. Scanline 2 recorded a set of NE/SW trending veins with an average aperture of 29.3 mm and an average spacing of 1.05 m/fracture. Scanline 3 recorded an average aperture of 28.5 and 13.6 mm with an average spacing of 3.14 and 3.23 m/fracture for NE/SW and NW/SE sets, respectively.

## **Station 2 (Salt Creek Canyon)**

The fractures at Station 2 are unique to the area and to the other study locations. These are discontinuities within the mudstone that do not incorporate mineral precipitation and occur as open or (more often) closed fractures. Green reduction spots and fracture borders are present at this location. The green spots typically halo a darker organic-rich center (Wu, 1969), while the green fracture borders surround and may run the entire length of the breakage, likely due to microbial organisms having lived within the fracture space and reducing the surrounding rock (Fig. 14b).

There are occurrences of open fractures in the area which expel saline fluids, this occurs within ~E/W trending fractures and contributes to the white salt encrusted surface from which the canyon gets its name. At the headwaters of the canyon are springs consisting of fracture sets and steeply dipping bedding planes. Another prominent aspect of this location is the inconsistent bedding strike in localized areas, two of which were recorded during this study. In one area, beds dip westward at 5° and then reverse dip direction to 8° eastward within a 25 m span along the

creek bed. The other area presents vertical or steeply dipping beds oriented at 90° towards one another. These features may be the result of unknown deltaic processes or, more likely, collapse features attributable to upper Cimarron Salts underlying the Chickasaw Formation.

At station 2, there were 132 recorded fractures (Appendix A) with nine scanlines that ranged from 1.5-18 m in length. The strike of the joints at Station 2 averaged 062/242° (ENE/WSW) with a standard deviation of 17.2° within Set 1 and in Set 2 averages were 129/309° (ESE/WNW) with a standard deviation of 19.2 (Fig. 14d). Fracture persistence was measured with overall lengths ranging from 30 cm - 46 m and an average of 6 m (Fig. 14e). Within the nine scanlines, the average spacing was 1.0 and 1.2 m/fracture for the ENE/WSW (Set 1) and ESE/WNW (Set 2) fracture sets, respectively. Average lengths for Set 1 joints were 5.4 m and ranged from 3 cm – 18 m. Average lengths for Set 2 joints were 3.6 m and ranged from 60 cm - 30 m.



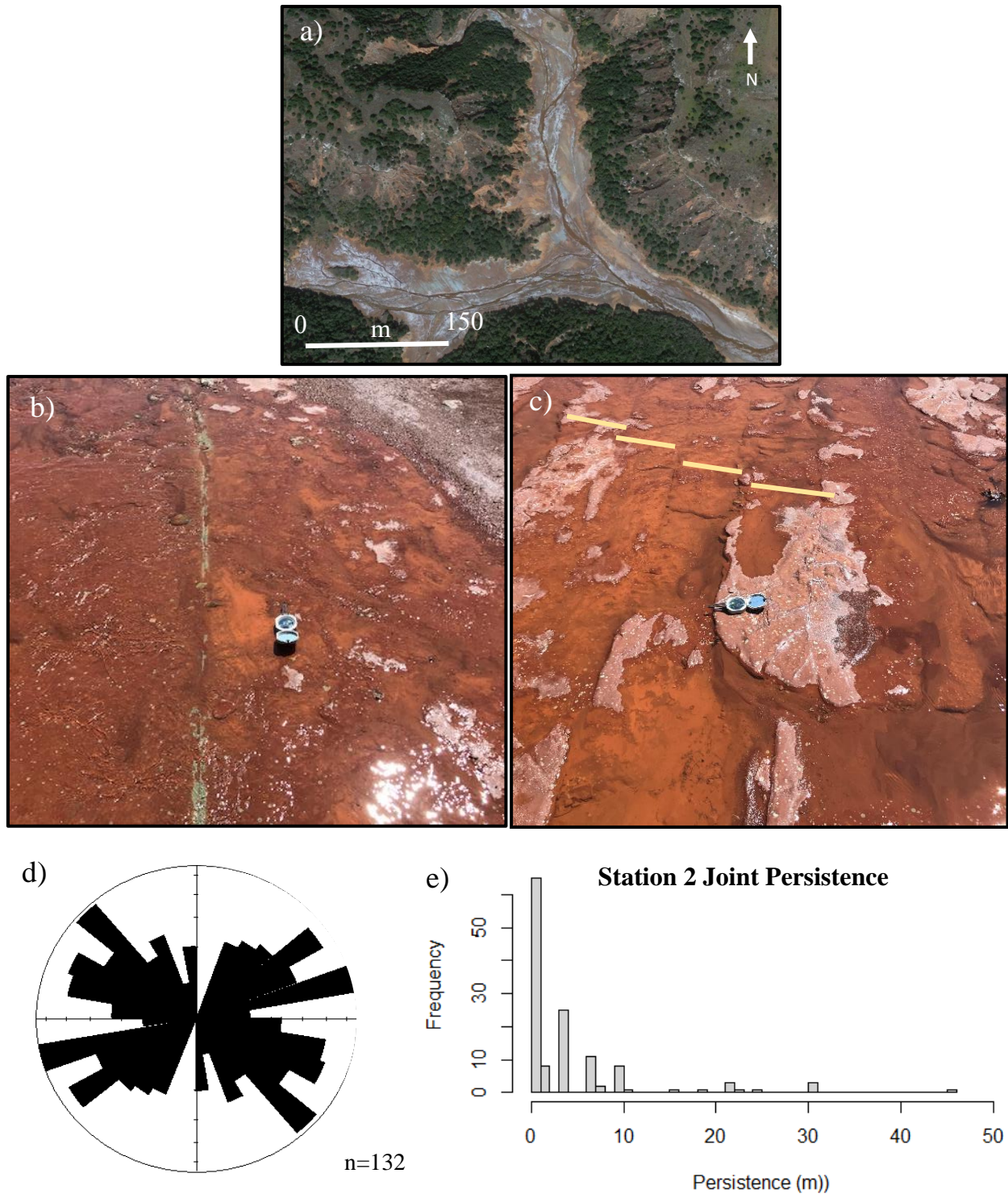


**Figure 14.** a) Satellite imagery of Salt Creek Canyon. b) Fracture with reduced zone due to organic reduction along fracture border. c) Regularly spaced fracture sets in mudstones. d) Rose diagram showing fracture orientations in Chickasaw Formation of Salt Creek Canyon. e) Histogram showing Station 2 fracture persistence frequency distributions.

### **Stations 3 & 4 (Gloss Mountain State Park and parts of Woods County)**

Stations 3 and 4 were grouped together because of extremely similar and simple characteristics. They are separated by approximately 10-15 miles along the Blaine Escarpment within Major County, northwest of Fairview, OK. The Medicine Lodge Gypsum grows quite thick in these northern locations and is underlain by the thick red/brown and thin green/grey shales of the Flowerpot Shale. The structure of the rock ranges from massive to granular, although not as distinctly granular or blocky as the shales of Station 1. The pedogenic features such as root traces and columnar peds were not observed throughout these study areas, nor did they appear in previous literary works, although the green/grey shale horizons have been attributed to organic reduction and paleosol formation (e.g., Fay, 1964; Wu, 1969; Sweet et al., 2013). The veins occurring within this shale occur in the uppermost section of the Flowerpot Shale; the upper 3.6 m of Station 3 and the upper 4.8 m of Station 4. Veins are dominantly sub-horizontal satin spar with occasional selenite (Fig. 15a, 15b). The satin spar is white to yellowish with fibers normal to fracture walls and no evidence of slippage during precipitation. These veins are similar to the Station 1 satin spar layer underlying the base of the Blaine Formation and likely represent a continuous network. The shales underlying this dense network are almost completely devoid of mineral veins.

At both stations, areal and scanline measurements were taken along with aperture recordings on various escarpment faces and mesas. Of the three areal grid measurements taken at Station 3, average vein density was recorded at 16 fractures/m<sup>2</sup>. At Station 4 the average vein density was 12 fractures/m<sup>2</sup>. Three vertical scanline measurements at 2.5 m lengths were also taken at each location. Average sub-horizontal vein spacing for Station 3 measured at 10.3

fractures/m and at Station 4, 11.8 fractures/m. Average vein aperture measured 4.4 and 6.2 mm for Stations 3 and 4, respectively (Fig. 15c, 15d).

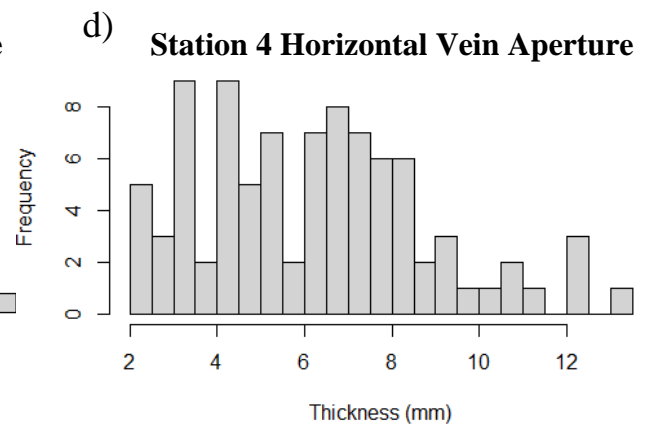
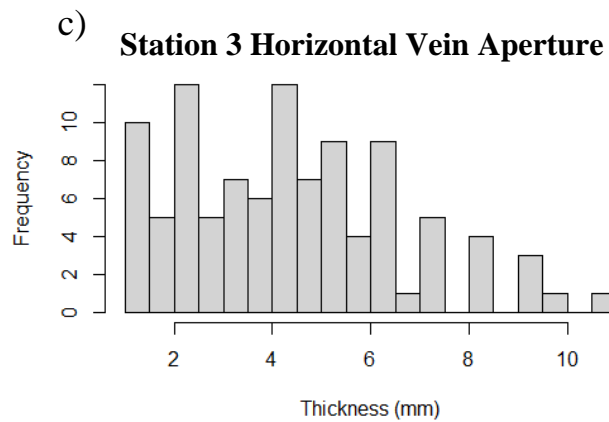


**Figure 15.** a) Sub-horizontal satin spar veins of Station 3. b) Sub-horizontal satin spar veins of Station 4. c) Histogram showing Station 3 aperture size distribution. d) Histogram showing Station 4 aperture size distribution.

## **Station 5 (Freedom, OK)**

Mineral veins outcropping at Station 5 display a contrast to previous locations. The Flowerpot Shales at this location underly a thick portion of the Medicine Lodge Gypsum of the Blaine Formation. They are once again of the thick red/brown and thin green/grey variety. These shales have no distinguishable structure and appear massive throughout the section, lacking any observable pedogenic features found in the southern stations (Stations 1, 2, 3, and 4). The dominant mineral veins of this location are satin spar, with little to no selenite being found. Thick sub-horizontal/bedding-parallel veins and gypsum-rich siltstone layers run between shale beds and are noticeably present upon changes from red/brown shale to green/grey shale.

The fibrous satin spar fill within the veins of Station 5 exhibits similar characteristics as the other locations, aside from the aperture, shear component of the fabric, and they occur at much greater depths from the Medicine Lodge Gypsum in the exposed shale section than other stations. These veins are both sub-vertical and sub-horizontal. They display antitaxial characteristics with medial scars that are approximately parallel to the fracture walls. Fibers at this location are white to yellowish with occasional grey, dark zones throughout. These darker vein fibers typically occur in or near the zones of the dark green/grey shales and likely incorporate the host material into the vein. Fiber width ranges from approximately 0.41 mm to 2.5 mm. These fibers constitute the thickest of any that have been observed within this study. Vein seams at this location tend to be more irregular than other observed locations, with much thicker or thinner variation in the upper or lower seams of the vein. Shear displacement within the growth fibers is a feature that is only observed at Station 5 (Fig. 16 a/b). The fibers appeared as sinusoidal, symmetric, or asymmetrical growths filling the fracture space. They occurred

within vertical veins to a small and inconsistent extent but were prominent and regular within the bedding-parallel veins them.

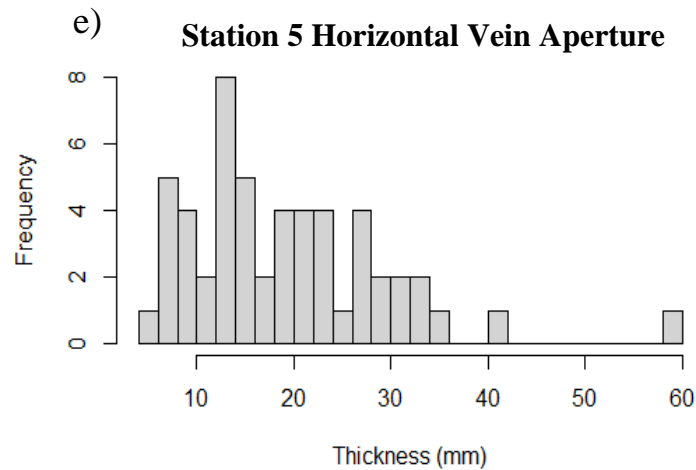
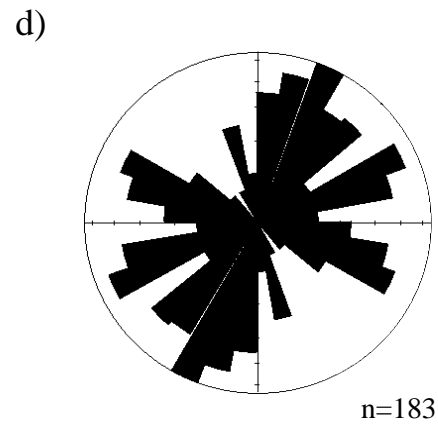
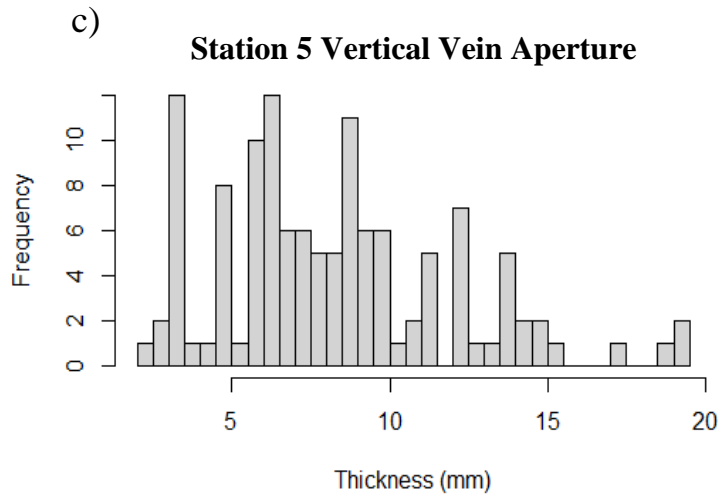
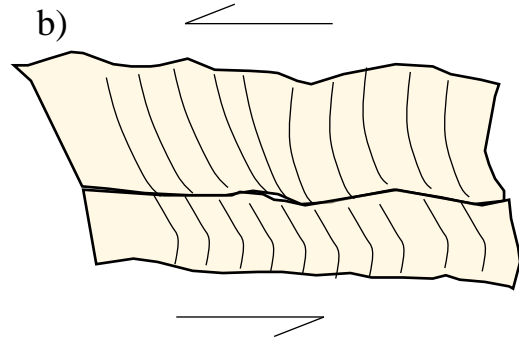


**Figure 16.** a/b) Common bedding-parallel antitaxial satin spar vein found at Station 5. Bent growth fibers indicate lateral shear movement in conjunction with fracture dilation and mineral precipitation. c) Histogram showing Station 5 vertical vein aperture distribution. d) Rose diagram showing vertical vein orientation distribution. e) Histogram showing horizontal vein aperture distribution.

Along the roadcut and along the riverside escarpment, there were 183 fractures measured with three horizontal scanlines running 30, 30, 18 m and three vertical scanlines running 4.5, 4.5, 13 m. Fracture aperture, orientation and spacing measurements were taken within these scanlines and along the hillsides. The three horizontal scanlines that measured vertical veining recorded average thicknesses of 8.2, 8.1, and 8.6 mm with a range of 2.1-19.1 mm and an average fracture spacing of 73, 78, and 71 cm/fracture. Combined these averages measure 8.4 mm aperture and 74 cm/fracture for the mostly bed-bound vertical veins (Fig. 16c). The three vertical scanlines which measured horizontal veining recorded average thicknesses of 17.5, 19.4, and 20.4 mm with a range of 3.64-58.97 mm and an average fracture spacing of 38, 35, and 44 cm/fracture (Fig. 16e). Combined these averages measure 19.06 mm aperture and 38 cm/fracture. There were three recorded vertical vein sets at Station 5 with strikes that trended heavily in the NNE/SSW (Set 1) and ENE/WSW (Set 2) directions with smaller trends in the NW/SE (Set 3) (Fig. 16d). Set 1 averaged  $023/203^{\circ}$  with a standard deviation of  $12.34^{\circ}$  and Set 2 averaged  $111/291^{\circ}$  with a standard deviation of  $8.35^{\circ}$ . The less dominant set of ENE/WSW (Set 3) trending veins averaged  $067/247^{\circ}$  and had a standard deviation of 9.65.

### **Station 6 (Big Salt Plains)**

Fracture/mineral vein natures change drastically in the short eight miles northwest from Station 5 to Station 6. This location takes place in the upper 20 m of the Flowerpot Shale, immediately underlying the Medicine Lodge Gypsum. The dominant, thick sub-horizontal satin spar veins with less thick and less dominant sub-vertical veining gives way to more dense, thin,

sub-vertical satin spar veins with regular spacing and no distinct signs of horizontal veining. Coloring is mostly whitish, yellowish, and dirty brownish. Fiber width is quite small and there are no indications of shear movement during or after dilation. Many of these veins appear to outcrop in a linear lateral fashion without penetrating far over or below the layer containing veins, likely indicating a bed-bounded pattern. This pattern is difficult to distinguish due to the highly weathered nature of these shales, which do not display anything other than a massive structure with no indication of paleosol conditions. Veins appear distinctly on the E/W sides on the small mesa that served as the study location, however, there are very few on the N/S faces, indicating an extremely dominant strike trend. This trend showed one distinguishable orientation to the NE/SW (Set 1) that averaged  $047/227^\circ$  with a standard deviation of  $33.23^\circ$  (Fig. 17a). Due to the scarcity of the vein outcrops, only two horizontal scanlines were taken at 8 m each, measuring 243 fractures in total. Aperture sizes along these scanlines ranged from 0.8-10.75 mm with an average of 4.4 mm (Fig. 17b). Spacing along these fractures was very regular and averaged 7 cm/fracture.

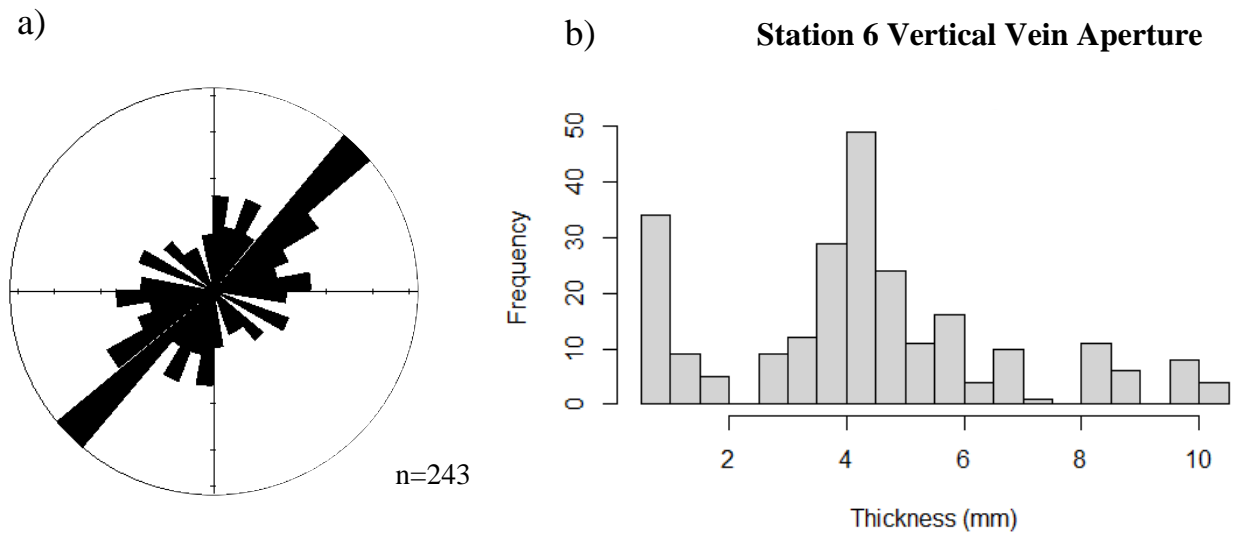


**Figure 17.** a) Rose diagram showing vein orientation distributions at Station 6. b) Histogram showing aperture size distribution.

## Results Summary

A complete summary of station results are as follows:

### Station 1

- Sub-vertical veining occurred dominantly as selenite while sub-horizontal veining occurred dominantly as satin spar.
- Aperture of sub-vertical veins had much greater average value and range than sub-horizontal veins.
  - Sub-vertical aperture averaged 8.2 mm with range of 0.8-153 mm.
  - Sub-horizontal aperture averaged 5.6 mm with a range of 2.6-33.7 mm.
- Vertical vein strike separated into three sets:
  - Set 1: NE/SW; avg. 066/246°; standard deviation of 18.4°.
  - Set 2: NW/SE; avg. 137/317°; standard deviation of 21.6°.
  - Set 3: N/S; avg. 179/359°; standard deviation of 3.19°.
- Shale structure found to be massive-granular in sub-horizontal satin spar vein zones and granular-blocky in sub-vertical selenite zones.
- Veins typically abut against NE/SW trending sets.
- Non-bed bound vertical veining.
- Proximal subsurface salt dissolution (~ 5 miles SE of Salt Creek Canyon).



## Station 2

- Closed opening mode joint sets with no mineral fill.
- Joint persistence averaged 6 m with a range of 0.15-46 m.
- Joints were separated into two sets:
  - Set 1: NE/SW; avg. 062/242°; standard deviation of 17.2°.
  - Set 2: NW/SE; avg. 129/309°; standard deviation of 19.2°.
- Joints hosted in mudstone conglomerates of the Chickasha Formation.
- Joints typically abut against NE/SW trending sets.
- Local subsurface salt dissolution of the Upper Cimarron Salt (Salt Creek Canyon).

## Stations 3 and 4

- Dominantly sub-horizontal satin spar veining.
- Sub-horizontal aperture of Station 3 averaged 4.4 mm with a range of 0.1-11 mm.
- Sub-horizontal aperture of Station 4 averaged 6.2 mm with a range of 2-13.5 mm.
- Average densities of Stations 3 and 4 are 16 and 12 fracture/m<sup>2</sup> respectively.
- Shale structure is massive-granular.
- No observed proximal sub-surface salt dissolution.

## Station 5

- Sub-vertical veining and sub-horizontal veining occur as satin spar.
- Aperture of sub-horizontal veins had much greater average value and range than sub-vertical veins.
  - Sub-vertical aperture averaged 7.96 mm with a range of 2.8-19.1 mm.
  - Sub-horizontal aperture averaged 19.06 mm with a range of 3.64-58.97 mm.
- Vertical vein strike separated into three sets:
  - Set 1: NNE/SSW; avg. 023/203°; standard deviation of 12.34°.
  - Set 2: ENE/WSW; avg. 111/291°; standard deviation of 8.35°.
  - Set 3: WNW/ESE; avg. 067/247°; standard deviation of 9.65°.
- Shale structure is massive-granular.
- Dominantly bed bound vertical veining.
- Shear fabrics within veins.
- Proximal subsurface salt dissolution (~ 3 miles SE of Big Salt Plains).

## Station 6

- Sub-vertical veining occurs as satin spar.
- Sub-vertical aperture averaged 4.3 mm with range of 0.8-10.2 mm.
- Vertical vein strike distinguished by one set:
  - Set 1: NE/SW; avg. 047/227°; standard deviation of 33.23°.
- Shale structure is massive-granular.
- Bed bound vertical veining.
- Proximal subsurface salt dissolution (Big Salt Plains)

## DISCUSSION

Fractures that occur at the six stations along the escarpment differ by location. These differences typically present themselves as variable vein or fracture characteristics. These characteristics will be analyzed in comparison with one another to gain a clearer understanding of how conditions are similar and how they are changing. Also, to gather insight into how and why fracturing occurred and its relationship to various locations and events throughout the escarpment and region.

### **Mineral Fill**

Variant mineral fills throughout the study region, even in the same section of rock, give indications of formation conditions. The most dominant fills within the region are selenite (the glassy form of gypsum identified by the platy, coarse-grained crystals (Fig. 18)) and satin spar (the fibrous form identified by thin radiating fibers within the mineral fill (Fig. 19)). Other vein filling material is present throughout the study, such as rock gypsum, but they are very low in frequency and only represent a fraction of the veins in the study.

### *Selenite*

Selenite veining occurs throughout the southern study regions but has immensely higher frequency and size distributions at Station 1 than in other locations. It also occurs within the upper Flowerpot Shale at Stations 3 and 4 with extremely low frequencies and thickness values.

It has been documented in core and logs from previous literature (e.g., Ward, 1961) in the Big Salt Plains region (Stations 5 and 6) but was not observed in this study.

Selenite formation, according to Mossop and Shearman (1973), results from a series of near-equilibrium hydration phases that enable slow, coarse grained crystal growth within porous or fractured rock. This slow growth of large and coarse crystals may indicate water levels with high salinity and low supersaturation with respect to gypsum (e.g., Peryt, 2001; Babel, 2004; Zaheri and Rafiei, 2020). The formation of this glassy form of gypsum is dependent upon stable growth conditions as well as the conditions mentioned above. These stable conditions are usually associated with depths greater than that of a fluctuating weathering profile (e.g., Maher et al., 2015; Rai et al., 2019). The arid climate of the deposition of this Permian sequence interpreted by Sweet et al. (2013) would allow for a relatively shallower weathering profile, assuming rock fracture took place during this climatic era.

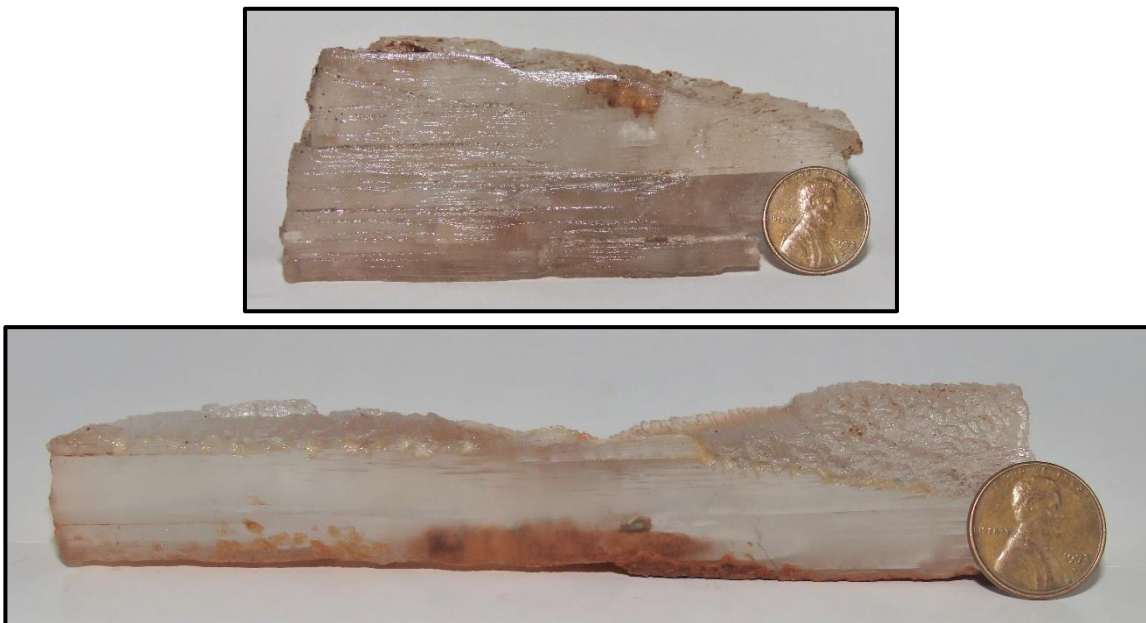


**Figure 18.** Two coarse grained selenite veins with linear, layered plating.

### *Satin Spar*

Satin spar, the fibrous form of gypsum, is found at every station location, although the orientation and frequency at which it occurs is highly variant (Fig. 19). At Stations 1, 3, and 4 this veining is dominantly sub-horizontal and found within the uppermost shales of the Flowerpot Shale, often directly underneath a layer of bedded or nodular gypsum.

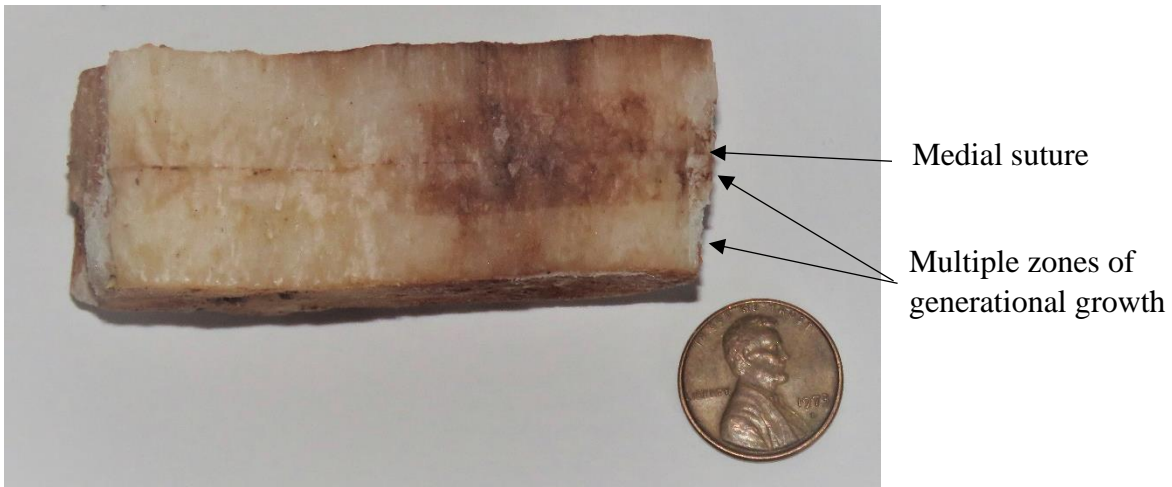


**Figure 19.** Fibrous satin spar vein showing multiple growth generations as identified through vein color variation zones radiating from medial suture.

Shear displacement within the growth fibers is only observed at Station 5. Due to weathering or various other circumstances, displacement of this nature was not observable or did not occur at other stations. It is obvious from the regular slip indicators of the bedding-parallel veins and the bed-bound nature of the vertical veins at Station 5 that the greatest slippage occurred predominantly along horizontal bedding planes. The bedding plane movement likely attributed to failure and fracture throughout the shale bed, producing vertical and bed bound veins that were themselves moving slightly as gypsum precipitated within them.

There are multiple works and interpreted causes of fibrous satin spar formation. Driving forces for the causation of satin spar have included mechanical forces through gypsum crystallization (e.g., Bundy, 1956), hydraulic fracture related to overpressure (e.g., Shearman et al., 1972), tectonically derived tensile forces (e.g., Machel, 1985; Cosgrove, 2001), and subsurface salt dissolution resulting in collapse (e.g., Gustavson et al., 1994). Fibrous natures have been linked to crystal growth rate that occurs at or near the same rate as fracture dilation (e.g., Machel, 1985; El Tabkh et al., 1998). This link between fibrous growth with dilation and glassy growth within pre-fractured rock likely accounts for the diverse vein arrays and transitions found at Station 1.

According to Machel (1985), hyper-concentrated waters in high volumes are necessary to create dense satin spar fibers. This supports the theory that the dense networks found in the upper Flowerpot Shales that immediately underly the Medicine Lodge Gypsum originated from the initial brine or resulted from dissolving Medicine Lodge Gypsum within the phreatic zone.

Extension oriented perpendicular to bedding and localized slumping of strata are considered to be dominant controls on satin spar orientation and development which are related to pervasive halite volume loss through dissolution in the presence of large volumes of freshwater (Gindre-Chanu, 2015). This case is evident at Stations 5 and 6 where the only observed accounts of high frequency vertical fracture have been filled with satin spar, subsurface salt dissolution is occurring, and local slumping has been recorded and observed (Johnson, 2019).

Ultimately, selenite and satin spar form under differing conditions within these shales. The formation of satin spar is linked to dynamic conditions and super-saturated fluids, while the formation of selenite is linked to stable conditions and fluids with a low  $\text{CaSO}_4$  saturation

(Machel, 1985; Peryt, 2001). These characteristics show a change of formational conditions from the northern to the southern escarpment even though both fracture zones show proximal salt dissolution. The reason for this variability may be from differing salinities or saturations of formation fluids (resulting from variable brine saturation or proximity from weathering gypsum beds), differing magnitudes of deformation, and the variable mechanical properties of the shale host.

### **Vertical/Sub-Vertical Fracture Orientation**

Fracture strikes trend in similar directions throughout the station locations. With degrees of variation in observed sets at Station 1, dominant orientations trend in NE/SW and NW/SE directions. This is true for the non or less-bed bounded selenite veins of Station 1, the joints and closed fractures of Station 2, and the bed bounded satin spar veins of Stations 5 and 6. The NE/SW orientations are akin to observed subsurface faulting that is prominent throughout the study region, where past and recent seismic activity has been recorded (Qin et al., 2019).

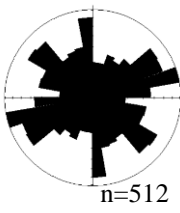
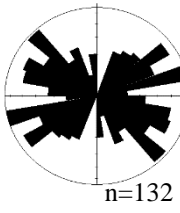
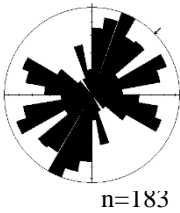
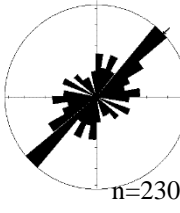
The sets of these regions are very similar despite Station 1 measurements recording veins within the Flowerpot Shale and Station 2 measurements recording joints within the Chickasaw mud rocks. The NE/SW sets of both these locations are within 4° of each other and the NW/SE sets are within 12° of each other.

These sets, especially the NE/SW set, display such a nearness in value and location that the formational stress should be concluded to be relational. This is further solidified when applying aperture and persistence values to fracture and vein orientations, as is done in the next

section. Stations 3 and 4 are excluded from this vertical fracture orientation section as a result of no significant vertical/sub-vertical veining.

The similarity in the strike orientation of Stations 5 and 6, as well as the bed-bounded nature of the vertical veins, displays a high likelihood that the causal stress which formed these filled fractures is related. The sets of these two locations have very dominant NE/SW directional trends once again, although they differ from the southern station by having a more north-striking attitude.

**Table 2.** Vertical fracture orientation trends by station.

Station 1	Station 2	Station 3	Station 4	Station 5	Station 6
		N/A	N/A		

The fracture orientations of this study can be compared to the fractures and lineations of previous studies done by Collins et al. (1974), Guo and George (1999), and Gauvey (2019). The linear features of the two lineation studies (Collins et al., 1974; Guo and George, 1999) were attributed to subsurface fault reactivation influencing the surface features of the region. The faults in this study region, as described in previous sections, have a dominant NE/SW strike pattern within the strike/slip regime (Marsh and Holland, 2016). Cavern systems throughout the Blaine Formation gypsum with linear passageways were recorded to trend in NE/SW and NW/SE directions by Gauvey (2019) and were found to follow joints in the Flowerpot Shale and Blaine Formation. This regional trend in both surface and subsurface conditions and in past



studies of relation to this research indicates a related stress that causes or influences the features found in the area. From the strike orientations of subsurface faulting in relation to surface deformational features, a strong causal relationship between the features is inferred.

### **Aperture/Persistence**

Fracture and vein size is measured in various ways. In this study the aperture sizes were collected at all stations except for Station 2, where rock jointing was measured in relation to persistence (or length). Density plots of aperture and persistence by set are shown below (Fig. 20 and 21). These are essentially smooth histograms that display continuous distributions of aperture and persistence values by set strike direction with the area under each curve of the graphed data adding to 1. This allows concentrated values to be identified by set.

Aperture is variable dependent upon all present vein characteristics, including azimuthal orientation, vertical or horizontal orientation, mineral fill, and location. 856 vein aperture measurements were taken along the various station locations. To simplify the results, the sequence of analysis will begin with the continuous layer of sub-horizontal satin spar veining located in the uppermost portions of the upper Flowerpot Shale, next will be the sub-horizontal/bedding parallel satin spar veins of Station 5, and, following these subjects, an analysis of the vertical vein aperture will be examined by station.

Beginning with the layer of continuous, thin, sub-horizontal satin spar vein-rich layer of the upper Flowerpot Shale. The aperture average and range of these veins varies by location. At Station 1, in a bed of massive, silty shales that is approximately 3 m thick, vein apertures average 5.6 mm. At Station 3, in a similar bed approximately 3.6 m thick, vein apertures average 4.4 mm. Finally, at Station 4, in another similar bed that is approximately 4.8 m thick, vein apertures average 6.2 mm. While there does not seem to be a relationship between bed thickness and average

aperture size, this may be because the beds and apertures are so similar that an appreciable trend cannot be distinguished in the available data. The distinct trends within the collected data show a relationship between bed thickness and average fracture density, and a small relationship between aperture and location. As the beds of this specific fracture layer thicken to the northwest, fracture density slightly decreases and aperture slightly increases (Fig. 20). Station comparisons between this layer of sub-horizontal satin spar confined to the uppermost sections of the Flowerpot Shale can be found in Table 3. This trend aligns with several studies that have observed correlations between increasing bed thickness and decreasing fracture densities (e.g., Ladeira and Price, 1981; Nelson and Sierra, 1993; Underwood et al., 2003), although this is not always the case. In relatively undeformed rocks, the mechanical properties of the stratigraphy will most often control the density and height of opening mode fractures ( Underwood et al., 2003). In the case of this shale layer within the Flowerpot Shale, the massive and structureless character of the rock results in fractures very different than the surrounding units.

The sub-horizontal/ bedding-parallel satin spar veins of Station 5 have much thicker aperture sizes and are continuous vertically throughout the entire section of exposed shale, not just the upper regions. As detailed in the previous section of this work, the average aperture of these features was 19.06 mm with a range from 3.64 to 58.97 mm. This included many of the thickest veins that were located at indistinct but somewhat interpretable bed boundaries and the thinner veins located within these beds.

In Table 4 the veins are described by their set orientation, to develop an idea of the relationship between vein thickness and its directional strike. These numbers are generated from scanline measurements at Stations 1, 5, and 6 with fracture sets accounting for average strike

orientation  $\pm 1$  standard deviation at the location. Bed thickness was not measured for these fractures because of indistinct bedding layers that could result in inaccurate analysis.

### Upper Flowerpot Shale Satin Spar Unit Aperture

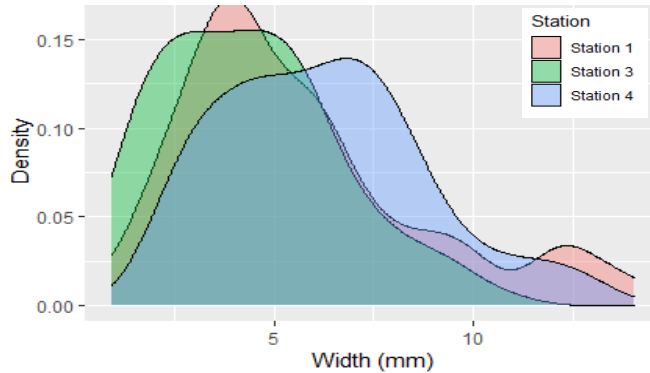


**Figure 20.** Density graph showing aperture of satin spar unit found continuously in uppermost Flowerpot Shale.

Station 1 shows a maximum average aperture within the Set 1 veins of 32.7 mm and a minimum in the Set 3 veins of 18.6 mm. Set 1 also displays the greatest range (1-153 mm) and largest maximum (153 mm). Set 2 displays a range of 0.8-84 mm with an average of 25 mm. Set 3 displays the smallest range (1-54 mm) (Fig. 21a). As fracture strike dominance decreases from Set 1 to Set 3, so too does the average spacing. Set 1 has an average spacing of 0.33 fractures/m while Set 3 has a spacing of 0.13 fractures/m (Table 4). This shows a decreasing relational trend between vein aperture, orientation, and spacing from the NE/SW veins of Set 1, to the NW/SE veins of Set 2, and finally to the N/S veins of Set 3.

Station 5 shows a maximum average aperture within the Set 2 veins of 8.7 mm and minimum average of 7.1 mm in the Set 1 veins (Table 4). The greatest range is seen in the Set 3 veins of 2.8-19.1 mm, which includes both the maximum and minimum aperture measurements along these scanlines (Fig. 21b). Despite showing the largest average aperture reading, Set 2 has the lowest spacing measurements at 0.23 fractures/m, compared to the greatest spacing frequency

of Set 1 at 0.72 fractures/m. Station 6 has the most regular fracture aperture with an average of 4.3 mm and a range of 0.8-10.2 mm. Spacing at this location measured 14.8 fractures/m. The veins of Station 6 show a much lower average aperture than the other sub-vertical vein locations but a much higher frequency (Table 4).

Comparing these three locations, it can be seen that there is a relationship between vein thickness, orientation, and spacing. The most dominant vein strikes trended in the NE/SW directions. These strike sets were also responsible for the greatest average aperture size, with varying degrees of offset. At Station 1, the aperture measurements were larger than anywhere else for all sets and the set spacing decreased along with the decrease in size. This case was the opposite at Station 5, where the set spacing increased with a decrease in aperture size. The average aperture measurements of Station 5 are very similar in value, however, and may be attributable to error. Considering the relationship between aperture, spacing, and orientation, the NE/SW trending sets of these locations favor a causal stress that trended in the same direction. This is also the case for Station 2 and the joints measured in relation to persistence rather than aperture.

The joints and fractures of Station 2 are separated into two sets; Set 1(NE/SW) and Set 2 (NW/SE). Fracture set measurements account for average orientation  $\pm 1$  standard deviation (Table 5). The greatest average length (5.4 m) and range (15 cm – 46 m) is found in the Set 1 fractures (Fig. 21c). Despite being relatively close in value, the fractures of Set 2 have a higher frequency with a spacing of 12.8 fractures/m. The joints of this location display relatable characteristics to the veins of the other study locations, especially its close neighbor, Station 1. The data implies a correlation between persistence, aperture, and orientation with relationships between dominant strike trends and the actual thickness of a vein and length of a fracture.

**Table 3.** Upper layer satin spar veining aperture and spacing for Stations 1, 3, and 4.

<b>Station</b>	<b>Avg. Aperture (mm)</b>	<b>Min. Aperture (mm)</b>	<b>Max. Aperture (mm)</b>	<b>Avg. Density (fracture/m<sup>2</sup>)</b>	<b>Avg. Spacing (fracture/m)</b>	<b>Bed Thickness (m)</b>
<u>Station 1</u>	5.6	0.9	14.05	18	23.3	3
<u>Station 3</u>	4.4	1.1	10.8	16	10.8	3.7
<u>Station 4</u>	6.2	2.4	13.1	12	20.3	4.8

**Table 4.** Sub-vertical veining aperture and spacing for Stations 1, 5, and 6.

<b>Station</b>	<b>Avg. Aperture by Set (mm)</b>	<b>Aperture Range by Set (mm)</b>	<b>Avg. Spacing by Set (fracture/m)</b>	<b>Avg. Total Aperture (mm)</b>	<b>Aperture Total Range (mm)</b>
<u>Station 1</u>				8.2	0.8-153
<i>Set 1</i>	32.7	1-153	0.33		
<i>Set 2</i>	25	0.8-84	0.2		
<i>Set 3</i>	18.6	1-54	0.13		
<u>Station 5</u>				7.96	2.8-19.1
<i>Set 1</i>	7.1	3.3-12.4	0.72		
<i>Set 2</i>	8.7	5.4-17.2	0.23		
<i>Set 3</i>	8.5	2.8-19.1	0.62		
<u>Station 6</u>				4.4	0.8-10.2
<i>Set 1</i>	4.3	0.8-10.2	14.76		

Scanline observations with station sets as ordered:

Station 1 (Set 1=NE/SW, Set 2=NW/SE, Set 3=N/S), Station 5 (Set 1=NNE/SSW, Set 2=ENE/WSW, Set 3=ESE/WNW), Station 6 (Set 1=NE/SE)

**Table 5.** Station 2 joint persistence and spacing.

<b>Station</b>	<b>Avg. Length by Set (m)</b>	<b>Length Range by Set (m)</b>	<b>Avg. Spacing by Set (fracture/m)</b>	<b>Avg. Total Length (m)</b>	<b>Length Total Range (m)</b>
<u>Station2</u>				6	0.15-46
<i>Set 1</i>	5.4	0.15-46	10.5		
<i>Set 2</i>	2.8	0.6-21	12.8		

Set 1=NE/SW, Set 2=NW/SE

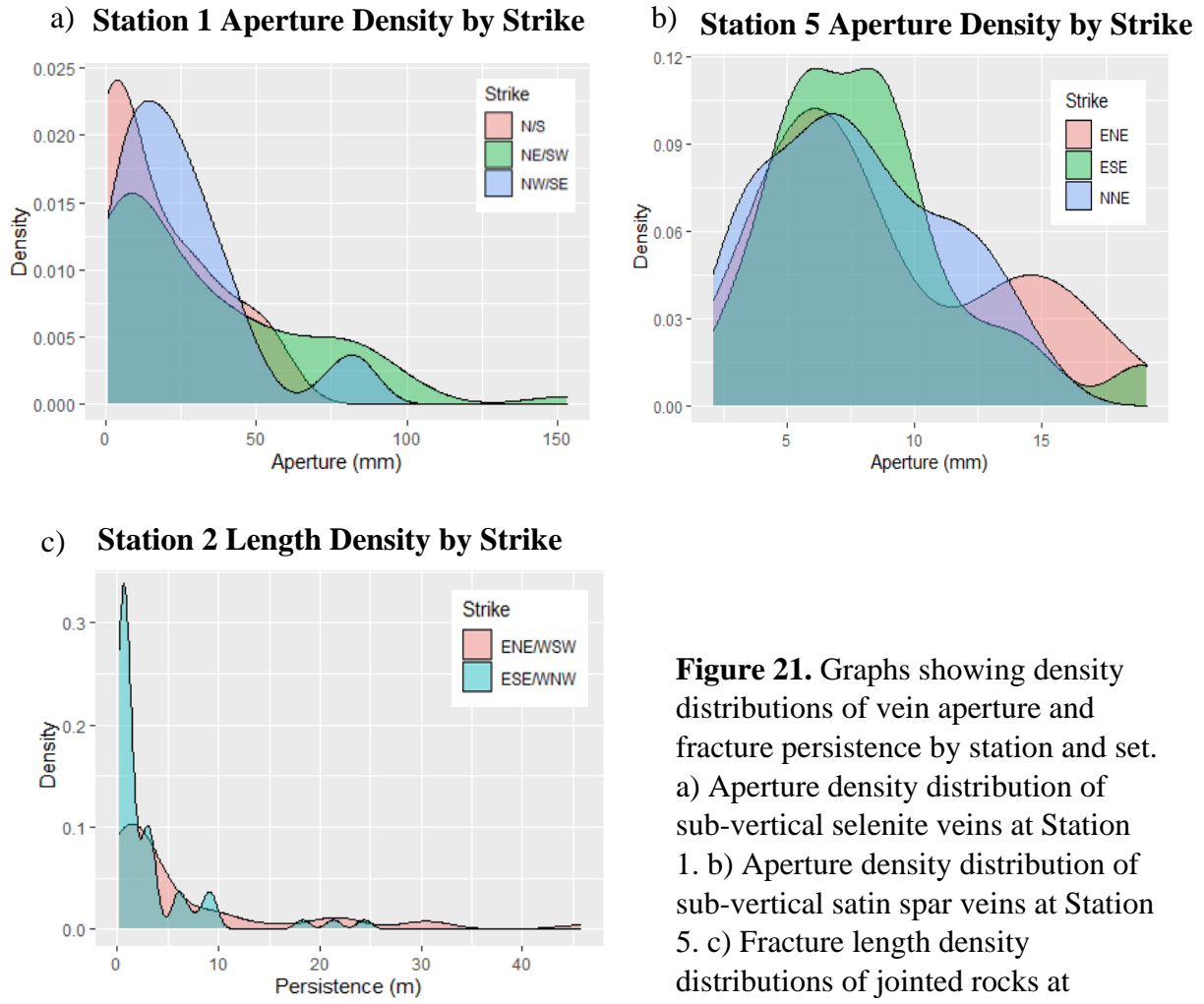


**Figure 21.** Graphs showing density distributions of vein aperture and fracture persistence by station and set. a) Aperture density distribution of sub-vertical selenite veins at Station 1. b) Aperture density distribution of sub-vertical satin spar veins at Station 5. c) Fracture length density distributions of jointed rocks at Station 2.

## Fracture Interactions

Fractures interact with each other in various ways within the Flowerpot Shales and Chickasaw Formation. There are many instances of isolated veins that occur without any observable contact with other veins as well as many vein interactions that have abutting and crosscutting relationships. Although it was difficult to get a distinctly clear idea of the vein relationships within the Flowerpot Shale, the veins that did interact were recorded and graphed.

The locations at which these events were best recorded are the areas that a plan-view of the fractures could be obtained, namely Stations 1 and 2. The other stations were analyzed upon the interactions between sub-horizontal fracture interactions and sub-vertical/sub-horizontal relationships.

Abutting fractures of Station 1 on the surface in plan-view display variable angles of connectivity, making both Y and T-shaped nodes (Fig. 22). The overall numbers calculated from the observations of which veins terminated against another, regardless of node type, can be seen in the density plots of Figure 23. These show a bimodal distribution between dominant vein strikes and whether they terminate against another vein or whether they have a vein terminate against them.

For the Set 1 (NE/SW) fractures of Station 1, these have more fractures terminating upon contact with them than them terminating upon contact with other fractures (Fig. 23a). For the Set 2 (NW/SE) fractures, there is a less defined relationship but a slightly more dominant trend in veins terminating against others. What this means is that the Set 1 fractures have a higher density of veins terminating against them than other sets. This is evidence of Set 1 fractures forming from an earlier deformational event or developing synchronously. This stems from many fractures of Set 2 having other fracture sets terminating upon contact with them as well as many observations of crosscutting occurring.

Vertical veining at Station 1 shales shows abutting, crosscutting, aperture change, and splaying interactions in both its relationship to other veins and changes in bedding. Upon encountering different bedding material, the veins will often terminate at or a short way into the different bed, they may run through the bed but change character (thickness or orientation), or they may splay through low angle bifurcation (Fig. 24).

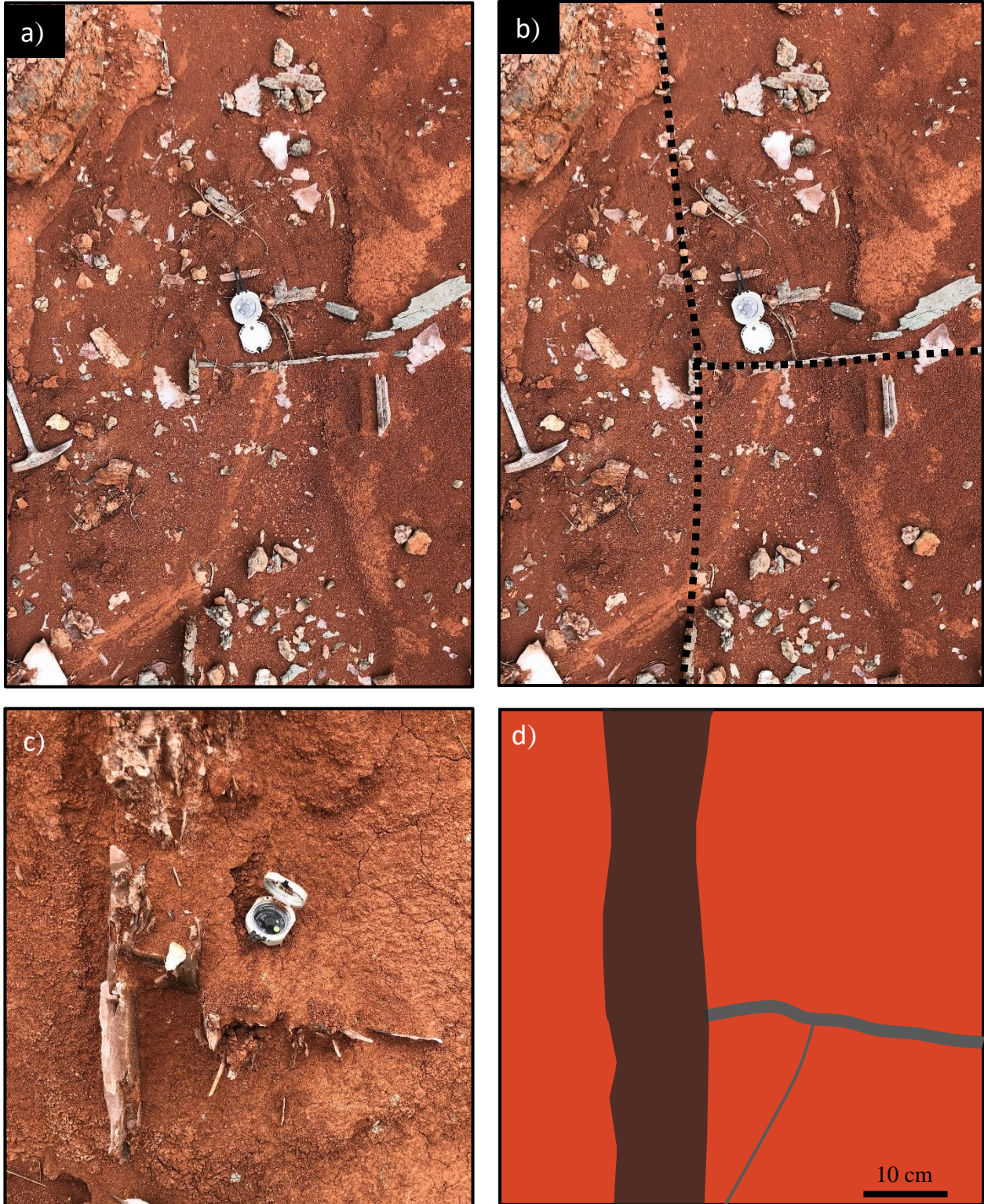


**Figure 22.** a/b) Vertical selenite veins of Station 1 intersecting at T-node with NE vein cutting NW vein. c/d) Thick (~120 mm) NE trending vertical selenite vein of Station 1 with NW vein abutting against it in T-node orientation.



Veins interact in variable ways at Station 1 in cross section view as well. Within the satin spar layer of the upper Flowerpot Shale at Stations 1, 3, and 4 there many interactions going on. There are observations of splaying, abutting, and crosscutting. This occurs between sub-horizontal veins, other sub-horizontal veins, and sub-vertical veins. This is the case throughout the continuous layers of satin spar near the base of the Blaine Formation gypsum, although significantly less vertical/sub-vertical veining occurs within this layer at the other locations outside of Station 1.

At Station 2 the joints within the mudstone display the same interactions as Station 1 apart from fracture splay. These fractures were only studied in plan-view with no cross-sectional outcrops occurring. The density distribution of these joints in comparison to Station 1 is slightly different. It still shows a bimodal distribution with Set 1 (NE/SW) and Set 2 (NW/SE) fractures being the dominant fracture upon which others terminate against (Fig. 23b). It also shows the more NNW/SSE fractures terminating against the main sets.

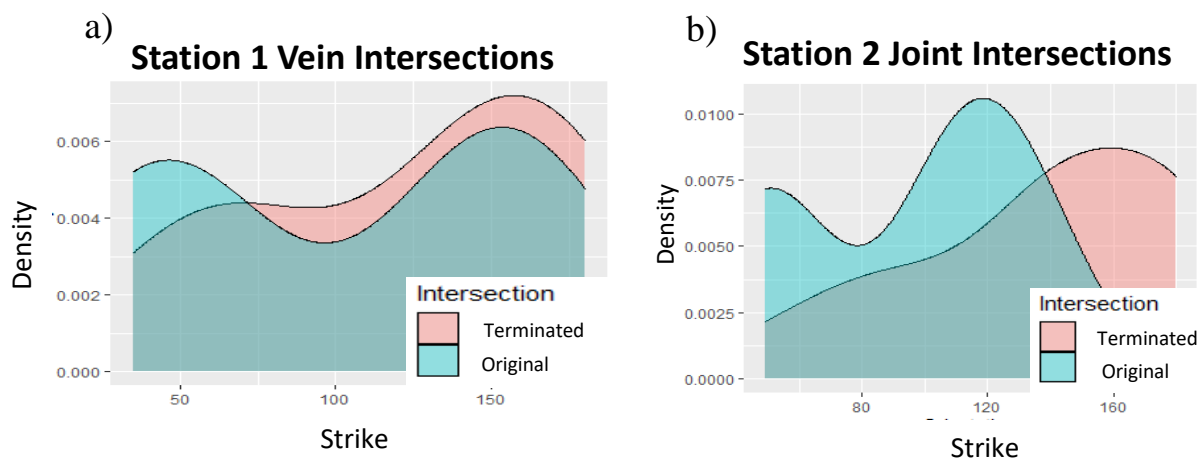


**Figure 23.** Density plots showing distributions of terminating and terminated against (original) veins and joints for both Station 1 (a) and Station 2 (b). Both show the vein terminations distributed by strike orientation. For both locations, the most common event is NE/SE and NW/SE trending fractures cutting and arresting NW/SE and NNW/SSE fractures.

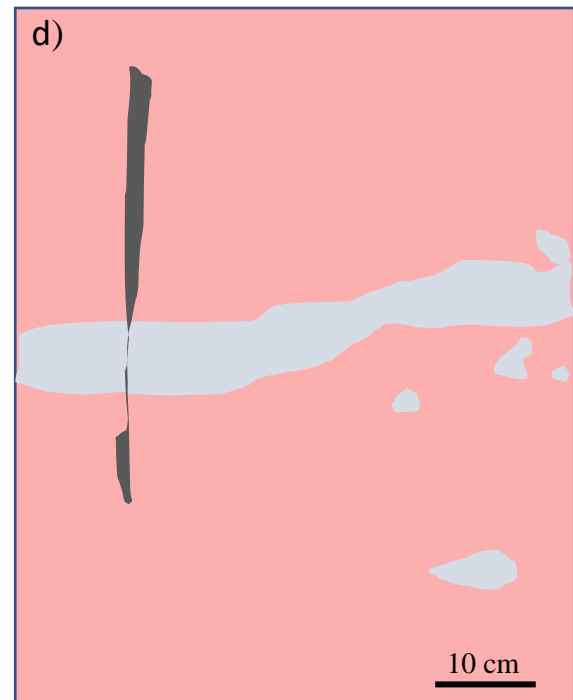
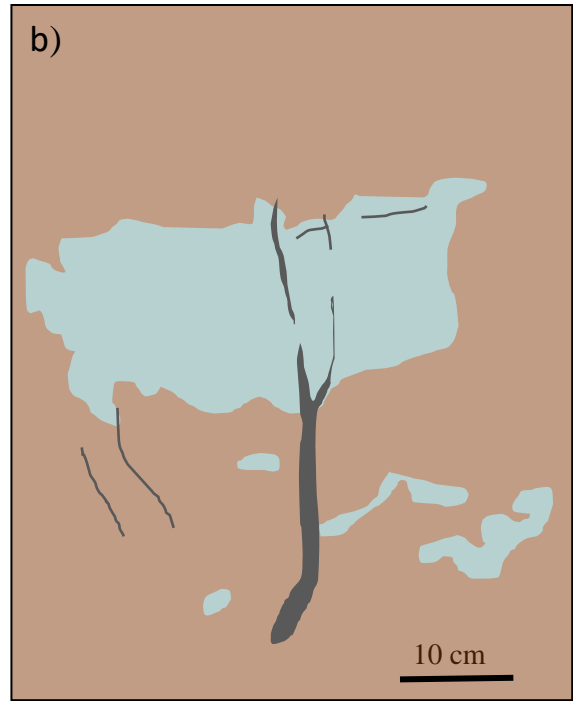


**Figure 24.** a/b) Gypsum vein bifurcating upon contact with gypsum nodule at Station 1. c/d) Gypsum vein thinning upon encountering a gypic unit and thickening past it.

The veins of Station 5 were only studied in cross-section view. They show many crosscutting and abutting relationships between sub-vertical and sub-horizontal veins, however, upon encountering the thick bedding-parallel veins or gypsum-rich layers, the sub-vertical veins typically terminate at the contact. This is discussed further in the next section.

### **Bed-bounded Fractures**

The bounded nature of a network of fractures or veins can show where stresses resulting in rock failure may have originated from. Fracture systems that are bed-bound and contained within fine-grained rocks have been attributed to diagenetic-related process such as volume change and compaction (e.g., Laubach et al., 2010; Maher and Shuster, 2012; Maher et al., 2015). Fracture systems that continue through host rock layers, hindered or not, are typically attributed to events aside from diagenesis, such as tectonic or slope stresses. The reason is that diagenetically driven fracturing will affect differing rock layers and materials in different ways, and the fractures are not expected to propagate in the same manner through multiple and variable layers. Many of the study locations exhibit bed-boundedness to some degree, with the most prominent examples of bed-bound vertical veining being in the northern regions, and the horizontal veining boundness occurring throughout the escarpment.

Selenite veins at Station 1 are of a hierarchical or unbounded nature, as according to Hooker et al. (2013). Many examples of veins cutting through bed boundaries were documented (Fig. 25 a/b), these typically being thicker and less weatherable selenite plates or rock gypsum. Alongside the few roadcuts or washouts that exposed the shale layering, many veins were arrested at or soon after encountering a composition change in the host material. Very large

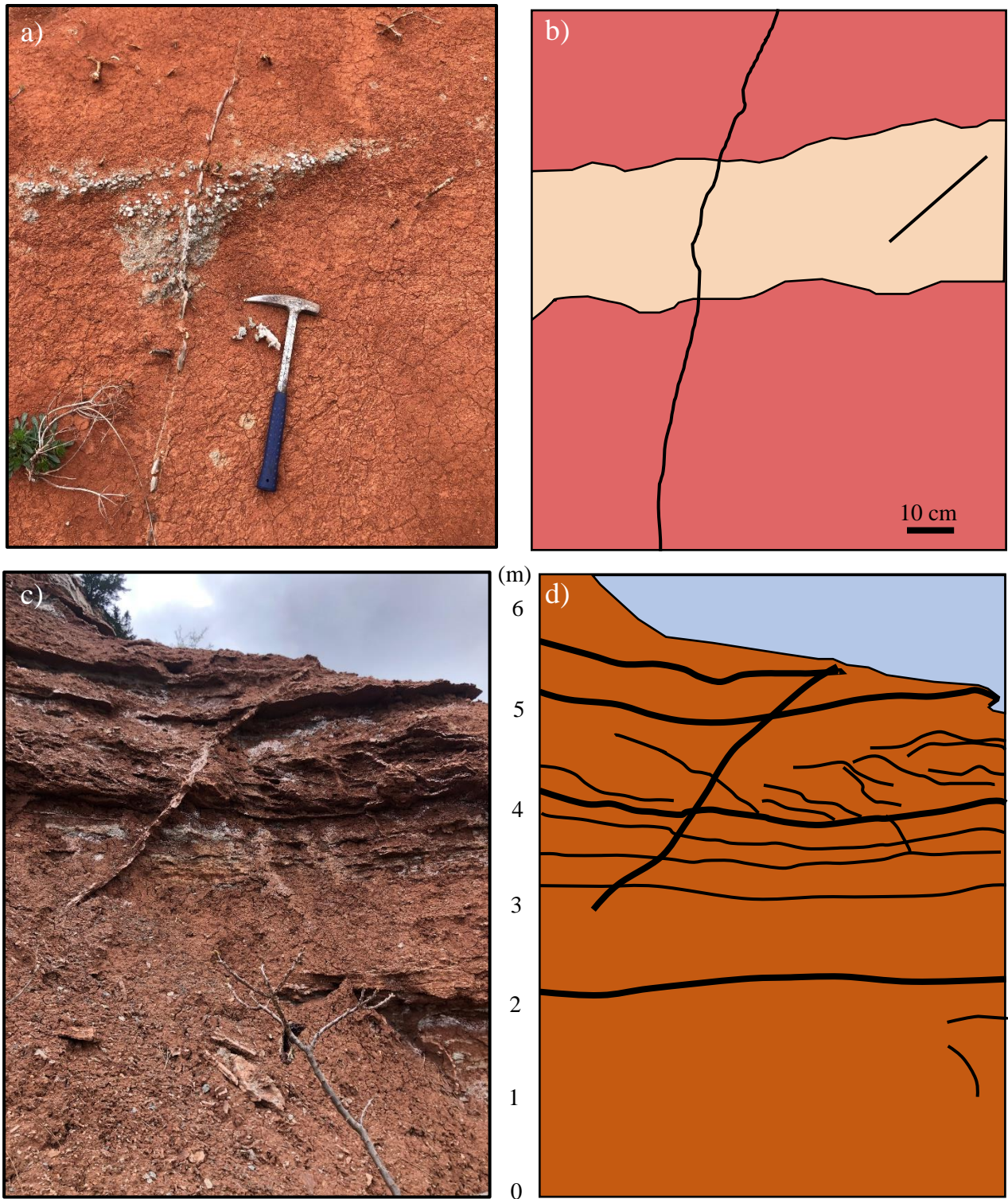


**Figure 25.** a/b) Non-bed bound, vertical selenite vein crosscutting through nodular gypsum layer at Station 1. c/d) Non-bed bound satin spar vein crosscutting multiple shale and vein layers at Station 5.

aperture veins were the most likely to cut through bedding and could indeed be seen running up the slope of the escarpment, slicing through multiple shale beds. The vertical persistence of many of these veins shows that layered stratigraphy within the shales played little importance in the growth of the fracture, indicative of externally derived sources of causal stress.

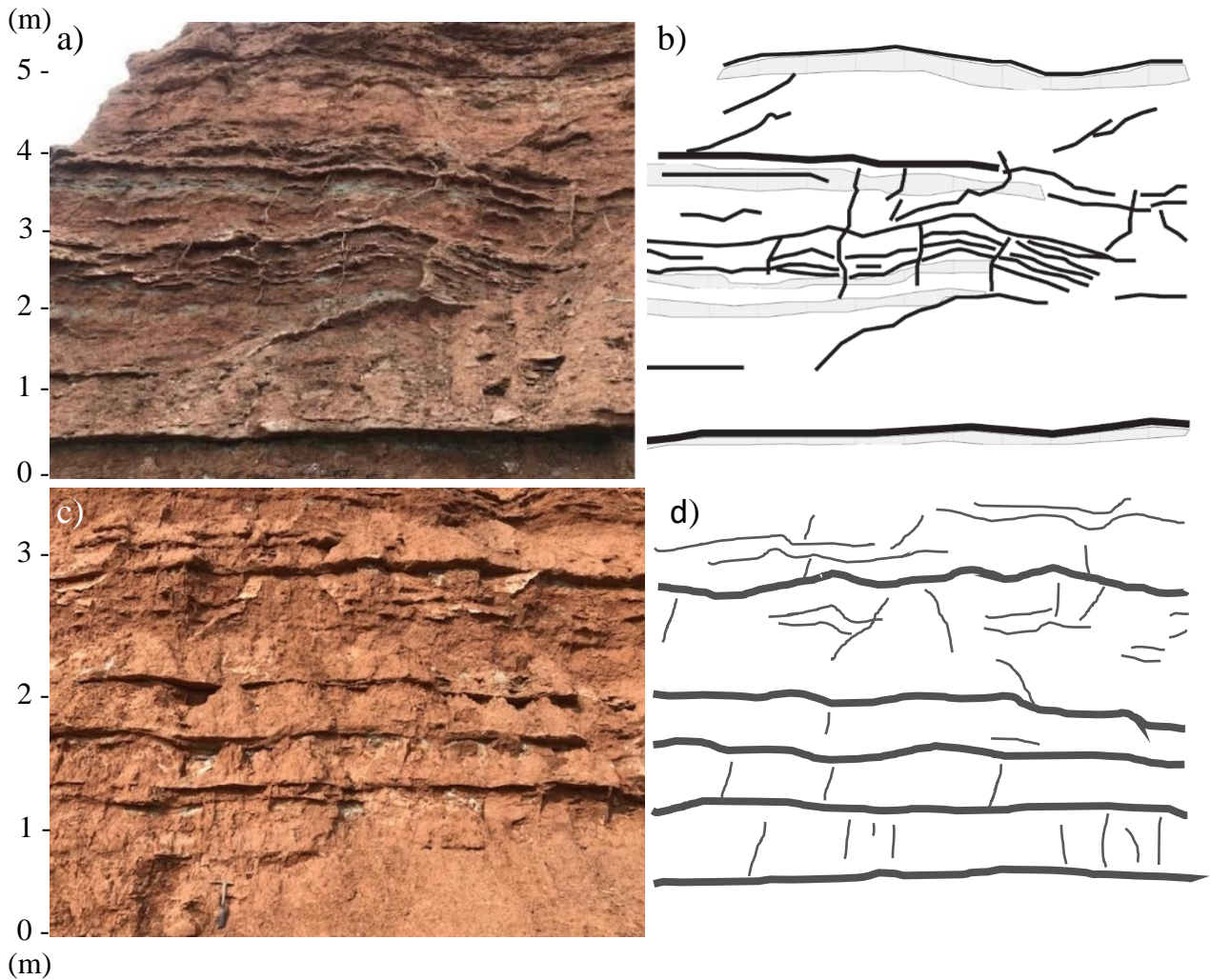


**Figure 26.**

a/b) Near perfect bed bounded or top bounded satin spar veins of Station 5 near river escarpment with small deformational folds present. c/d) Near perfect bed bounded or top bounded satin spar veins of Station 5 at roadcut.

The mineral veins of Station 5 exhibited occasional crosscutting of veins through beds (Fig. 25 c/d), but typically displayed bed-bounded fracture networks in the vertical/sub-vertical orientations (Fig. 26). The thick vertical veins of Station 5 can often be observed to be terminating at the even thicker bedding-parallel veins or gypsic siltstone layers that seem to occur at bed boundaries, as identified by the color changes from red/brown shales to green/grey shales present with thick vein fill (Fig. 26a). Many of these vertical veins merge with or crosscut sub-horizontal veins within the shale beds, indicating contemporaneous genesis, but they terminate at the thickest bed-boundary veins (Fig. 26b).

### **Shale Character**

The structure of the rock in which the veins appear plays an important role in fracture development and the transition between shale material, from massive and structureless to blocky and pedogenic, and is often a factor of what type of vein and fill is present. If the massive-granular shales have veins within them, they are often (though not always) sub-horizontal, satin spar. The dense networks of these veins are correspondent to this type of material throughout Station 1 and other study locations. The vein types are also present within the green/grey shale layers in which Wu (1963) measured higher levels of silt than surrounding shales (Fig. 27, 28a).

The transition in shale structure also marks a transition in vein and fracture nature (Fig. 27). Upon entering blocky and granular shales, the fractures are oriented vertical to sub-vertically and are mostly filled with selenite. This complete change in nature of shale fracture and fill may be linked to the host materials composition and, therefore, the vertical or horizontal orientations of the veins and their fill. The blocky and columnar peds in some of the lower shales

contributes to pre-fractured void spaced left to be filled with gypsum-saturated fluids. Often, when digging through or pulling apart pedogenic columns or blocks (Fig. 28b), one will typically see thin selenite within the small fracture space that separates these features.



**Figure 27.** Station 1 transitional layer from red/brown shale to green/grey back to red/brown. There is a change in shale structure from the top red shales to the bottom. The top is mostly massive and structureless with dense sub-horizontal satin spar veining. The bottom has changed to a more granular and blocky shale with root traces (left) and vertical selenite veins (right).

The appearance and interpretation of paleosols in the study area could play a part in the structure of these shales. These paleosol layers, as reported by Sweet et al. (2013), through a process of shrink/swell conditions acting upon the clay materials, results in pedogenic structures within the material (i.e., granular nature, blocky and columnar peds, etc.) (Fig. 28b). These structures provide breakage planes along which veins may develop. While these have been attributed to desiccation, the measurements and observations of this study suggest that desiccation and mud cracks are not the only factor of fracture propagation. It is unlikely that the great aperture values, non-bed bound veins, and strike trends throughout multiple locations along the escarpment are the result of desiccation alone. This being the case, an external force (dissolution subsidence or seismic activity) capable of producing the features previously mentioned might fracture rock along preferential orientations within this granular and brittle medium while hindering it within silty and structureless layers. In summary, blocky/brittle units are the dominant material within which are found vertical/sub-vertical vein that have been filled with selenite as observed at Station 1 and in the drill logs of Ward (1961).



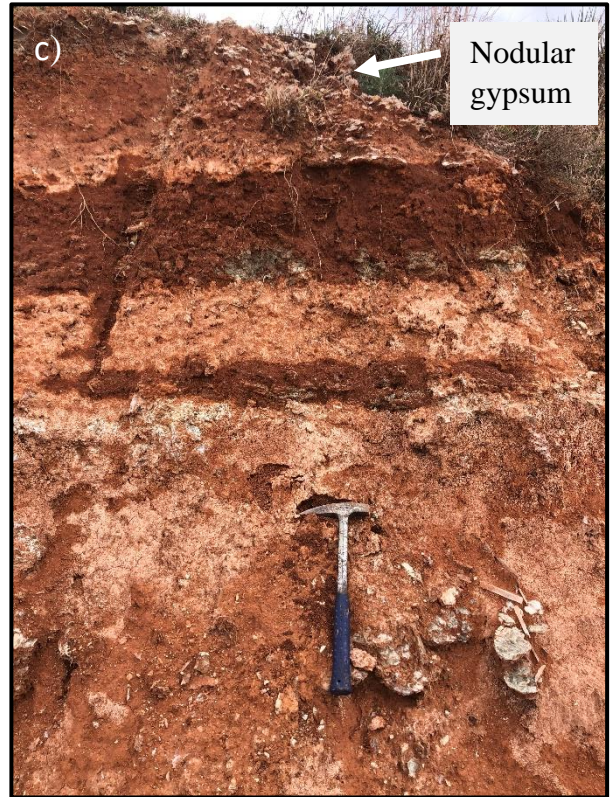
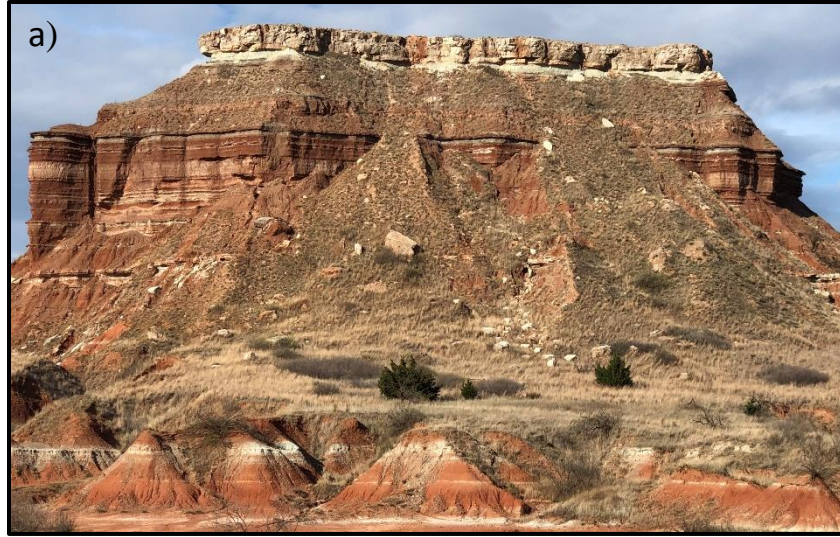


**Figure 28.** Photographs showing various paleosol and reduction-related features found throughout the study area. a) Photo showing multiple layers of reduced horizons that are slightly richer in silt content at Lone Peak near Station 3. b) Closed and closely spaced fractures within blocky pedogenic shale that strike NW/SE at Station 1. c) Nodular gypsum horizon with layer of water retentive clay located immediately below it at Station 1.

## **Subsurface Salt Layer Proximity**

Permian strata within this region are layered with evaporites, many of which include salts and shaly salts. Again, the evaporite strata of significance to this study is the Upper Cimarron Salt and the Flowerpot Salt based upon the location interpretation of Vosburg (1963). These salts have been theorized, in all likelihood, to be the primary contributors to surface salt precipitation within Big Salt Plains, Salt Creek Canyon, Okeene Salt Plains, and other smaller patches of observed salt pans (Johnson, 2019). The ground surface at these locations is covered in a salt crust that may accumulate to a great thickness, especially at Big Salt Plains where active surface salt mining currently takes place.

Stations 1, 2, 5, and 6 are zones of dominant vertical fracture, aside from Station 5 in which horizontal fracture is dominant but vertical fracture is still frequent. These stations are also located within proximal distance to active and shallow dissolution fronts as compared to the stations that display sub-horizontal satin spar veins in the uppermost Flowerpot Shale only. Sub-horizontal veins lacking frequent vertical veins were found within more central zones of subsurface salt bodies or near salt fronts of significant depths, and therefore less likely to dissolve significant loads of halite.

The salt fronts were interpreted by Vosburg (1963) from well logs and core that showed brecciated and collapse zones at the depth that the salt was expected to be present on the eastern front while on the west the salt was found at the appropriate depth. This loss of salt that resulted in brecciated and collapsed material occurred in a non-uniform but systematic zone that is likely to impact surface features to some degree. The degree of surface deformation depends upon the extent of dissolution and the thickness of the salt which previously occupied the zone.

## Research Comparison

### *Comparable Fracture Studies*

Previous studies relating subsurface faulting and regional stresses with overlying sedimentary structures are quite common (e.g., Butler et al., 1997; Lorenz, 2002; Burberry, 2015; Burberry et al., 2018; Pisani et al., 2019; Kolawole et al., 2019; Kolawole et al., 2020) and show that deep structures and stress regimes can influence overhead rock and sediments, as is suggested by the current study. These are determined through similarities in the strikes of the deep and shallow structures.

Burberry et al. (2018) has published work showing how reactivation of basement faults can influence and control surface features within the Midcontinent of the United States. Joint networks that appear in successively younger strata and surface lineaments within the midcontinent were recorded throughout multiple regions of Kansas and Nebraska and were found to mirror deep-seated basement faults oriented in NE/SW and NW/SE directions. These features were attributed to far-field stresses likely related to Laramide or Ancestral Rocky Mountain orogenic events and reactivation of Mid-continent rift fault systems. In relation to the current thesis work, the study of Burberry et al. (2018) shows how basement structures can influence surface features in the absence of large-scale structural development and deformation within a regional setting, as in the case of the region surrounding the Blaine Escarpment.

An additional study completed by Pisani et al. (2019) shows how gypsum cave orientations are controlled by structural trends in the northern Apennines of Italy. Deformation trends identified by faulting and folding in this region show a well-developed relationship with directions of karst development. As in the study of Gauvey (2019), Pisani et al. (2019) shows

how joints related to deep seated structures (determined through strike orientations) allow for fluid migration that results in preferred cavern passageway orientation through dissolution.

Kolawole et al. (2019) published a study concerning exposed and fractured basement within Oklahoma. This study showed that fault and fracture trends within the Precambrian basement of southern Oklahoma were similar to recent earthquake lineament trends of north-central Oklahoma (NE/SW, NW/SE, and a slight N/S directional trend). The faults trending NE/SW and NW/SE are favorably oriented for reactivation within the present-day stress field (Kolawole, et al., 2019). These trends closely resemble the surface shale fractures within the Flowerpot Shale, especially in the southern escarpment region.

Observed Precambrian igneous intrusions (analyzed through geochronological and structural analysis) that occur within the exposed basement trend in the prominent strike directions of NE/SW and NW/SE, indicating that the fractures are Precambrian in age (Kolawole et al., 2019). This means that NE/SW trending faults within the basement of the current study area may range in age from Precambrian to the last influential tectonic influence (the Laramide Orogeny during the late Cretaceous). Reactivation of these faults likely occurred in the past up to the present. Deformation resulting from this reactivation could occur within the Permian Flowerpot Shales anytime after deposition and lithification, however, the proximity of deformation zones and dissolving salt fronts suggests that during times of water influx (shallow seas, glacial melt, etc.), large amounts of dissolution would have taken place and weakened the overlying rock, leaving it further susceptible to deformation.

### *Stress Regime Deformation*

Deformation and sub-surface structures occur throughout regions surrounding the research area and may relate to features seen along the Blaine Escarpment. Kolawole et al. (2020) shows that basement structures control overlying sedimentary sequences along the Anadarko Shelf and that NE, NW, and ~ N trending faults that root in the basement have penetrated into the sedimentary rocks overhead. The trend of the structures in this region along the Anadarko Shelf are attributed to tectonic forces created as the Anadarko Basin subsided in Southern Oklahoma (Kolawole et al., 2020). These features occur proximal to the current study and suggest a relatable stress-regime origin.

Additional studies attribute features from stress related to other processes, such as far field orogenic deformation. Sedimentary rock fracture within the Spraberry Formation of the Midland Basin has been attributed to far field stress induced by events of the Laramide Orogeny or residual Laramide stress by Lorenz et al. (2002). This conclusion is reached through the parallelism of natural fractures and veins within core that trend in dominant NE/SW directions and the NE-directed Laramide compression. According to Lorenz et al. (2002), there have been few tectonic events affecting Cretaceous rocks of this region since deposition aside from the basement-involved Laramide orogeny thrusting several hundred kilometers to the west. This is also the conclusion of Burberry et al. (2018), in the case of surface joints mirroring sub-surface fault systems with dominant NE/SW and NW/SE trends.

Stress regimes regionally proximal to the current study area are inherited from various events (i.e., orogenic events (Laramide, Ancestral Rocky Mountain, Central Plains, etc.), Nemaha Uplift, Midcontinent Rift System, basin subsidence, etc.). The structures produced from these events often control sedimentary sequences overlying them through ductile and brittle

deformation (i.e., fault penetration, folding, etc.) (Kolawole, 2020). Faults oriented optimally to the contemporary stress field have a higher likelihood of slipping and inducing seismic events that are responsible for deformation (Burberry et al., 2018). In the case of northwestern Oklahoma, NE/SW trending sub-surface faults are optimally oriented with the present stress regime and show the highest likelihood of earthquake potential (Qin et al., 2019). Along the Blaine Escarpment, the fractures of interest often mirror the NE/SW trending faults, indicating a relationship between these features through recent or ancient seismic deformation.

## CONCLUSIONS

There are many circumstances that affect the nature of rock fracture along the escarpment and various processes that influence fracture propagation. Additionally, once created, mineral infill of fracture voids show precipitation that took place under varied conditions. These conditions include shale character (massive, granular, or blocky), stability or speed of propagation, and proximal parent material (material from which gypsum-saturated fluids were derived. (e.g., the weathering of bedded or nodular gypsum, rehydrated anhydrite accumulations, etc.)). The layer of thin, sub-horizontal satin spar found at Stations 1, 3, and 4 is proposed to form via weathering of gypsum layers or hydration of anhydrite that crystalizes within the massive shales in a sub-horizontal-preferred orientation. The chaotic fracture interactions within this unit show that fracturing of all orientations happened synchronously. The satin spar indicates growth through a saturated fluid precipitating in a desiccated layer or through force of crystallization via volume expansion, or both.

The formation of vertical veining and jointing is proposed to be a separate deformational event than the previously discussed veins. Sets of these features display reliable strike orientations with a slight northern shift at the northernmost locations (Stations 5 and 6). There is also an observed alignment between these measured fractures and previously studied regional faults and lineaments. This relationship and alignment suggests an association between subsurface features and the measured fracture zones on the surface. The influence of these subsurface faults appears likely from the evidence gathered; however, the question is whether fault activity initiated rock fracture or whether it guided propagation when initiation was caused by a separate event or load. This event or load could come in the form of a salt or evaporite layer within the shale dissolving and deforming the surface through subsidence. As a result, salt-related deformation is proposed to have induced a load upon the rocks of the area, while strike orientation was controlled through a regionally applied stress field or the upward propagation of sub-surface fault systems into a weakened zone resulting from underlying material loss through dissolution.

The case for Stations 1 and 2 relates to the previously discussed paragraph. Both exhibit very similar fracture orientations with the greatest intensities of aperture and persistence lying in the NE/SW directions. The great lengths of straight linear fractures at Station 2 and the thick, non-bedbound veins of Station 1 point towards an external cause aside from diagenetic-related deformation. At Station 1, the influence of the shale character is apparent throughout the section. While this may occur from pedogenic processes, the important aspect is that the shales vary from massive to granular and blocky and that changing concentrations of silt, clay, and gypsum throughout rock changes the character of the veins that precipitate.

Chaotic bed dips and strikes within Salt Creek Canyon (Station 2) indicate that these rocks do undergo dissolution-related failure. However, these features are typically confined to small areas. The joints may run for great enough lengths to be seen on Google Earth (up to 46 m) and are often extremely linear and common. This commonality and linear continuity isn't what would be expected of a surface suffering from dissolution induced deformation, although that is dependent upon rate and intensity of dissolving salts. Fracturing within the collapse features was not observed. Because of the large scale and regular fracture sets and the smaller scale collapse structures, these joints may pre-date dissolution and have acted as the initial conduit from which saline waters escaped the subsurface.

The directional trends of fractures seen at the northern locations (Stations 5 and 6) are interpreted to be closely related to bedding-parallel slip. While the alignment of vertical fracture with sub-surface faulting and lineaments is clear, this orientation has a higher likelihood of being an effect of movement along the bedding planes. This is obvious at Station 5 in the shear fibers of the thick satin spar veins that the vertical veins are mostly bound within. Rock failure within the slipping beds would be a function of the direction and intensity of movement. Since many of the sub-horizontal veins and sub-vertical veins contained within the beds crosscut and merge without pattern, it is inferred that they formed synchronously while slip was happening along weak bedding planes. Proximity to a very shallow salt layer, intense surface accumulation, and chaotically dipping beds near this region make the case that salt dissolution induced subsidence is responsible for the least compressive stress being oriented vertically and resulting in horizontal fracture dilation. During dilation satin spar precipitated and bedding planes moved laterally, forming shear fibers in the veins and fractures within the bedding.



Summarily, the purpose of this study was to characterize, analyze, and interpret fracture systems within the Permian strata of Blaine County, Oklahoma, and the surrounding regions. In reference to the initial questions regarding this fracture project: 1) The nature and characteristics of surface fracture within the research area have been observed, measured, and recorded. These characteristics (e.g., mineral fill, strike orientation, aperture, persistence, shale host character, salt layer proximity, etc.) have then been analyzed in juxtaposition with other locations and previous literature. 2) The relationship between these surface fractures and regional stress/sub-surface fault systems is evident in strike patterns seen throughout fracture zones along the escarpment. The upward propagation of faults and/or an influential stress regime are controlling factors in how fractures along the Blaine Escarpment organize in regards to strike and magnitude of the rock failure (e.g., aperture, persistence, bed-boundedness, etc.) 3) In an area of stratified salt layers where active dissolution takes place near the zones of vertical fracture, it is evident that while fractures may organize in association with or under the influence of stress regimes or sub-surface fault systems, they are closely related to sub-surface material removal or flow. Proximity to salt plains, inferred salt fronts by Vosburg (1963), and zones of the greatest deformation display a relationship between the layers of salt and surficial rock failure. Regions of no observed or cited vertical fracture (Stations 3 and 4) occur where no shallow salt front or salt plains exist. Ultimately, fractures along the Blaine Escarpment are the result of multiple influencing forces and local characteristics. Stress fields and sub-surface fault systems organize fracture sets under a stress load created from sub-surface material removal and are also subject to controlling properties within the shale themselves (e.g., shale structure, proximity to gypsum-rich strata, etc.).

This study of fractures along the Blaine Escarpment of Northern Oklahoma adds value to the limited literature of the features in the rock units mentioned throughout the work, however, further research is needed to ascertain specific relationships between proximal salt dissolution regions and areas of effect throughout this and other evaporite basins. This would be best completed through study zones at specified ranges from observed salt dissolution-induced surface locations and through the study of core above and below the salt layers in these zones and zones of no observed vertical fracture deformation or salt dissolution.

Additional work is also needed on the influence of unit structure upon the formation of gypsum polymorphs. This would include further geochemical analysis on the layers of the same section in which veins both propagate and fill differently than surrounding layers. These, along with other contributions, would further academic understanding of gypsum veining and fracture within shales and mud rocks. It would also serve to increase our knowledge of salt dissolution and tectonic events in relation to their impact on surficial features.

## REFERENCES

- Alt, R. C., & Zoback, M. D. (2017). In situ stress and active faulting in Oklahoma. *Bulletin of the Seismological Society of America*, 107(1), 216–228.
- Babel, M. (2004). Models for evaporite, selenite and gypsum microbialite deposition in ancient saline basins. *Acta Geologica Polonica*, 54, 219–249.
- Bozeman, J. & Bozeman, S. (2002). Speleology of Gypsum Caves in Oklahoma. *Carbonates and Evaporites*, 17(2), 107-113.
- Bundy, W.M. (1956). Petrology of gypsum anhydrite deposits in southwestern Indiana. *Journal of Sedimentary Petrology*, 26, 240–252.
- Burberry, C. M. (2015). The effect of basement fault reactivation on the Triassic – Recent geology of Kurdistan, North Iraq. *Journal of Petroleum Geology*, 38, 37-58.
- Burberry, C. M., Swiatlowski, J. L., Searls, M. L., & Filina, I. (2018). Joint and lineament patterns across the midcontinent indicate repeated reactivation of basement-involved faults. *Geosciences*, 8, 215
- Butler, R. W. H., Holdsworth, R. E., & Lloyd, G. E. (1997). The role of basement reactivation in continental deformation. *Journal of Geological Society, London*, 154, 69-71.
- Carter, L. S., Kelley, S. A., Blackwell, D. D., & Naeser, N. D. (1998). Heat flow and thermal history of the Anadarko Basin, Oklahoma. *American Association of Petroleum Geologists Bulletin*, 82, 291-316.
- Cobbold, P. R., Zanella, A., Rodriques, N., & Loseth, H. (2013). Bedding-parallel fibrous veins (beef and cone-in-cone): Worldwide occurrence and possible significance in terms of fluid overpressure, hydrocarbon generation and mineralization. *Marine and Petroleum Geology*, 43, 1-20.
- Collins, E. W. (1984) Styles of deformation in Permian strata, Texas Panhandle: University of Texas at Austin, *Bureau of Economic Geology Geological Circular*, 84(4), 4-11.
- Collins, R. J., McCown, F. P., Stonis, L. P., Petzel, G. J. & Everett, J. R. (1974). An Evaluation of ERTS Data for the Purposes of Petroleum Exploration. *Final report prepared for Goddard Space Flight Center*.
- Cosgrove, J. W. (2001). Hydraulic fracturing during the formation and deformation of a basin a factor in the dewatering of low-permeability. *AAPG Bulletin*, 85, 737–748.

- Cunningham, V. F. (2018). Identifying brittle deformation with remote sensing of geomorphic landforms on the Southern High Plains, West Texas (Unpublished master's thesis). Texas Tech University.
- Dart, R. L. (1990). In situ stress analysis of wellbore break-outs from Oklahoma and the Texas Panhandle. U.S. Geological Survey Bulletin 1866-F. doi:10.3133/b1866f.
- Engelder, T. (1982). Is there a genetic relationship between selected regional joints and contemporary stress within the lithosphere of North America? *Tectonics*, 1(2), 161-177. doi:10.1029/tc001i002p00161.
- Everett, A. G., (1962). Clay petrology and geochemistry of the Blaine Formation (Permian), northern Blaine County, Oklahoma. (Unpublished master's thesis). University of Oklahoma.
- Fay, R. (1964). Blaine Formation Northwestern Oklahoma. *Oklahoma Geological Survey Bulletin* 98.
- Fay, R. (1959). Guide to Roman Nose State Park, Blaine County, Oklahoma. *Oklahoma Geologic Survey Guide Book IX*.
- Frumkin, A., (2013). Salt karst. In: Shroder, J. (Editor in Chief), Frumkin, A.(Ed.), *Treatise on Geomorphology*. Academic Press, San Diego, CA, v. 6, Karst Geomorphology, pp. 407–424.
- Gale, J., Laubach, S., Olson, J., Eichhubl, P., & Fall, A. (2014). Natural Fractures in shale: A review and new observations. *AAPG Bulletin*, 98(11), 2165-2216. doi:10.1306/08121413151.
- Gauvey, K. (2019). Gypsum Karst Speleogenesis in Barber County, Kansas of the Permian Blaine Formation. (Unpublished master's thesis). Fort Hays State University.
- Ghosh, S., Milad, B., Prasun, S., & Ghosh, S. S. (2018). Origin and Characterization of Joints in Sedimentary Rocks: A Review. *Petroleum & Petrochemical Engineering Journal*, 2(5).
- Gindre-Chanu, L., Warren, J. K., Puigdefabregas, C., Sharp, I. R., Peacock, D. C. P., Swarts, R., Poulsen, R., Ferreira, H., & Henrique, L. (2015). Diagenetic evolution of Aptian evaporites in the Namibe Basin (south-west Angola). *Sedimentology*, 62, 204-233.
- Goldstein, A. G., & Collins, E. W. (1984). Deformation of Permian strata overlying a zone of salt dissolution and collapse in the Texas Panhandle. *Geology*, 12(5), 314. doi:10.1130/0091-7613(1984)122.0.co;2

- Goldstein, R. H., Anderson, J. E., & Bowman, M. W. (1991). Diagenetic responses to sea-level change: Integration of field, stable isotope, paleosol, paleokarst, fluid inclusion, and cement stratigraphy research to determine history and magnitude of sea-level fluctuation. *Kansas Geological Survey Bulletin*, 233, 139-162.
- Gross, M. R., & Engelder, T. (1991). A case for neotectonic joints along the Niagara Escarpment. *Tectonics*, 10(3), 631-641. doi:10.1029/90tc02702
- Guo, G., & George, S. A. (1999). An analysis of Surface and Subsurface Lineaments and Fractures for Oil and Gas Exploration in the Mid-Continent Region (Rep. No. NIPER/BDA4-0223). Tulsa, OK: National Petroleum Technology Office.
- Guðmundsson, A. (2011). *Rock Fractures in Geological Processes*. Cambridge: Cambridge University Press.
- Gustavson, T. C. (1986). Geomorphic development of the Canadian River Valley, Texas Panhandle: An example of regional salt dissolution and subsidence. *Geological Society of America Bulletin*, 97(4), 459. doi:10.1130/0016-7606(1986)972.0.co;2
- Gustavson, T. C., Hovorka, S. D., & Dutton, A. R. (1994). Origin of Satin Spar Veins in Evaporite Basins. *SEPM Journal of Sedimentary Research*, 64A. doi:10.1306/d4267d1b-2b26-11d7-8648000102c1865d
- Gustavson, T., & Simpkins, W. (1989). Geomorphic Processes and Rates of Retreat Affecting the Caprock Escarpment, Texas Panhandle. Report Investigation. doi:10.23867/ri0180d.
- Heidbach, O., Rajabi, M., Cui, X., Fuchs, K., Müller, B., Reinecker, J., Reiter, K., Tingay, M., Wenzel, F., Xie, F., Ziegler, M. O., Zoback, M. L., & Zoback, M. D. (2018). The World Stress Map database release 2016: Crustal stress pattern across scales. *Tectonophysics*, 744, 484-498.
- Hemmerich, M. J. & Kelley, S. A. (2000). Patterns of Cenozoic denudation on the Southern High Plains. *Association of Petroleum Geologists Bulletin*, 84, 1239.
- Hooker, J., Laubach, S., & Marret, R. (2013). Fracture-aperture size frequency, spatial distribution, and growth processes in strata – bounded and non-strata bounded fractures, Cambrian Mesón Group, NW Argentina. *Journal of Structural Geology*, 54, 54-71.
- Johnson, K. S. (2019). Geology of salt plains on the Cimarron River in northwest Oklahoma; Big Salt Plain, Little Salt Plain, Salt Creek Canyon, and Okeene Salt Plain. Norman, OK: *Oklahoma Geological Survey*.
- Jordan, L. & Vosburg, D.L. (1963). Permian Salt and Associated evaporites in the Anadarko Basin of western Oklahoma-Texas Panhandle region. *Oklahoma Geological Survey Bulletin*, 102, 76.

- Kolawole, F., Turko, M., & Carpenter, B. (2020). Basement-controlled deformation of Sedimentary Sequences, Anadarko Shelf, Oklahoma. doi:10.31223/osf.io/up497.
- Kolawole, F., Johnson, C. S., Morgan, C. B., Chang, J. C., Marfurt, K. J., Lockner, D. A., Reches, Z., Carpenter, B. M. (2019). The susceptibility of Oklahoma's basement to seismic reactivation. *Nature Geoscience*, 12, 839-844. <https://doi.org/10.1038/s41561-019-0440-5>
- Ladeira, F. L., Price, N. J. (1981). Relationship between fracture spacing and bed thickness: *Journal of Structural Geology*, v. 3, no. 2, p. 179–183.
- Laubach, S. E., Eichhubl, P., Hilgers, C., & Lander, R. H. (2010). Structural Diagenesis. *Journal of Structural Geology* 32(12): 1866-1872. doi: 10.1016/j.jsg.2010.10.001.
- Levandowski, W., Herrmann, R. B., Briggs, R., Boyd, O., & Gold, R. (2018). An updated stress map of the continental United States reveals heterogeneous intraplate stress. *Nature Geoscience*, 11(6), 433-437. doi:10.1038/s41561-018-0120-x
- Lockamy, D. (2014). Preservation Potential of Permian Gypsum Beds, Nippewalla Group, USA (Unpublished master's thesis). Wichita State University.
- Lorenz, J. C., Sterling, J. L., Schechter, D. S., Whigham, C. L., & Jensen, J. L. (2002). Natural fractures in the Spraberry Formation, Midland Basin, Texas: The effects of mechanical stratigraphy on fracture variability and reservoir behavior. *AAPG Bulletin*, 86(3), 505-524.
- Mack, G. H., James, W. C., & Monger, H. C. (1993). Classification of paleosols. *Geological Society of America Bulletin*, 105, 129-136.
- Machel, H.G. (1985). Fibrous gypsum and fibrous anhydrite in veins. *Sedimentology*, 32, 443–454.
- Maher, H., Ferguson, S., Korth, R., Marshall, J., & Pickett, L. (2015). Strata-bound vein array in the basal Pierre Shale, Lake Francis Case, South Dakota, U.S.A. *Rocky Mountain Geology* 50 (2): 153–165.
- Maher, H. & Shuster, R. (2012). Chalcedony vein horizons and clastic dikes in the White River Group as products of diagenetically driven deformation. *Lithosphere* 4(3): 167-186. doi: 10.1130/L187.1
- McGregor, D. J. (1954). Gypsum and Anhydrite Deposits of Southwestern Indiana. Indiana Department of Conservation: *Geological Survey, Report of Progress no. 8*.
- Morton, S. L., Peterie, S. L., Parsons, R. L., Ivanov, J., Miller, R. D., & Livers-Douglas, A. J. (2018). Time-lapse Monitoring of Subsidence Features within the Hutchinson Salt in Kansas. *SEG Technical Program Expanded Abstracts 2018*. doi: 10.1190/segam2018-2997153.1.

- Nelson, R. A., Serra, s. (1993) Vertical and lateral variations in fracture spacing in folded carbonate sections and its relation to locating horizontal wells: Canadian SPE/CIM/CANMET International Conference on Recent Advances in Horizontal Well Applications, *Canadian Society of Petroleum Engineers*, Paper HWC94-41, 10.
- Peacock, D. C. P., Nixon, C. W., Rotevatn, A., Sanderson, D. J. & Zuluaga, L. F. (2016). Glossary of fault and other fracture networks. *Journal of Structural Geology*. 92, 12-29.
- Peacock, D. C. P., Sanderson, D., & Rotevatn, A. (2017). Relationships between fractures. *Journal of Structural Geology*. 106. doi:10.1016/j.jsg.2017.11.010.
- Peryt, T.M. (2001). Gypsum facies transitions in basin–marginal evaporites: middle miocene (Badenian) of west Ukraine. *Sedimentology*, 48, 1103–1119.
- Pisani, L., Antonellini, M., Waele, J. D. (2019). Structural control on epigenic gypsum caves: evidences from Messinian evaporites (Northern Apennines, Italy). *Geomorphology*, 332, 170-186.
- Qin, Y., Chen, X., Walter, J. I., Haffener, J., Trugman, D. T., Carpenter, B. M., Kolawole, F. (2019). Deciphering the Stress State of Seismogenic Faults in Oklahoma and Southern Kansas Based on an Improved Stress Map. *Journal of Geophysical Research: Solid Earth*, 124(12), 12920-12934. doi:10.1029/2019jb018377.
- Rai, A. K., Pati, J. K., Parigger, C. G. & Rai, A. K. (2019). Plasma spectroscopy of various types of gypsum: An ideal terrestrial analogue. *Atoms*, 7(3), 72, doi: 10.3390/atoms7030072.
- Ramsay, J. G. (1980). The crack–seal mechanism of rock deformation. *Nature*, 284(5752), 135-139. doi:10.1038/284135a0.
- Rascoe, B. & Baars, D. L. (1972). The Permian System, in Geologic Atlas of the Rocky Mountain Region: *Rocky Mt. Assoc. of Geologists*, Denver, Colo., 143-165.
- Reinhardt, J., & Sigleo, W. R. (1988). Paleosols and weathering through geologic time: Principles and applications. Boulder, CO: *Geological Society of America*. doi: 10.1130/spe216.
- Retallack, G. J. (1988). Field Recognition of Paleosols. *Special Paper of the Geological Society of America*. doi:10.1130/SPE216.
- Schultz, R. A. & Fossen, H. (2008). Terminology for structural discontinuities. *American Association of Petroleum Geologists Bulletin*, 92, 853-867.

- Shearman, D. J., Mossop, G., Dunsmore, H., & Martin, H. (1972) Origin of gypsum veins by hydraulic fracture. *Transaction of the American Institute of Mining and Metallurgical Engineers*, 82B, 65–67.
- Singhal, B. B., & Gupta, R. P. (1999). Fractures and discontinuities. *Applied Hydrogeology of Fractured Rocks*, doi:10.1007/978-94-015-9208-6\_2.
- Sweet, A. C., Soreghan, G. S., Sweet, D. E., Soreghan, M. J., & Madden, A. S. (2013). Permian dust in Oklahoma: Source and origin for Middle Permian (Flowerpot-Blaine) redbeds in Western Tropical Pangaea. *Sedimentary Geology*, 284-285, 181-196. doi:10.1016/j.sedgeo.2012.12.006.
- Tabakh, M., Schreiber, B. & Warren, John. (1998). Origin of fibrous gypsum in the Newark Rift Basin, Eastern North America. *Journal of Sedimentary Research*, 68. 88-99. doi:10.2110/jsr.68.88.
- Tabor, N., Myers, T. & Michel, L. (2017). Sedimentologist's Guide for Recognition, Description, and Classification of Paleosols. *Terrestrial Depositional Systems*, 165-208. doi:10.1016/b978-0-12-803243-5.00004-2.
- Underwood, C. A., Cooke, M. L., Simo, J. A. & Muldoon, M. A., (2003). Stratigraphic controls on vertical fracture patterns in Silurian dolomite, northeastern Wisconsin: *American Association of Petroleum Geologists Bulletin*, 87(1), 121–142.
- Vosburg, D. L. (1963). Permian subsurface evaporites in the Anadarko Basin of the western Oklahoma-Texas panhandle region. University of Oklahoma.
- Warren, J. K. (2016) *Evaporites: A Geological Compendium* (2nd Ed.). Springer International Publishing. doi: 10.1007/978-3-319-13512-0.
- Ward, P. E. (1961). Shallow halite deposits in northern Woodward and southern Woods Counties, Oklahoma. *Oklahoma Geological Survey. Geology Notes*, 21(9), 150-151.
- Wu, D. C. (1969). Clay Mineralogy and Geochemistry of the Upper Flowerpot Shale in Major and Blaine Counties, Oklahoma. (Unpublished dissertation). University of Oklahoma.
- Zabawa, P. J. (1976). Investigation of Surficial Structural Geology of Portions of Beckham, Custer, Roger Mills, and Washita Counties, Oklahoma (Unpublished master's thesis). University of Oklahoma.
- Zaheri, M. & Rafiei, B. (2020). Facies analysis, petrography and geochemistry of the Neogene gypsum deposits in the Eshtehard area, Alborz Province, Iran. *Geopersia* 10(2), 289-303. doi: 10.22059/GEOPE.2019.291757.648510.



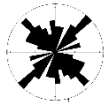

Zhang, X., & Jeffrey, R. G. (2012), Fluid-driven multiple fracture growth from a permeable bedding plane intersected by an ascending hydraulic fracture, *J. Geophys. Res.*, 117, B12402, doi:10.1029/2012JB009609.

# APPENDIX A

## Data Tables

### Station 1

**Table 6.** Unit Data

<b>Section Unit</b>	<b>Avg. Aperture (mm)</b>	<b>Dominant Fill</b>	<b>Orientation</b>
Upper Veins	13.01	Selenite	
Middle Veins	5.66	Satin Spar	N/A
Lower Veins	25.5	Selenite	

**Table 7.** Scanline Data of Veins

<b>Section Unit</b>	<b>Aperture (mm)</b>	<b>Avg. Spacing (m/fracture)</b>	<b>Avg. Frequency (fracture/m)</b>
<b>Upper Veins</b>			
<u>Scanline 1</u>	16.4	2.16	0.46
<i>Set 1</i>	8.35	1.5	0.7
<i>Set 2</i>	19.64	2.2	0.45
<b>Middle Veins</b>			
<u>Scanline 1</u>	7.1	0.12	8.4
<u>Scanline 2</u>	3.5	0.13	8
<u>Scanline 3</u>	7.0	0.1	9.9
<b>Lower Veins</b>			
<u>Scanline 1</u>	20	2.44	0.41
<i>Set 1</i>	23.3	5.9	0.17
<i>Set 2</i>	18.3	6.2	0.16
<i>Set 3</i>	17.4	8	0.13
<u>Scanline 2</u>	26.8	1.07	0.95
<i>Set 1</i>	29.2	1.05	0.95
<u>Scanline 3</u>	24.8	2.6	0.39
<i>Set 1</i>	28.5	3.14	0.32
<i>Set 2</i>	13.6	3.23	0.31

Set 1 – NE/SW trending fractures

Set 2 – NW/SE trending fractures

Set 3 – N/S trending fractures

## Station 2

**Table 8.** Scanline Data of Joints

Station	Persistence (m)	Spacing (m/fracture)	Frequency (fracture/m)
<u>Scanline 1</u> <i>Set 1</i>	1.5	2.04	0.5
<u>Scanline 2</u> <i>Set 1</i>	0.6	0.7	1.5
<u>Scanline 3</u> <i>Set 1</i>	6	0.7	1.5
<u>Scanline 4</u> <i>Set 2</i>	0.6	1.7	0.6
<u>Scanline 5</u> <i>Set 2</i>	0.6	1.4	0.72
<u>Scanline 6</u> <i>Set 2</i>	3	0.38	2.6
<u>Scanline 7</u> <i>Set 1</i>	0.6	0.61	1.6
<u>Scanline 8</u> <i>Set 2</i>	0.6	1.5	0.7
<u>Scanline 9</u> <i>Set 1</i>	3	0.76	1.3

Set 1 – NE/SW trending fractures

Set 2 – NW/SE trending fractures

### Stations 3 and 4

**Table 9.** Scanline Data of Sub-Horizontal Veins

<b>Station</b>	<b>Avg. Aperture (mm)</b>	<b>Avg. Spacing (m/fracture)</b>	<b>Avg. Frequency (fracture/m)</b>	<b>Density (fracture/m<sup>2</sup>)</b>	<b>Fill</b>
<b>Station 3</b>	4.4	1	0.98	16	Satin Spar
<u>Scanline 1</u>	4.1	0.76	1.3		
<u>Scanline 2</u>	5.04	1.19	0.85		
<u>Scanline 3</u>	4.0	0.8	1.25		
<b>Station 4</b>	6.2	0.9	1.08	12	Satin Spar
<u>Scanline 1</u>	6.03	0.7	1.4		
<u>Scanline 2</u>	5.56	1.5	0.66		
<u>Scanline 3</u>	7.37	0.8	1.2		

## Station 5

**Table 10.** Scanline Data of Sub-Horizontal Veins

<b>Vertical Scanline</b>	<b>Avg. Aperture (mm)</b>	<b>Avg. Spacing (m/fracture)</b>	<b>Avg. Frequency (fracture/m)</b>
<u>Scanline 1</u>	17.48	0.38	2.6
<u>Scanline 2</u>	19.35	0.35	2.9
<u>Scanline 3</u>	20.4	0.44	2.3

**Table 11.** Scanline Data of Sub-Vertical Veins

<b>Horizontal Scanline</b>	<b>Avg. Aperture (mm)</b>	<b>Avg. Spacing (m/fracture)</b>	<b>Avg. Frequency (fracture/m)</b>
<u>Scanline 1</u>	8.2	0.73	1.4
<i>Set 1</i>	8.09	1.98	0.5
<i>Set 2</i>	8.02	1.1	0.9
<u>Scanline 2</u>	8.1	0.78	1.3
<i>Set 1</i>	7.44	2.6	0.4
<i>Set 2</i>	7.85	1.5	0.7
<i>Set 3</i>	9.96	4.3	0.23
<u>Scanline 3</u>	8.6	0.71	1.4
<i>Set 1</i>	7.99	0.82	1.2

Set 1 – NNE/SSW trending fractures  
Set 2 – WNW/ESE trending fractures  
Set 3 – ENE/WSW trending fractures

## Station 6

**Table 12.** Scanline data of sub-vertical veins

<b>Horizontal Scanline</b>	<b>Aperture (mm)</b>	<b>Avg. Spacing (m/fracture)</b>	<b>Avg. Frequency (fracture/m)</b>
<u>Scanline 1</u>	4.24	1.27	0.78
<u>Scanline 2</u>	4.58	1.54	0.62

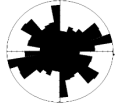
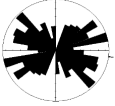


## All Stations

**Table 13.** Data table of comparable station characteristics

<b>Station</b>	<b>Fill (Dominant/Less Dominant)</b>	<b>Proximal Shallow Salt</b>	<b>Observed Paleosol</b>	<b>Dominant Bed-Boundedness</b>
<u>Station 1</u>	Selenite/satin spar	Yes	Yes	No
<u>Station 2</u>	N/A (closed joints)	Yes	N/A	No
<u>Station 3</u>	Satin spar/selenite	No	Possible	Yes
<u>Station 4</u>	Satin spar/selenite	No	Possible	Yes
<u>Station 5</u>	Satin spar	Yes	No	Yes
<u>Station 6</u>	Satin spar	Yes	No	Likely



**Table 14.** Data Table of comparable station characteristics

<b>Station</b>	<b>Vertical SC* Spacing (fracture/m)</b>	<b>Horizontal SC* Spacing (fracture/m)</b>	<b>Horizontal Vein Density (fracture/m<sup>2</sup>)</b>	<b>Horizontal Vein Aperture (mm)</b>	<b>Vertical Vein Aperture (mm)</b>	<b>Trend</b>
<u>Station 1</u>	23.3 <sup>×</sup>	5.3	18 <sup>×</sup>	5.6 <sup>×</sup>	8.2	
<u>Station 2</u>	N/A	0.79	N/A	Closed	N/A	
<u>Station 3</u>	11.2 <sup>×</sup>	N/A	16 <sup>×</sup>	4.8 <sup>×</sup>	N/A	N/A
<u>Station 4</u>	10.2 <sup>×</sup>	N/A	12 <sup>×</sup>	6.1 <sup>×</sup>	N/A	N/A
<u>Station 5</u>	2.3	1.25	N/A	18.42	7.98	
<u>Station 6</u>	N/A	15.1	N/A	N/A	4.4	

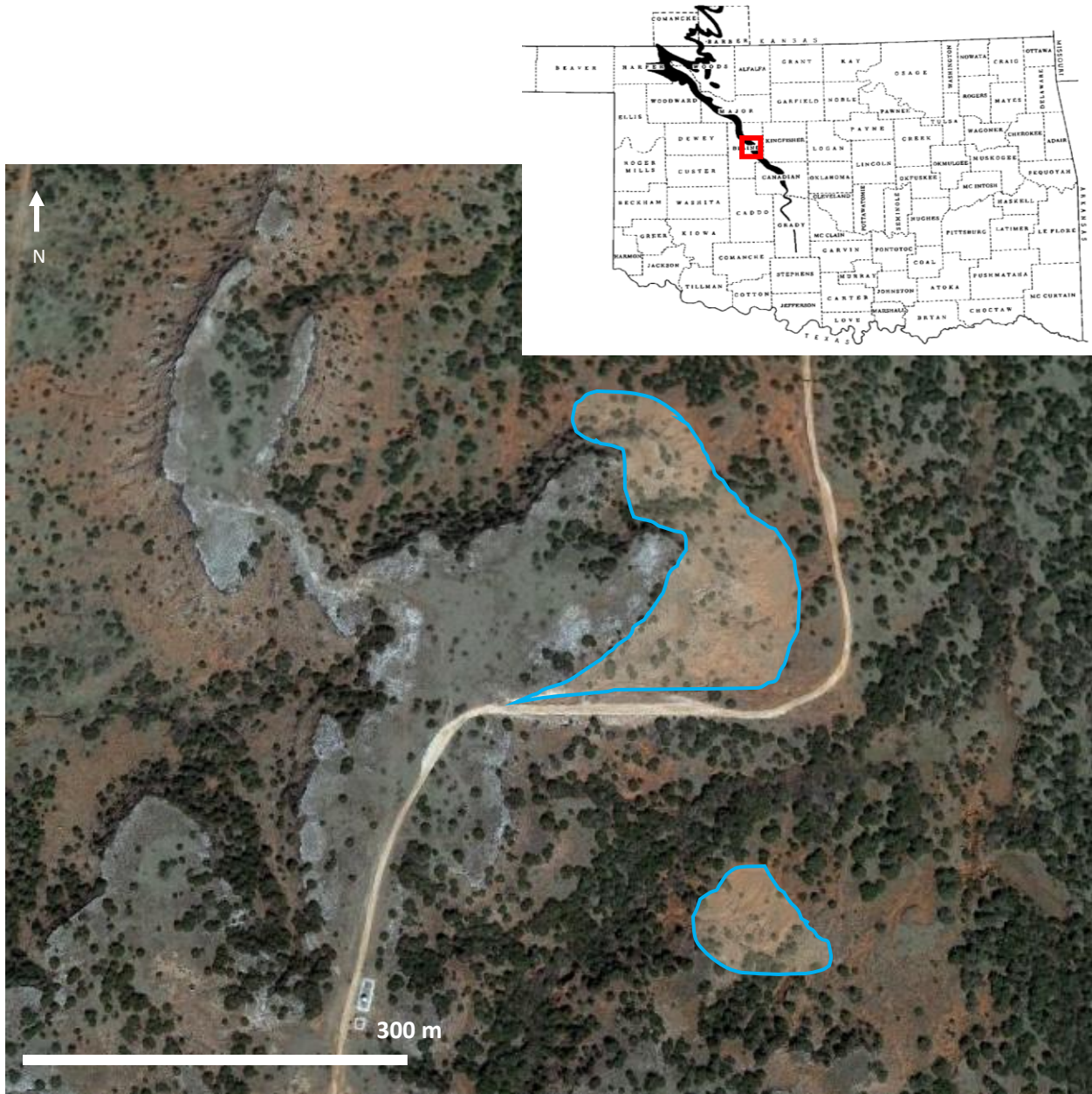
\* - Scanline measurements

× - indicates measurements taken in the thin, dense vein networks located in the upper portion of the Flowerpot Shale

# APPENDIX B

## Station Maps

### Station 1



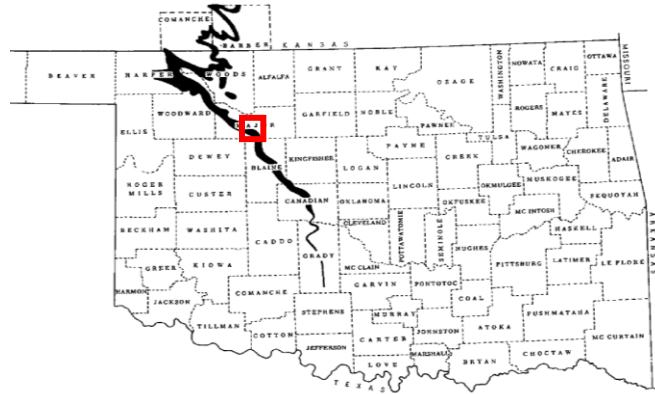
Hitchcock, OK: Blue outlined polygon represents fracture zones of study.

## Station 2



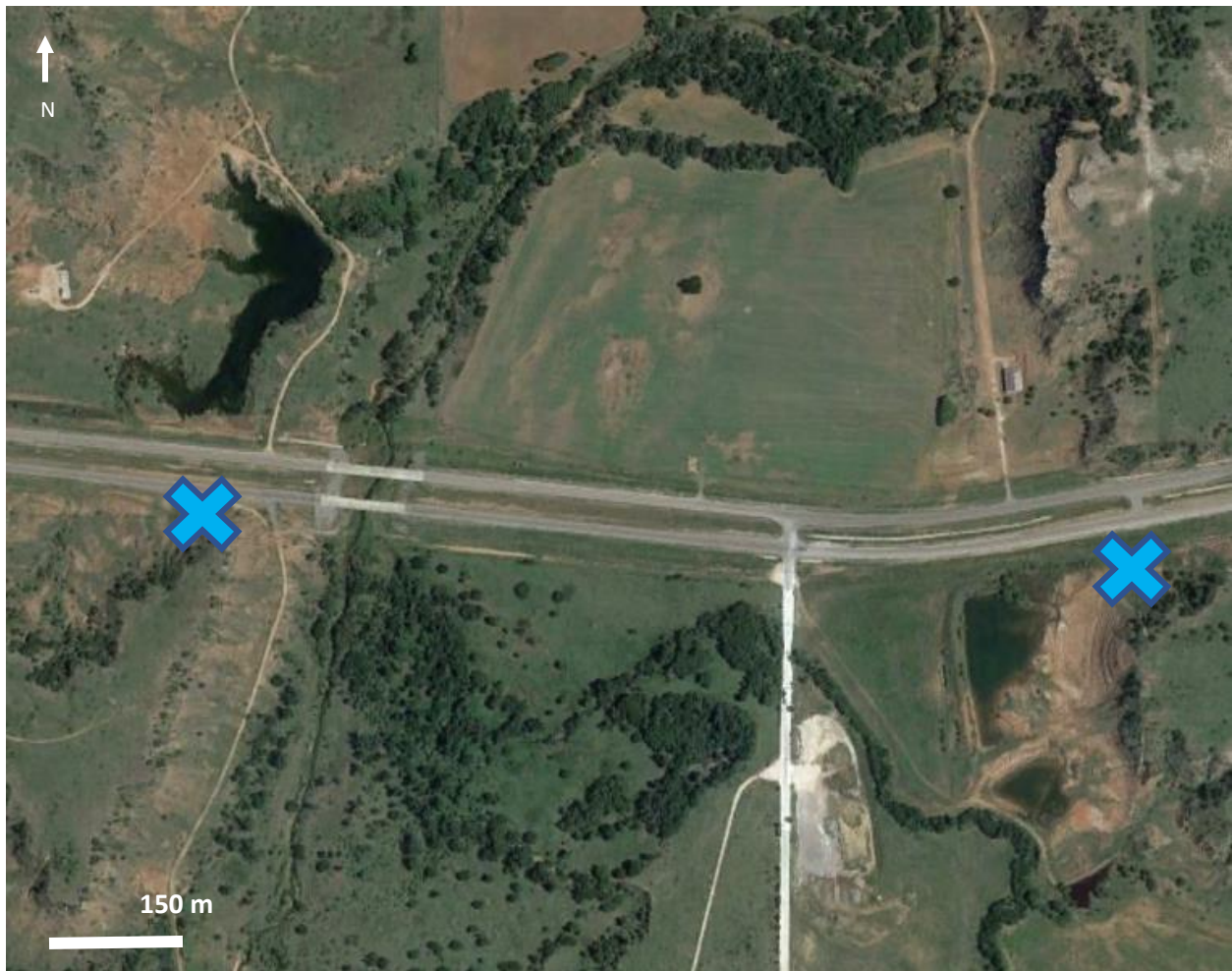
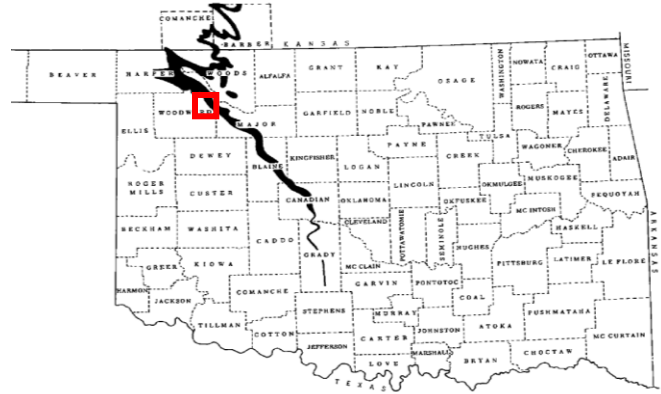
Salt Creek Canyon: Blue outlined polygon represents fracture zones of study.

### Station 3



Fairview, OK: Blue X's represent fracture zones of study.

# Station 4



Mooreland, OK: Blue X's represent fracture zones of study.

# Station 5



Freedom, OK: Blue X's and line represent fracture zones of study.

### Station 6



Big Salt Plains, OK: Blue X represents fracture zones of study.